PAPER SPRAY MASS SPECTROMETRY (PS-MS) FOR TOXICOLOGICAL DRUG SCREENS AND BIOMONITORING OF CHEMICAL WARFARE AGENT EXPOSURE

by

Josiah Michael McKenna

A Thesis

Submitted to the Faculty of Purdue University

In Partial Fulfillment of the Requirements for the degree of

Master of Science

Department of Forensic & Investigative Sciences

Indianapolis, Indiana

August 2017

THE PURDUE UNIVERSITY GRADUATE SCHOOL
STATEMENT OF COMMITTEE APPROVAL

Dr. Nicholas Manicke, Chair
Department of Chemistry & Chemical Biology
Dr. John Goodpaster
Department of Chemistry & Chemical Biology
Dr. Frederique Deiss
Department of Chemistry & Chemical Biology

Approved by:
Dr. Eric Long
Head of the Graduate Program

ACKNOWLEDGEMENTS

I would like to sincerely thank my advisor, Dr. Nick Manicke, for all of his help and guidance throughout the course of my graduate career. If not for his patience in dealing with me as I gained my footing in research, I would not have accomplished nearly as much as I did. I also want to thank everyone in the Manicke group—especially Greta Ren, Brandon Bills, and Dr. Chengsen Zhang—who provided technical, practical, and moral support when it was quite often needed, and I wish them the best as they each finish out their tenures here.

I would be remiss if I failed to mention those who came before me and those who made the journey through this master's program with me. Both Rachel Jett and Jordan Ash have been influential in my success, Rachel especially for teaching me the fundamentals of paper spray and doing the extensive preliminary work for one of the projects presented herein. Wesli Kay Stubbs, who joined the program when I did and will complete it alongside me, has been a valued support while we took and taught classes together.

I would also like to thank the U.S. Army Edgewood Chemical Biological Center, specifically Dr. Trevor Glaros and the rest of his group at the Mass Spectrometry Core Facility. The research they do is vital in protecting the safety of our men and women both on the battlefield and at home. Not only that, but they have taken their time to earnestly listen to the advice this 24-year-old has to offer from his relatively narrow field of experience, and I consider myself lucky to have been given the opportunity to work with them.

Additionally, but not with any less importance, I would like to thank all the teachers that I have had the good fortune of learning from throughout my lifetime. There are far too many to name here, but all have been instrumental in shaping me into the person I am today. Without their countless valuable lessons and insights in subjects concerning not only science and math, but also the expressive worlds of English, theatre, and life in general, I would have never made it this far. From questions as small and deceptively simple as "What is an atom?" to infinitely larger concepts concerning the nature of existence and how we relate to the universe around us, I have always been humbled by the knowledge others have to offer. More than just knowledge, though, they have taught me how to think, and for that I am eternally grateful.

TABLE OF CONTENTS

LIST OF TABLES vii
LIST OF FIGURES viii
LIST OF ABBREVIATIONS xi
ABSTRACT xiii
CHAPTER 1. INTRODUCTION 1
Introduction to Paper Spray Mass Spectrometry (PS-MS) 1
Project Overview 5
CHAPTER 2. DEVELOPING PS-MS IN NEGATIVE ION MODE 6
Introduction 6
Materials and Methods 10
Chemical Materials 10
Paper Spray Ionization 11
Mass Spectrometry 13
Data Visualization 14
Negative Ion Drug Screen 14
Results and Discussion 16
Demonstrating the Discharge Problem 16
Polyethylene Substrates 20
Resistor-Aided Negative Ion Spray 26
Discharge Susceptibility in Velox Sample Cartridges 28
Spray Solvent Optimization 31
Negative Ion Drug Screen 39
Future Work 43
Conclusion 47
CHAPTER 3. DETECTION OF CHEMICAL WARFARE AGENT HYDROLYSIS PRODUCTS USING PS-MS 49
Author's Note 49
Introduction 49
Materials and Methods 54
Chemical Materials 54

Sample Preparation 54
Paper Spray Ionization 55
Mass Spectrometry 55
Data Processing 57
Results and Discussion 58
Conclusion 62
CHAPTER 4. APPLYING A PS-MS/MS DRUG SCREEN TO POSTMORTEM BLOOD SAMPLES 64
Introduction 64
High-Resolution Mass Spectrometry 64
Drug Screening 66
Materials and Methods 70
Chemical Materials 70
Sample Preparation 70
Paper Spray Ionization 71
Mass Spectrometry 71
Data Processing 76
Postmortem Sample Drug Screen 76
Results and Discussion 77
Paper Spray Screening on a Quadrupole-Orbitrap Mass Spectrometer 77
Method Optimization for Postmortem Samples 80
Limits of Reporting 84
Evaluating the PS-MS/MS Drug Screen 89
Future Work 92
Conclusion 93
REFERENCES 95
VITA 105

LIST OF TABLES

Table 1. Fragmentation of the analytes and ISTDs used in the negative ion drug screen. 15

Table 2. Experimental parameters and discharge diagnostic data for manual cartridges and VSCs. 30

Table 3. Calibration curve data for each analyte from the negative ion drug screen. Screening cutoffs can be found in Table 1. 39

Table 4. Fragmentation of each CWA hydrolysis product and their SIL ISTDs for both positive and negative ion MS/MS, the latter of which is highlighted. 57

Table 5. Comparison of quantitative capabilities of positive and negative ionization in the detection of CWA hydrolysis products in blood and urine matrices. 58

Table 6. Fragmentation of each analyte and SIL ISTD used in the PS-MS/MS drug screen. The fragment ion indicated was the primary fragment ion used for quantitation. 72

Table 7. Raw ISTD MS/MS signal in the PM and calibrant samples when sprayed using the new method (85:10:5:0.01 acetonitrile:acetone:water:acetic acid with thinned blood samples) as compared to the original method (95:5:0.01 methanol:water:acetic acid). 82

Table 8. Quantitative measurements for each of the analyte calibration curves which ran concurrently with the PM samples in the PS-MS/MS drug screen. 84

Table 9. Results from the PS-MS/MS drug screen for each of the 30 PM samples. 88

Table 10. Qualitative results of the HPLC- and PS-based drug screens..... 90

LIST OF FIGURES

Figure 1. Operation of (a) LC-ESI-MS and (b) PS-MS. 3

Figure 2. (a) The PS-MS negative ion circuit. Electron current (e^-) naturally flows to the tip, which emits electrons due to the high electric field around it. (b) The chain reaction of electron-releasing ionizations that propagates the avalanche, each arrow split indicating an ionization event. (c) A primary electron avalanche releasing photons, the circled charges representative of approximate space charge distributions. The electrospray gap is very large compared to the high-field region, so the electric field around the distant anode has no influence over the propagation of avalanches. 7

Figure 3. (a) Manual cartridges and (b) Velox Sample Cartridges (VSCs) used for PS-MS, as well as the spotting method for the former. 12

Figure 4. (a) Full-MS and (b) MS/MS of m/z 205 TIC plots of a single discharging PS-MS sample. Inset in (a) is a camera-aided visualization of corona discharge on paper tips. At 0.44 min, the discharge intensified to more noticeable levels, (c) and (d) showing the full mass spectra before and after this point, respectively. In the mass spectra, m/z 205 is ibuprofen's precursor ion, m/z 60 is CO_3^-, and m/z 62 is NO_3^-. 17

Figure 5. Full-MS precursor ion intensities for ibuprofen, phenobarbital, ibufenac, and phenobarbital-d5 sprayed from both paper and methanol-washed PE (7-12 μm pore size) tips across three different matrices (neat, human whole blood, and bovine plasma). Five replicates were run for each sample. 21

Figure 6. MS/MS fragment ion signal for phenobarbital, warfarin, ibufenac, and phenobarbital-d5 sprayed from both paper and unwashed PE (7-12 μm pore size) tips across neat and blood matrices. All samples were run in triplicate. 22

Figure 7. Ratio of analyte/ISTD signal for (a) phenobarbital and (b) warfarin at 1× and 10× their given concentrations of 2000 ng/mL and 500 ng/mL. All samples were run in triplicate; RSDs are given above or below each plot. 23

Figure 8. MS/MS fragment ion signal obtained for each of the five compounds in neat and whole blood matrices with and without use of the 10-GΩ resistor in the PS-MS circuit. Five replicates were run for each sample. 27

Figure 9. MS/MS fragment ion signal for ibuprofen (10000 ng/mL), naproxen (30000 ng/mL), furosemide (1000 ng/mL), amobarbital (500 ng/mL), butabarbital (500 ng/mL), and butalbital (500 ng/mL) in both neat and blood matrices, sprayed from manual cartridges and VSCs. All samples were run in triplicate. 29

Figure 10. Full-MS CO_3^- measurement distributions for spray solvents containing different amounts of CCl_4. The remaining solvent consisted of methanol with 0.01% NH_4OH, spraying from neat samples on manual cartridges at 3.3 kV. Eight replicates were run with each spray solvent. 33

Figure 11. Comparison of discharge measurements between the optimized solvent (90:10:0.01 methanol:CCl_4:NH_4OH), a methanol solvent (100:0.01 methanol:NH_4OH), and a conventional PS solvent (95:5:0.01 methanol:water:acetic acid), all run at 3.5 kV on the Velox 360 source. 35 replicates were run with each spray solvent. 36

Figure 12. Ratio of analyte/ISTD signal for hydrochlorothiazide, phenobarbital, and pentobarbital acquired using (1) the optimized solvent (90:10:0.01 methanol:CCl_4:NH_4OH), (2) a pure methanol solvent (100:0.01 methanol:NH_4OH), and (3) a conventional PS solvent (95:5:0.01 methanol:water:acetic acid). 30 replicates were run with each solvent; RSDs are given above each plot. 37

Figure 13. Ratio of analyte/ISTD signal for phenobarbital and warfarin at 1× and 10× their given concentrations of 2000 ng/mL and 500 ng/mL in blood, sprayed using the optimized solvent (90:10:0.01 methanol:CCl_4:NH_4OH) and a conventional solvent (95:5:0.01 methanol:water:acetic acid). All samples were run in triplicate; RSDs are given above each plot. 38

Figure 14. Calibration curves for (a) butabarbital, (b) butalbital, (c) amobarbital, (d) pentobarbital, (e) phenobarbital, (f) secobarbital, (g) thiopental, and (h) phenytoin. The y-axes are the ratio of the respective fragment ion signal to that of phenobarbital-d5, and each point is the average of three replicates of these measurements. Inset in (d) is a calibration curve for pentobarbital run from a different set of samples. 40

Figure 15. Calibration curve for ibuprofen in blood samples. 42

Figure 16. Raw MS/MS signal for (a) ibuprofen and (b) levetiracetam in the matrix blanks and calibration samples. 43

Figure 17. Chemical structures of five nerve agents: GB (sarin), GD (soman), GF (cyclosarin), VX, and VR ("Russian VX"). 50

Figure 18. Successive hydrolysis reactions of a CWA, where X = F or $S(CH_2)_2NR'_2$ and R = C_2-C_6. 53

Figure 19. Negative ion transitions of the five CWA hydrolysis products. Red and blue bolded atom labels indicate the locations of the ^2H (d) and ^{13}C isotopes, respectively, in the SIL analogs. 56

Figure 20. Positive ion calibration curves for EMPA, IMPA, iBuMPA, CHMPA, and PinMPA in both blood (a-e) and urine (f-j) matrices. Each data point is the average of three replicates. 59

Figure 21. (a) Positive and (b) negative ion calibration curves for IMPA in blood, showing each individual analyte/ISTD measurement against its known concentration. 60

Figure 22. Negative ion calibration curves for EMPA, IMPA, iBuMPA, CHMPA, and PinMPA in both blood (a-e) and urine (f-j) matrices. Each data point is the average of three replicates. 61

Figure 23. Schematic diagram of a Q-Exactive mass spectrometer from Thermo Fisher Scientific, which utilizes a hybrid quadrupole-orbitrap to achieve high mass resolution. 69

Figure 24. (a) Total ion chronogram (all scans combined). (b) Extracted ion chronogram from MS/MS scans of cocaine. (c) Tandem mass spectrum for a neat standard of cocaine at 200 ng/mL, infused via commercial ESI. (d) Tandem mass spectrum for blood spiked with 16 ng/mL cocaine (0.33× its cutoff), sprayed via paper spray. 78

Figure 25. MS/MS signals between the original (a-d) and new (e-h) methods of sample preparation and spraying for the ISTDs benzoylecgonine-d8, flunitrazepam-d7, gabapentin-d10, and metaxalone-d6. Average values for half of the PM samples, run in triplicate, are shown along with an average value for calibrants run alongside them, with the error bars indicating one standard deviation above and below these values. 83

Figure 26. Comparison of concentrations for the drugs detected and quantitated from the PM samples by both HPLC- and PS-based screening methods. The dashed line represents two methods whose quantitative performances are identical. 92

LIST OF ABBREVIATIONS

APCI	atmospheric pressure chemical ionization
AUC	area under curve
CE	collision energy
CHMPA	cyclohexyl methylphosphonic acid
CID	collision-induced dissociation
CWA	chemical warfare agent
CWC	Chemical Weapons Convention
DART	direct analysis in real time
DBS	dried blood spot
DESI	desorption electrospray ionization
DIMP	diisopropyl methylphosphonate
DMMP	dimethyl methylphosphonate
DMSO	dimethyl sulfoxide
EMPA	ethyl methylphosphonic acid
ESI	electrospray ionization
FN	false negative
FP	false positive
FT-ICR	Fourier transform ion cyclotron resonance
GB	O-isopropyl methylphosphonofluoridate (sarin)
GC	gas chromatography
GD	O-pinacolyl methylphosphonofluoridate (soman)
GF	O-cyclohexyl methylphosphonofluoridate (cyclosarin)
HCD	high-energy collisional dissociation
HDPE	high-density polyethylene
HPLC	high-performance liquid chromatography
HR-MS	high-resolution mass spectrometry
IARC	International Agency for Research on Cancer
iBuMPA	isobutyl methylphosphonic acid
IMPA	isopropyl methylphosphonic acid

ISTD	internal standard
LC	liquid chromatography
LOD	limit of detection
LOQ	limit of quantitation
LOR	limit of reporting
MPA	methylphosphonic acid
MS	mass spectrometry
MS/MS	tandem mass spectrometry
NPV	negative predictive value
PE	polyethylene
PES	polyester
PinMPA	pinacolyl methylphosphonic acid
PM	postmortem
PPV	positive predictive value
PS	paper spray
RSD	relative standard deviation
SIL	stable isotope labeled
SIM	selected ion monitoring
SPME	solid-phase microextraction
TCNQ	7,7,8,8-tetracyanoquinodimethane
TIC	total ion current
TMP	trimethyl phosphate
TN	true negative
TOF	time-of-flight
TP	true positive
UHPLC	ultra-high-performance liquid chromatography
VR	O-isobutyl-S-(2-diethylamino)ethyl methylphosphonothiolate
VSC	Velox Sample Cartridge
VX	O-ethyl-S-(2-diisopropylamino)ethyl methylphosphonothiolate

ABSTRACT

Author: McKenna, Josiah Michael MS
Institution: Purdue University
Degree Received: August 2017
Title: Paper Spray Mass Spectrometry (PS-MS) for Toxicological Drug Screens and Biomonitoring of Chemical Warfare Agent Exposure
Major Professor: Nicholas Manicke

Paper spray is an ambient ionization technique for mass spectrometry that is well-known for its ability to accomplish rapid and sensitive analyses without any need for sample preparation. This work further develops the technique in two major areas: negative ionization and drug screening. Negative ionization has always been an obstacle to electrospray-based ion sources because of its vulnerability to corona discharge, but methods are presented here to both quantify and suppress this electrical phenomenon, thus preventing it from interfering with qualitative/quantitative analyses. The validity of the discharge-suppressing method is demonstrated for both a simple screen of barbiturates and other acidic drugs (Chapter 2) and the detection and quantitation of chemical warfare agent hydrolysis products (Chapter 3). Additionally, a positive ion drug screen is applied to the analysis of postmortem blood samples (Chapter 4), achieving rapid and effective screening of 137 different drugs ranging from pharmaceuticals to drugs of abuse. The performance of this screen is also evaluated by comparing the results of the postmortem samples to those obtained using a more established series of assays. The research contained herein presents strides toward forensic application of paper spray mass spectrometry, especially in disciplines related to forensic toxicology.

CHAPTER 1. INTRODUCTION

Introduction to Paper Spray Mass Spectrometry (PS-MS)

For many forensic laboratories, mass spectrometry (MS) serves as the gold standard for identification of unknown chemical samples. The ability to detect analytes by mass as well as filter them for subsequent fragmentation to monitor the resulting masses—a technique referred to as tandem MS, or MS/MS—lends to the impressive selectivity put forth by the method. However, up until the 1980s, MS could only viably be paired with the separating capabilities of gas chromatography (GC) systems, primarily because of the need for ions to be in the gas phase and under vacuum pressures for accurate mass analysis.[1] While GC-MS still remains one of the go-to techniques for volatile samples, the eventual development of electrospray ionization (ESI) established the bridge to allow effective and direct coupling of liquid chromatography (LC) systems with MS in open air.[2-4] This in turn provided a simpler means for the previously difficult mass analysis of nonvolatile samples, further enabling the implementation of MS as an analytical technique.

Even with the ability to connect the two chromatographic systems to MS, though, proper analysis still requires a relatively large amount of sample preparation both before and including the separation. Such preparatory requirements can be both time-consuming and costly, which are non-negligible obstacles when trying to streamline sample processing. To address the limitations imposed by chromatography, techniques have been developed within the past couple decades that allow for direct ionization of samples within their ambient environments (e.g., in blood or on metal surfaces) under atmospheric pressure before introduction to the vacuum for MS analysis. Desorption electrospray ionization

(DESI)[5] and direct analysis in real time (DART)[6] were the pioneering ambient ionization techniques developed to this extent, with many more to follow.[7]

Notable among the growing list of ambient ionization techniques is paper spray (PS). PS was first explored conceptually by Tepper and Kessick using porous polymer wicks in 2009[8] and then with more application in following years, chiefly out of Cooks' and Ouyang's laboratories at Purdue University.[9-14] Operationally, PS functions in the same manner as ESI, where a high voltage—usually between 2-5 kV—is applied to a liquid on a point to get it to spray toward the MS inlet as shown in Figure 1. The only difference is that instead of eluent from a chromatography column flowing through a narrow needle to generate the electrospray, the sample is first transferred onto a pointed porous substrate and allowed to dry before a spray solvent—equivalent to the mobile phase in LC—is applied. The spray solvent wicks through the entirety of the substrate and the dried sample, extracting the analytes and conveying them to the tip; an elevated electric field exists around the tip of the substrate due to its small radius, which expels charged droplets in the form of electrospray toward the MS inlet. Once these droplets are airborne, remaining solvent molecules quickly evaporate and successive Coulombic fissions, arising from the repulsive forces felt by many charged molecules occupying the same droplet volume, generate gas-phase ions that are then drawn into the vacuum of the mass spectrometer.

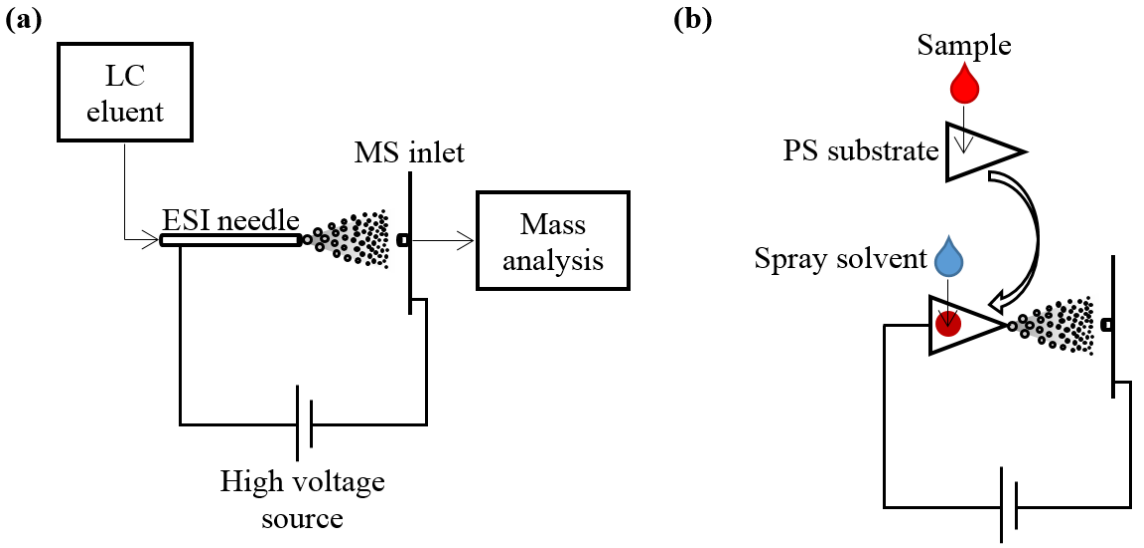

Figure 1. Operation of (a) LC-ESI-MS and (b) PS-MS.

By name alone, PS implies ionization from a paper substrate, but this is not necessarily true. The term "paper" itself can be associated with many different types of materials, all of which may in fact spray very differently. The physical and chemical differences between filter paper and chromatography paper, for instance, causes them to spray with different efficiencies.[9] In general, though, any porous material which allows for quick solvent travel through or on it can be used as a spray substrate. To this extent, carbon-nanotube-coated filter paper,[15] polymer-blend fibers,[8] porous polymer pen nibs,[16,17] wooden toothpicks,[16-18] and even intact plant material such as leaves[19] have been successfully tested as PS substrates.

The conventional and clinically-minded method of transferring samples onto the substrate is via direct pipetting, or spotting. Other sampling methods involve wiping the substrate on or dipping it into samples, which permits the PS-MS analysis of a much broader range of samples[9,18,20,21] and demonstrates the ease of applying the technique to forensic science and the types of evidence typically encountered at crime scenes. In terms of spray solvents, an organic solvent is usually employed with a small amount of aqueous

phase to increase the surface tension. To this is added a modifier such as acetic acid or formic acid that assists in ionizing the analytes. While chromatography paper substrates are versatile and function well for most applications, proper choice of the substrate-solvent system in PS is often crucial in optimizing the analytical method.

The utilization of PS-MS confers many advantages to the sampling and analytical processes. Among these advantages are: ease of patient-end sampling due to the small sample volumes required; biological samples spotted and dried on paper, such as dried blood spots (DBSs), present a reduced biohazard in storage/transport compared to traditional liquid samples; little-to-no sample preparation; reduced matrix effects from the rudimentary separation that takes place on the substrate; speedy data acquisition and analysis; and cost-effective materials for high throughput. Good quantitation of analytes can also be achieved through the use of stable isotope labeled (SIL) internal standards (ISTDs). And while adding ISTD to a sample may indicate a small amount of required sample preparation, studies have demonstrated the successful quantitation of analytes by either pre-treating the substrate with ISTD or including it in the spray solvent, avoiding any need to alter the sample.[10,11] All of these factors have aided the implementation of PS-MS in miniature and field-forward MS systems designed for use outside of laboratory environments.[22,23]

The breadth of PS-MS applications is wide and constantly growing. The technique has proven effective for the quantitative analysis of small molecules such as drugs in biofluids, which could be highly beneficial in clinical settings as it is capable of providing a rapid means for therapeutic drug monitoring of individuals.[10,11,24-26] PS-MS has been successfully demonstrated for dye analysis, even after quick chromatographic separation

from an ink sample.[12,18,27] It has also been used for the detection of contaminants on foodstuffs[28] and, due to the small sample sizes needed, coupled with microfluidic chips to detect products of microchemical reactions.[29] Biochemical species of interest such as proteins,[9,12,17,18] nucleic acids,[17] and phospholipids[12] have all been investigated using PS-MS, and it has even been used for the direct analysis of tissue samples.[13] The application of PS-MS to neonatal screening—specifically through the detection of acylcarnitines, which are used in monitoring metabolic deficiencies—has also been demonstrated.[30] Additionally, such already-established applications can be translated to their corresponding forensic science disciplines. For example, ink- and drug-based analyses could be relevant for purposes of questioned document examination[31,32] and forensic toxicology.

Project Overview

The research presented in this thesis further develops PS-MS in two areas: negative ionization and drug screening of blood samples. Chapter 2 addresses the plaguing issue of corona discharge encountered in negative mode ESI techniques and investigates means to suppress it such that sensitive and reliable detection can be accomplished. Also demonstrated in Chapter 2 is the application of the developed negative ion PS-MS method to a toxicological screen of 19 acidic drugs, with barbiturates and ethanol metabolites included among them; a few drugs capable of positive ionization were also analyzed in this screen to see how well they could be detected in negative ion mode. Chapter 3 investigates the detection and quantitation of chemical warfare agent hydrolysis products in biomatrices using PS-MS in both polarities of ionization. Chapter 4 sees the adaptation of a PS-based drug screen for 137 analytes[33,34] to postmortem samples, which, when developed further, would be an invaluable tool for forensic toxicology.

CHAPTER 2. DEVELOPING PS-MS IN NEGATIVE ION MODE

Introduction

Despite the significant developments that PS has seen over the past decade to increase the scope of its applicability, much of this development has only covered positive ionization. Few studies have implemented negative ion PS in the detection of analytes, and fewer still have discussed the reason behind this relative lack of research.[9,12,13,16,18,35] This reason is an issue facing not only PS but negative ESI in general: corona discharge.[35] Corona discharge is a glowing electrical event caused by rapid ionization of gas molecules which, when applied to ESI systems, overwhelms stable electrosprays. Accompanied by a drastic increase in spray current, the appearance of this discharge is known for leading to poor reproducibility and sensitivity of the electrospray technique,[36] hence why forays into PS in the negative ion mode are often brief and underdeveloped compared to those into positive ion mode.

To demonstrate why the occurrence of corona discharge is detrimental to the fundamental ESI process, it is important to discuss the electrical nature of the circuit created and how the discharge manifests itself. Figure 2a shows the electrical circuit created in negative ion PS, with the high voltage source flipped compared to that of positive ionization to apply a negative potential to the paper tip. The high-field region that is responsible for propelling negative ions toward the distant and positively charged MS inlet is represented by the dashed circle. Ions that scatter around the inlet rather than pass through are neutralized via oxidation, establishing the flow of electrons (e^-) opposite the current (I). Since electron current flows in this direction, individual electrons are readily

released by the elevated electric field around the negative cathode in a process known as field emission.[37,38] These free electrons quickly accelerate and collide with gas molecules in the region, leading to either electrochemical reduction of gas molecules along with subsequent ion-molecule reactions[39] or electron avalanches.[38,40]

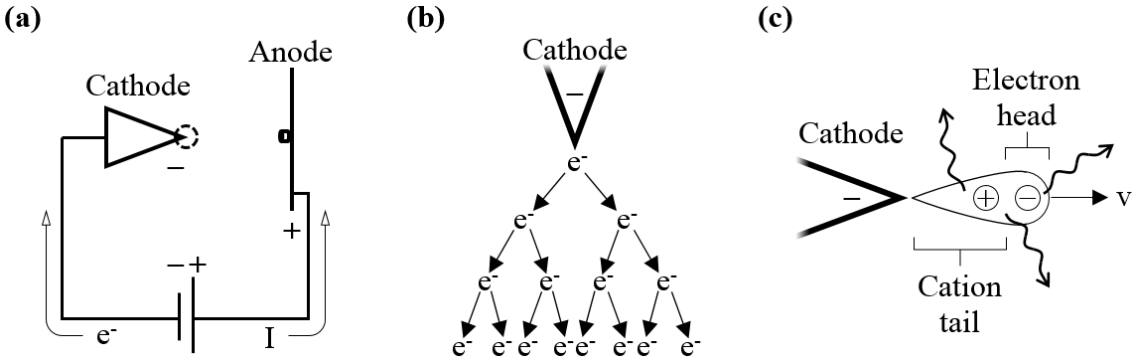

Figure 2. (a) The PS-MS negative ion circuit. Electron current (e^-) naturally flows to the tip, which emits electrons due to the high electric field around it. (b) The chain reaction of electron-releasing ionizations that propagates the avalanche, each arrow split indicating an ionization event. (c) A primary electron avalanche releasing photons, the circled charges representative of approximate space charge distributions. The electrospray gap is very large compared to the high-field region, so the electric field around the distant anode has no influence over the propagation of avalanches.

Electron avalanches are the primary cause for discharging and electrical breakdowns. They occur when an accelerated electron, still within the high-field region, has enough energy to completely ionize a molecule, liberating an electron and re-accelerating to ionizing speeds. This process leads to a chain reaction of electron-induced ionizations, producing a swarm of electrons trailed by the slower-moving ionized molecules—the avalanche, shown in Figures 2b and 2c—and releasing the photons perceived as the glow in corona discharge; the emitted electrons can also trigger secondary avalanches that propagate around the primary avalanche.[38,40] As long as the electric field remains high enough in the vicinity of an avalanche, this propagation can continue indefinitely until it bridges the gap to the opposing electrode, leading to a complete spark breakdown of the gap.[40]

However, when considering an ESI source charged with a negative potential such as the tip in PS-MS shown in Figure 2, the avalanching develops away from and beyond the high-field region. Any further propagation is quenched because the lower field strength is insufficient to accelerate electrons to ionizing speeds, preventing formation of full breakdown streamers and limiting discharge to the visible corona around the cathode. Alternatively, when operating positive ESI, any avalanching develops toward the positively charged anode that is the source and into the high-field region; because of this, every primary avalanche is guaranteed to fully propagate to the anode, forming partial streamers that visually extend outward from the source, leading to the conclusion that partial breakdown of the gap occurs at lower voltages for positive ion mode than it does for negative ion mode.[38,40,41]

While seemingly conflicting with the notion that corona discharge is more of a problem in negative ion mode, this only notes the small voltage difference between corona discharge in positive ion mode and the onset of breakdown streamers. In actuality, the onset of corona discharge itself occurs at higher voltages in positive ionization due to the higher energies needed to ionize gases and generate the free electrons that begin the avalanching process in the first place.[37,38] Since free electrons are readily released via field emission in negative ionization, though, it does not require the higher energies or voltages that positive ion mode needs. In fact, because of the nature of the electrical circuit created, there is a very small and unreliably defined range of operating voltages in which negative ESI can be achieved normally and without discharge.

Corona discharge affects sensitivity primarily through its overproduction of ions. Those generated from gaseous ion-molecule reactions—O_3^-, CO_3^-, CO_4^-, and NO_3^-, to name

a few[39]—are all of small mass. As such, they travel faster than most analytes and reach the inlet more quickly than their larger counterparts. And in instruments such as ion traps that are limited by the number of ions that can be introduced into the system, the increased presence of small ions restricts the number of heavier ions that are available for mass analysis. Furthermore, when compounded with the overabundance of electrons from the unending cascade of avalanches, these ions increase the charge density in the inlet-bound ion beam, which causes the noticeable rise in spray current. This increase also enhances the space charge effect, which is responsible for defocusing the ion beam and deflecting heavier and slower-moving ions by Coulombic repulsion.[42] Discharge can also affect sensitivity by preventing the Taylor cone from forming at all and therefore inhibiting the fundamental electrospray process. When taken together with the fact that negative ion mode is naturally prone to discharge, this sensitivity loss is the motivating factor behind the lack of negative ESI development, especially for the relatively new PS-MS.

Among the primary experimental parameters that influence the susceptibility of the tip to discharge are the electrospray gap length (the tip-to-inlet distance in PS-MS) and the applied voltage, which directly affect the strength of the electric field at the cathode. When ionizing with PS, the presence of stray fibers or burring at paper tip also increases the propensity for discharge due to the high electric field at these protuberances. There have been studies, however, that address problems with discharge and show successful ESI in negative ion mode by incorporating new or different elements into the experimental setup. For example, introducing electron-scavenging gases such as SF_6[36,43] or O_2[44] into the electrospray gap has been shown to suppress discharge. Using chlorinated solvents as a mobile phase effectively increases the voltage required for the onset of corona discharge

without affecting the voltage required for proper Taylor cone formation.[2,45,46] Strong resistors—on the order of GΩ—positioned between the high voltage source and the ESI needle have also demonstrated discharge-suppressing abilities.[47-49] And in PS specifically, the utilization of alternative substrates such as polyethylene or polyester has shown acceptable detection in negative ion mode.[16]

The goal of this study was to investigate the issue of corona discharge in negative ion PS-MS and its various remedies as they might be applicable to field-forward PS instrumentation. This involved optimization of the experimental setup such that discharge could be quantified and reproducibly avoided between samples, preventing it from interfering with quantitative analyses. The optimized negative ion method is ultimately demonstrated through its use in a drug screen targeting barbiturates—which, while not as prevalent or abused today as they have been in the past, still see therapeutic use[50]—as well as several other acidic analytes.

Materials and Methods

Chemical Materials

High-performance liquid chromatography (HPLC) grade methanol, Optima grade ammonium hydroxide (NH_4OH), and glacial acetic acid were purchased from Fisher Scientific (Pittsburgh, PA, USA). Anhydrous carbon tetrachloride was purchased from Sigma Aldrich (St. Louis, MO, USA). Most standards—ibuprofen, naproxen, levetiracetam, tadalafil, furosemide, hydrochlorothiazide, warfarin, phenytoin, amobarbital, butabarbital, butalbital, pentobarbital, phenobarbital, phenobarbital-d5, and ethyl-beta-D-glucuronide—were purchased from Cerilliant (Round Rock, TX, USA) at concentrations of either 1.0 mg/mL or 100 μg/mL in methanol. Secobarbital and thiopental

were purchased from Sigma Aldrich as 1.0 mg/mL standards. Salicylic acid, valproic acid, and sodium ethyl sulfate powders were also purchased from Sigma Aldrich and were dissolved in water to generate stock solutions. Ibufenac powder was purchased from Sigma and dissolved in dimethyl sulfoxide (DMSO) to create a stock solution.

Since the majority of this chapter is dedicated to the development of an optimized method, many different samples were made to test different parameters. As such, these samples were prepared as described in the Results and Discussion section. For biological samples, human whole blood was provided by a single donor and bovine plasma was purchased from Lampire Biological Laboratories (Pipersville, PA, USA). All solvent mixtures, unless otherwise indicated, were mixed by volume (v:v).

Paper Spray Ionization

PS was accomplished using both manual cartridges and the Velox Sample Cartridges (VSCs) designed for use with the automated Velox 360 PS source (Prosolia, Indianapolis, IN, USA). The former type of cartridge, shown in Figure 3a, was made by using a Sherline milling machine (Vista, CA, USA) to create the holes and slot in a bar of Delrin plastic (Quadrant, Fort Wayne, IN, USA). For all experiments, cellulose-based Whatman 31ET CHR chromatography paper (Piscataway, NJ, USA) was used as the substrate for the punch, onto which 3.5 μL of sample were deposited before drying at room temperature. Various substrates were tested as the PS tip, including: Whatman chromatography paper; porous polyethylene with assorted pore sizes of 7-12 μm, 15-45 μm, and 15-50 μm (Porex, Fairburn, GA, USA); and high-density polyethylene (Pore Technology, Marietta, TX, USA). These substrates were all cut into the irregular pentagons shown and inserted into the cartridge for spraying, positioned ~4-5 mm in front of the MS

inlet. Before the voltage was turned on, 40-60 µL of spray solvent was applied into the well on top of the sample-spotted paper punch. A Pulnix TM-200 camera (Jai, San Jose, CA, USA) with a Navitar Precise Eye adapter tube and lens (Rochester, NY, USA) was used in visualizing the PS process for all cartridges sprayed manually.

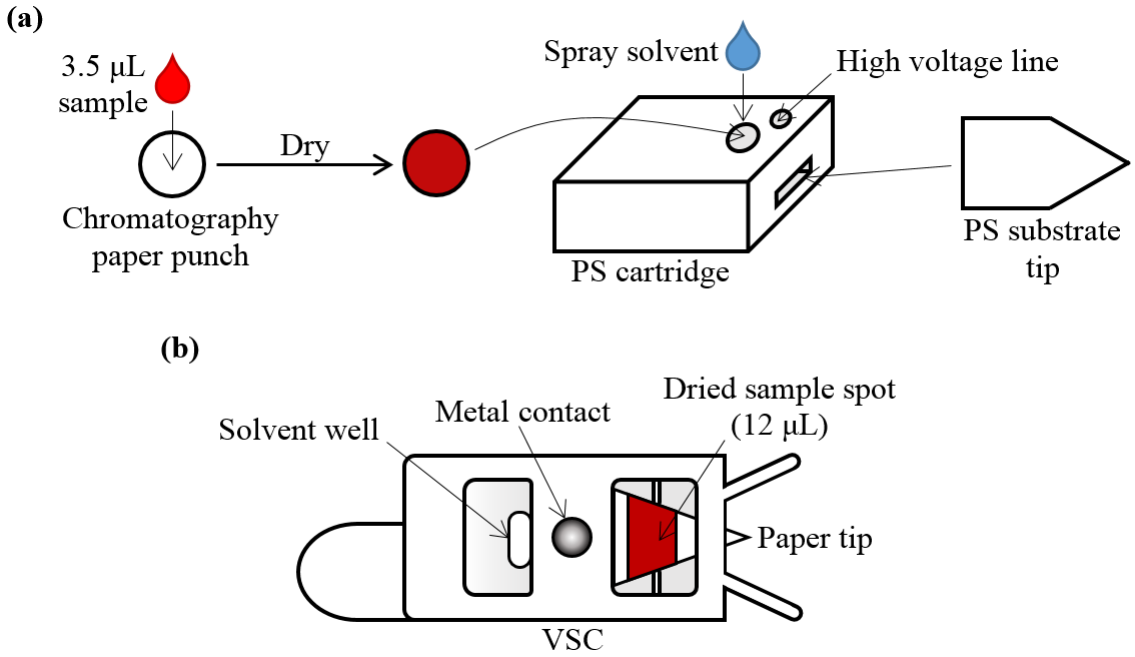

Figure 3. (a) Manual cartridges and (b) Velox Sample Cartridges (VSCs) used for PS-MS, as well as the spotting method for the former.

When using the VSCs (Figure 3b), 12 µL of sample were spotted onto the paper tip through the sample window and allowed to dry at room temperature. The Velox 360 source uses two pumps to apply solvent to the paper tip: pump A, which dispenses in 3-µL increments, for application straight onto the dried sample spot, and pump B, which dispenses in 10-µL increments, for application into the solvent well. When the VSCs were sprayed with this automated PS source, 142 µL of solvent were applied to the cartridge—12 µL from pump A and 130 µL from pump B. Most often, a large delay was incorporated only before the first dispensation of solvent onto the sample, all subsequent delays occurring in a quick succession of 2-second intervals. Whenever it was used for automated

PS-MS, the Velox 360 source was locked into place against the rim of its mounting flange, allowing for no user-end control over the tip-to-inlet distance to keep it consistent between sampling across multiple days. VSCs were also occasionally sprayed manually using a specially milled bar of Delrin plastic to simply hold them in place in front of the MS inlet—in these cases, the solvent was applied in such a way as to mimic the dual action of the pumps, using it to first wet the sample spot and then dispensing it into the solvent well.

To test the discharge-suppressing capabilities of including a resistor in the high voltage line, a 10-GΩ-equivalent resistor was created by soldering together ten 1-GΩ Ohmite (Warrenville, IL, USA) resistors in series. This large resistor was then connected in series between the high voltage source of the mass spectrometer and the PS cartridge. When using this resistor as such, cartridges were only ever run manually without the aid of the Velox 360 PS source.

Mass Spectrometry

All data were acquired in negative ionization mode using either an LTQ-XL linear ion trap mass spectrometer or a Q-Exactive Focus orbitrap mass spectrometer (Thermo Fisher Scientific, San Jose, CA, USA). When optimizing the method, both full-MS and MS/MS scans were utilized, fragmenting all analytes via collision-induced dissociation (CID) at the collision energies (CEs) given in Table 1, which were determined via direct infusion ESI of analyte solutions. Onset voltages were typically within the 3.0-4.0 kV range—or up to 8.0 kV when using the resistor—with method lengths between 1.0 and 1.4 minutes. All data were analyzed using Xcalibur v. 4.0 (Thermo Fisher Scientific) and, unless otherwise noted, defined signal as the area-under-curve (AUC) response for any given precursor or fragment ion.

Data Visualization

Two types of graphs were employed to visualize the data acquired. Bar graphs were used to compare average signals—taken from three to five individual measurements—across different variables, with the error bars indicating the magnitude of one standard deviation above and below these values. To visualize measurement distribution and precision of the compared methods, box-and-whisker plots were used. The median of a set of measurements was used as the central tendency of such plots, with the box encasing the interquartile range between the 25^{th} and 75^{th} percentiles; the whiskers extended outward to encompass the 0^{th} and 100^{th} percentiles.

Negative Ion Drug Screen

Several acidic analytes were tested, all of which are given in Table 1 along with their precursor and MS/MS fragment ions. Due to the limitations of MS in not being able to differentiate structural isomers such as amobarbital and pentobarbital, this initial drug screen was separated into two methods to deal with the quantitation of each separately. Phenobarbital-d5, a SIL ISTD of phenobarbital, was used in quantitating all barbiturates and related structural analogs (amobarbital, butabarbital, butalbital, pentobarbital, phenobarbital, secobarbital, thiopental, and phenytoin); ibufenac, a structural analog for ibuprofen containing a –COOH moiety, was used as a catch-all ISTD for the remaining analytes.

Table 1. Fragmentation of the analytes and ISTDs used in the negative ion drug screen.

Compound	Precursor Ion [m/z]	Fragment Ion [m/z]	CE [V]	Screening Cutoff [ng/mL]
Butabarbital	211.1088	168.1029	11	500
Butalbital	223.1088	180.1030	10	500
Amobarbital	225.1245	182.1185	11	500
Pentobarbital	225.1245	182.1185	11	500
Phenobarbital	231.0775	188.0718	10	1000
Secobarbital	237.1245	194.1187	10	500
Thiopental	241.1017	100.9812	14	2000
Phenytoin	251.0824	102.0345	22	1000
Salicylic acid	137.0244	93.0342	16	9000
Valproic acid	143.1077	143.1077	10	5000
Levetiracetam	169.0983	84.0450	10	2000
Ibuprofen	205.1233	159.1179	10	1000
Naproxen	229.0869	158.0374	15	1000
Hydrochlorothiazide	295.9571	268.9460	20	100
Warfarin	307.0974	161.0245	21	500
Furosemide	329.0004	285.0103	14	1000
Tadalafil	388.1307	262.0871	19	100
Ethyl sulfate	124.9914	96.9598	17	100
Ethyl-beta-D-glucuronide	221.0668	75.0082	15	100
Ibufenac	191.1079	107.0500	10	---
Phenobarbital-d5	236.1090	193.1032	10	---

The analytes were spiked into blood to generate samples at 15× their respective screening cutoff concentrations, which were then serially diluted in blood to generate a 5-point calibration series of 1×, 3×, 6×, 10×, and 15×. 5 µL of an ISTD mixture of phenobarbital-d5 and ibufenac were then spiked into 100 µL of each sample to generate ISTD concentrations of 0.4 µg/mL and 5.3 µg/mL, respectively. These blood samples were spotted in triplicate on VSCs and sprayed from the Velox 360 PS source using 142 µL of 90:10:0.01 methanol:CCl_4:NH_4OH.

All samples were acquired on the Q-Exactive Focus mass spectrometer using MS/MS scans for each analyte and a temperature of 320°C; the isolation width of each precursor ion by the first quadrupole was ±0.5 m/z. The method was 1.4 minutes long, with the voltage on at 4.0 kV for the first 1.1 minutes and then off at 0 kV for the final 0.3

minutes. This no-voltage time was included to allow for automated data analysis using TraceFinder v. 3.3 (Thermo Fisher Scientific), which integrated m/z signals within a 5-ppm window of the target fragment ion. Concentrations were plotted against the measured analyte/ISTD signal and lines of best fit were determined using 1/x weighting; LODs were calculated with a k-factor of 3 multiplied by the standard error of the y-intercept and divided by the slope of the calibration curve.

Results and Discussion

Demonstrating the Discharge Problem

An example of a PS-MS sample discharging is shown in Figure 4. In this case, the analyte—10 μg/mL ibuprofen—was included in the spray solvent, which was a 95:5:0.01 methanol:water:NH_4OH mixture. NH_4OH was used as a solvent modifier to facilitate negative ion production, the hydroxide ions deprotonating the ibuprofen molecules to form $[M-H]^-$ molecular ions at m/z 205. The voltage was turned on to 4.0 kV for the middle 0.8 minutes of the acquisition to allow the sample to spray. In an ideal sample, the total ion current (TIC) would remain relatively constant over this window, producing a box-like shape from the voltage being switched on and off. During the first half of this acquisition, however, light discharge was already occurring, producing spray currents between 1 and 2 μA along with an unstable TIC; halfway through, the discharge intensified to currents around 20 μA, halving the full-MS signal and decreasing the measured ibuprofen precursor ion signal by a factor of 40. This loss of signal is readily apparent in the difference between the instrumental response for m/z 205 in the mass spectra shown in Figures 4c and 4d. The decreased presence of the precursor ion in turn adversely affected the capability of the method to adequately perform MS/MS via fragmentation of ions at m/z 205, the resulting

MS/MS spectra seeing a 110-fold decrease in the measured fragment ion (m/z 161) signal. This significant drop in sensitivity is demonstrated in the MS/MS TIC plot seen in Figure 4b, where almost all signal virtually vanishes with the onset of heavy discharge.

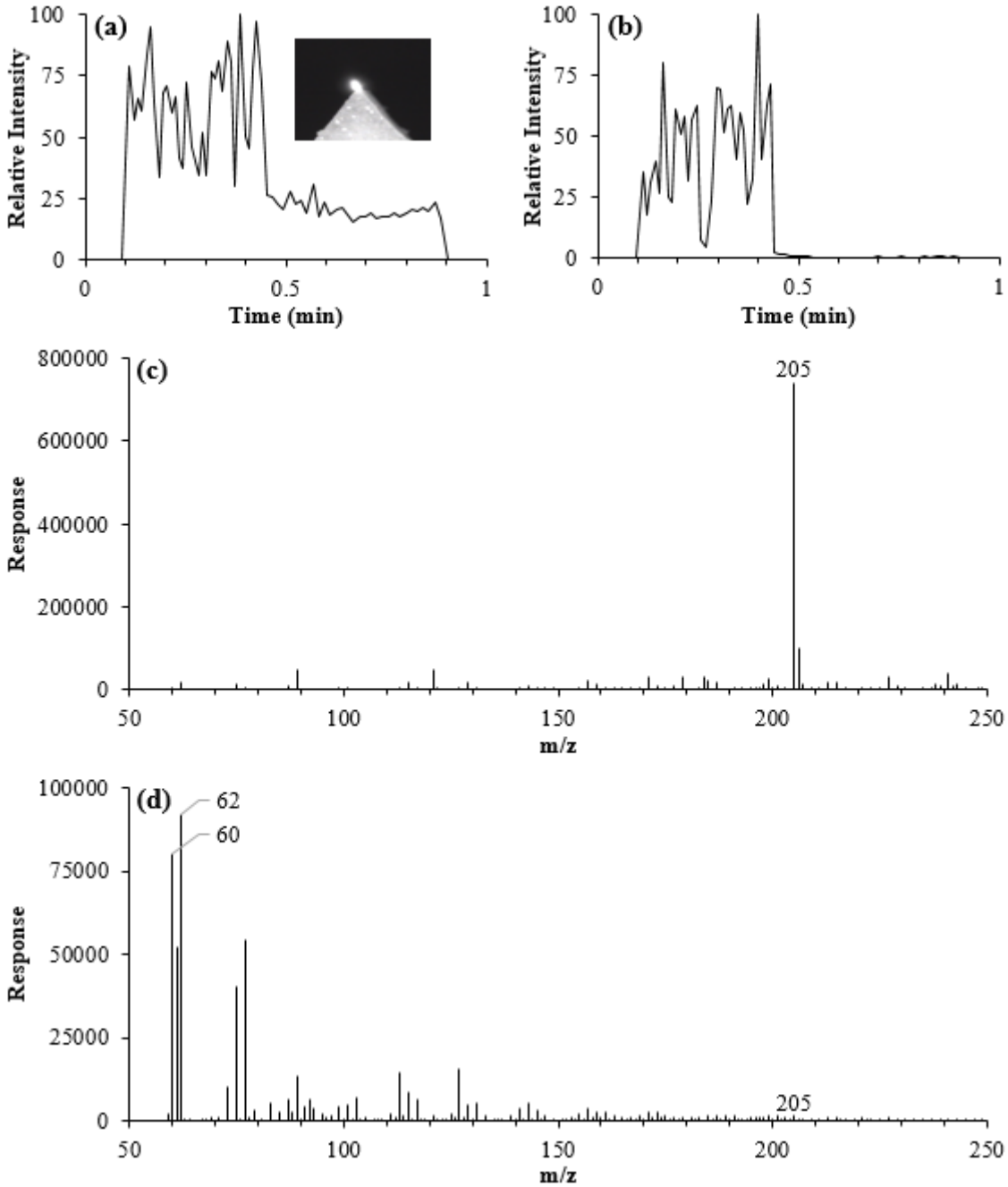

Figure 4. (a) Full-MS and (b) MS/MS of m/z 205 TIC plots of a single discharging PS-MS sample. Inset in (a) is a camera-aided visualization of corona discharge on paper tips. At 0.44 min, the discharge intensified to more noticeable levels, (c) and (d) showing the full mass spectra before and after this point, respectively. In the mass spectra, m/z 205 is ibuprofen's precursor ion, m/z 60 is CO_3^-, and m/z 62 is NO_3^-.

Depending on the strength of any occurring discharge across multiple samples (e.g., the difference between 2 μA and 20 μA), such decreases in sensitivity can take a toll on reproducibility of single-concentration measurements, driving up standard deviations and, when generating calibration curves, impairing limits of detection (LODs) and quantitation (LOQs). Theoretically, the use of ISTDs when attempting to quantitate should prevent any occurrence of discharge from significantly affecting analyses. But when different masses exhibit different extents of sensitivity loss by nature of the discharge itself and the effects of space charge, measuring analyte/ISTD responses produces values that significantly disagree with those of non-discharging samples, further harming any attempted quantitation.

Aside from the dramatic decrease in analyte sensitivity apparent in Figure 4d, it is also important to observe the overwhelming presence of m/z 60 and 62. These masses respectively correspond to CO_3^- and NO_3^-, two ions which are produced in negative corona.[39] Expressed as a percentage of the full-MS TIC, they comprised 12.81% and 14.67% of all signal during the period of heavy discharge (~20 μA) seen over the last half of the acquisition. To a lesser extent, m/z 60 and 62 can even be seen in Figure 4c, where the weaker discharge (1-2 μA) was occurring, although they only comprised 0.44% and 1.15% of the TIC in this section. It thus follows that tracking these two specific ions in full-MS can serve as an indicator of corona discharge, providing an easily measurable means to monitor differences in discharge between samples. This tracking of ions with relation to discharge is not novel; previous experiments have utilized the discharge-driven production of ions—specifically $CH_3OH_2^+$—for similar diagnostic purposes.[36,51] While any such applications have only been performed for positive ion ESI, the tracking of CO_3^-

and NO_3^- in negative ion mode effectively served to indicate and quantify discharge where and when it occurred. Combined with the frequency of occurring discharge in a given sample set, this removed the need to visually observe samples as they spray, which was crucial when moving toward the high-throughput and automated PS-MS methods that are ideal for drug screens.

However, this ability to quantify and track corona discharge is not without its limitations. First, abrupt changes in signal due to a disruption in the normal spraying process—such as what might be seen when the Taylor cone collapses mid-acquisition or when the spray is generally unstable—can cause the measured m/z 60 and 62 signals in full-MS to artificially increase, even in the absence of the complementary increase in spray current that would definitively indicate discharge. Whereas the measurements that were performed on the mass spectra in Figure 4 were taken from each section individually, all other such discharge measurements presented here were taken across the entirety of a single acquisition; if the signal was not relatively constant throughout the acquisition, the discharge measurements rose and led to false positives. If necessary, such samples could be processed individually, but in terms of PS-MS method optimization, having information about spray stability—even if masked as potential discharge—was also useful, as samples should spray consistently between multiple trials and achieve a constant spray strength over the entire acquisition.

Second, the interpretation of these discharge measurements can only reliably be taken into consideration as a relative measure between experimental setups that differ in only one variable. Differences in terms of tip-to-inlet distance, applied voltage, and even instrumentation can affect the magnitude of these measurements. Non-discharging samples

acquired alongside the discharging sample of Figure 4 showed CO_3^- measurements close to 0%, whereas a different set of conditions on a different instrument saw non-discharging samples produce CO_3^- measurements around 0.5%. Additionally, some instruments may see background signal at the two ions observed, making those measurements less reliable. For example, the Q-Exactive Focus used in much of these experiments did not see a strong correlation between NO_3^- signal and the presence of discharge, hence why the CO_3^- signal alone was used to gauge discharge for all data presented. As will be seen, though, when used to compare similarly acquired samples, the CO_3^- discharge measurements proved indispensable.

Polyethylene Substrates

Recently reported was a negative ion PS-MS method for improved sensitivity in the detection of nitrobenzene and nitrophenol derivatives, achieved by using porous polyethylene (PE) and polyester (PES) as tip substrates.[16] To investigate its discharge-suppressing ability, PE was tested alongside paper as a PS substrate, and initial forays into this as a substrate were encouraging. As Figure 5 demonstrates, full-MS precursor ion intensities were slightly stronger and generally more precise when using methanol-washed Porex PE (7-12 μm pore size) instead of paper. This increase in signal was observed across three different sample matrices—methanol (neat), human whole blood, and bovine plasma, each containing ibuprofen and phenobarbital and spotted on paper punches—when tested with a methanol spray solvent containing ibufenac and phenobarbital-d5. Washing the tips with methanol first and allowing them to dry before use was found to increase precursor ion signal by ~2×, so it can be inferred that unwashed tips would present precursor ion intensities at about the same levels as paper tips. Additional porous PE substrates were

tested, including PE with larger pore sizes from the same manufacturer and high-density PE (HDPE) from a separate manufacturer, but none showed stronger signals than those which were obtained using the small-pore (7-12 μm) PE.

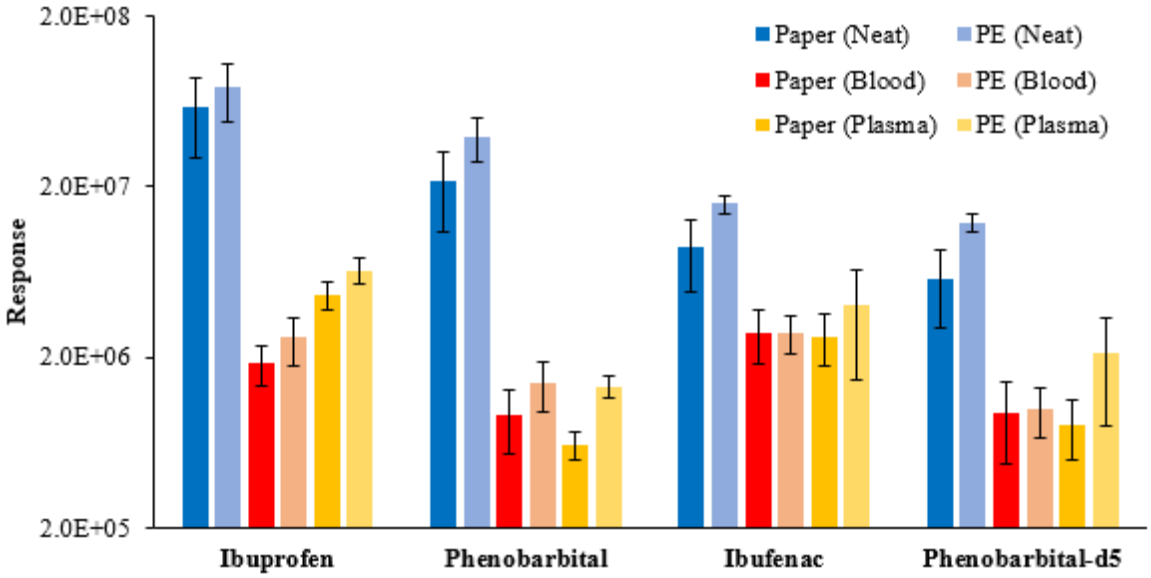

Figure 5. Full-MS precursor ion intensities for ibuprofen, phenobarbital, ibufenac, and phenobarbital-d5 sprayed from both paper and methanol-washed PE (7-12 μm pore size) tips across three different matrices (neat, human whole blood, and bovine plasma). Five replicates were run for each sample.

Continuing with the small-pore PE substrate, experiments were then performed to simulate quantitative conditions, such as what might be seen when preparing calibration curves. Phenobarbital and warfarin were tested in both neat and blood matrices at concentrations of 2000 ng/mL and 500 ng/mL, respectively, as well as at concentrations 10× greater. A constant amount of an ISTD mixture containing both ibufenac and phenobarbital-d5 was added to each sample before spotting to allow for better quantitation. All samples were sprayed at 3.5 kV with the same conventional PS solvent—95:5:0.01 methanol:water:acetic acid.

The raw MS/MS signals obtained for each of the four compounds in the most concentrated sample are shown in Figure 6. As can be seen, PE tips, though unwashed, actually saw a decrease in sensitivity that the precursor ions did not experience in full-MS.

The fact that the PE tips were unwashed is not likely to have been the cause for this decrease since the intensity of the precursor ions, and therefore the fragment ion signal, should have been approximately the same as with the paper tips; it would also fail to explain why phenobarbital-d5 in blood experienced such a drastic decrease in signal when sprayed from PE. Instead, the different experimental conditions between Figure 5 and Figure 6 were the likely cause for this loss in signal when transitioning to MS/MS. The spray solvents as well as the tip-to-inlet distances were different, and depending on how well PE sprays compared to paper, this could have affected the sensitivity.

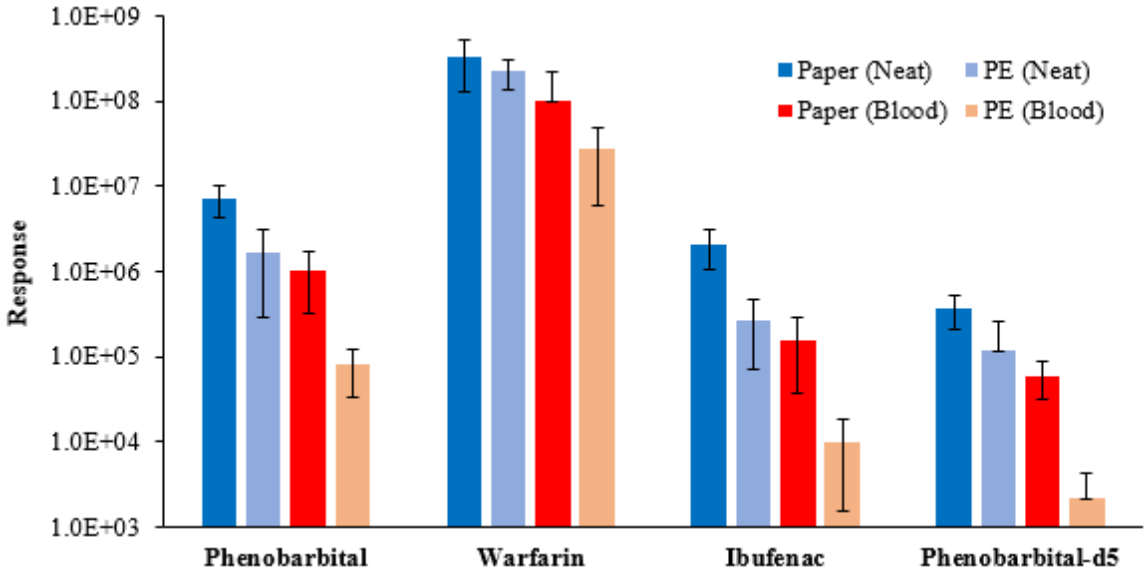

Figure 6. MS/MS fragment ion signal for phenobarbital, warfarin, ibufenac, and phenobarbital-d5 sprayed from both paper and unwashed PE (7-12 µm pore size) tips across neat and blood matrices. All samples were run in triplicate.

Furthermore, the average full-MS CO_3^- signal across all paper samples was 1.06% of the TIC, with 8 out of 18 samples manifesting some amount of discharge during the acquisition that was reflected in the recorded spray current. For PE, the average CO_3^- signal was 2.16%, with 14 out of 18 samples exhibiting high currents and visual discharge. These results would suggest that, despite the fact that a non-optimized spray solvent was used, PE was less capable than paper as a PS substrate when it came to suppressing discharge.

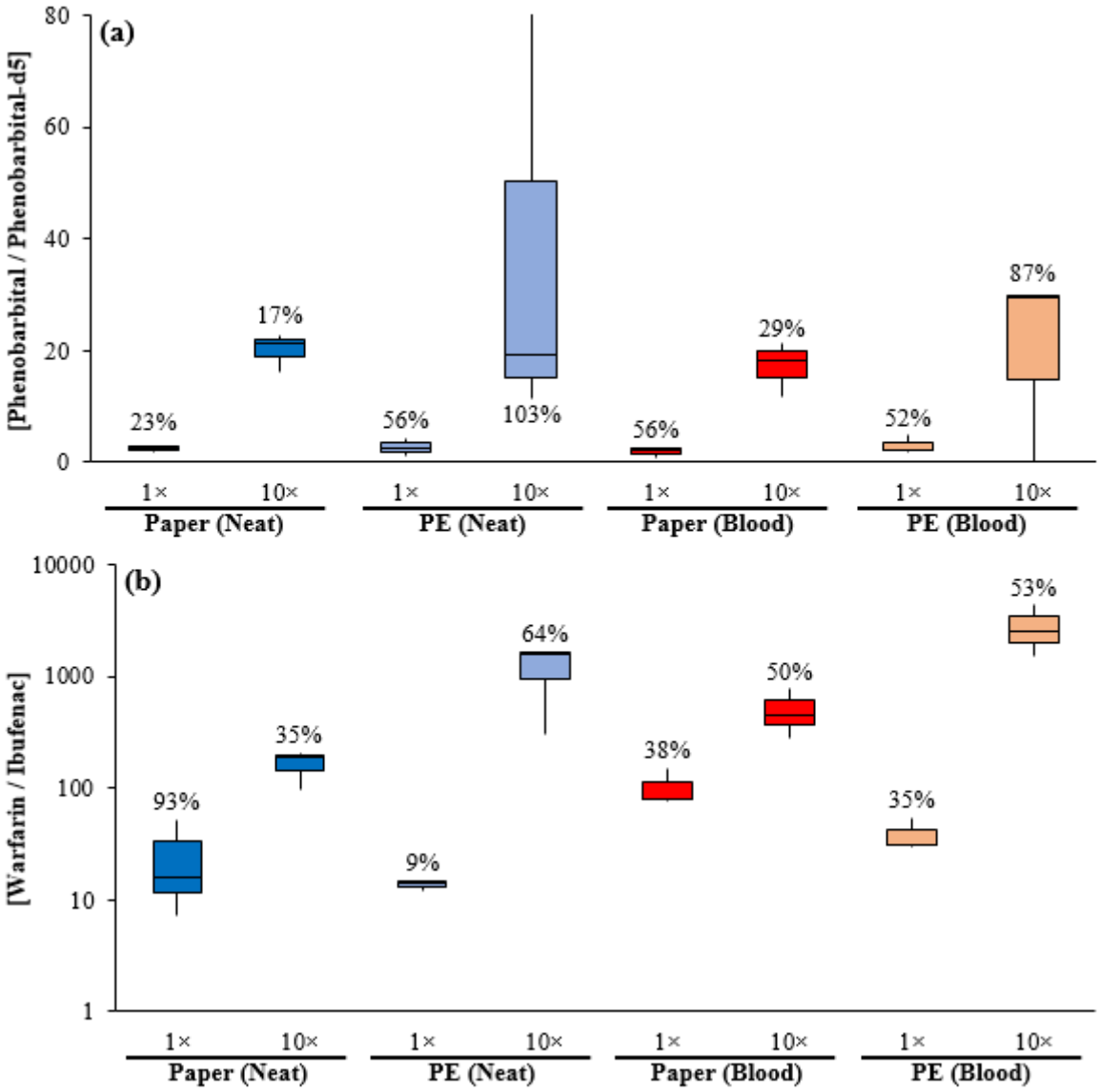

Figure 7. Ratio of analyte/ISTD signal for (a) phenobarbital and (b) warfarin at 1× and 10× their given concentrations of 2000 ng/mL and 500 ng/mL. All samples were run in triplicate; RSDs are given above or below each plot.

Figures 7a and 7b show the analyte/ISTD measurements for phenobarbital and warfarin, respectively. Phenobarbital, using an ideal SIL ISTD, saw better performance and precision spraying from paper than it did from PE, producing a narrow range of values that would in turn result in smaller errors when generating calibration curves. The largest relative standard deviation (RSD) for paper tips was at the lower concentration in blood, all others lying under 30%; RSDs from the PE tips were always above 50%, the largest

being 103%, which would hinder potential quantitation. Warfarin, on the other hand, saw less concrete differences between paper and PE in terms of RSDs. What was apparent, though, was that the warfarin/ibufenac measurements for the more concentrated sample were higher when using PE as opposed to paper, whereas the less concentrated samples were about the same. If used for actual quantitation, this would result in very steep calibration curves with a PE substrate, which would potentially correspond to increased sensitivity and lower LODs.

While the barbiturate data contradict the idea that PE provides enhanced detection in negative ion mode when used as a PS substrate, none of this is to refute the work presented by Wong et al.[16] In their paper, the authors describe two mechanisms of negative ion formation, the first of which being electron-capture ionization. They observed that the ability to detect radical anions of nitrobenzene derivatives was proportional to a given compound's electron affinity, which, with knowledge of the negative ESI circuit (Figure 2a), suggests that the flow of electrons to the PS tip may have aided the production of analyte ions. Combined with the ability of PE to accumulate electrons—more so than paper, for example, owing to its greater electrostatic charging capabilities[52]—the increased sensitivity when detecting such radical anions may have given the appearance of resolving the discharge problem when in fact it was more of an analyte-specific effect that they were observing. Additionally, and perhaps more importantly, while Wong et al. were operating at a normal tip-to-inlet distance of 5 mm, they were also working within a low voltage range, between 1.4 and 1.6 kV. They mentioned that these low voltages were what aided the second mechanism of negative ion formation—deprotonation—for the improved detection of nitrophenol derivatives, commenting that PS above 3.0 kV in negative ion

mode, even with PE and PES, showed worse sensitivities than conventional ESI precisely because of the discharge problem. And since the aim of these studies was to develop a negative ion PS-MS method specifically to suppress corona discharge under the usual 3.5-4.0 kV spraying conditions—the typical onset voltages required for proper and reliable Taylor cone formation which would allow for maximal sensitivity without having to rely on the vacuum of the MS for ionization[53]—alternative substrates alone were not the best avenue to approach such optimization.

Furthermore, it is important to note that in spite of what potential advantages PE may confer over paper when it comes to deprotonation and subsequent fragmentation, additional studies would be needed to optimize the specific substrate, examining in greater detail the effects and limitations of pore size. The PE substrate used most often here was one with a small pore size (7-12 μm). While this was easily cut into sharp tips, biofluids such as blood could not soak into it and would only bead up on the surface, preventing samples from being spotted directly onto the substrate; thick matrices had to first be spotted onto chromatography paper punches through which the spray solvent would travel before the substrate, such mixing of substrates potentially confounding results. Conversely, PE substrates with larger pore sizes (15-50 μm) were permeable to thick matrices like blood and were capable of being spotted, but they produced tips which were more prone to abrasive damage due to the less compact nature of the material. As such, the tips were more likely to have lost any semblance of being sharply pointed through handling or even the cutting process alone. This in turn generated microstructures at the tip which were small enough to see elevated electric fields beyond that which a single, sharp point would have produced, increasing the likelihood for discharge to occur and leading to more erratic and

unpredictable spraying. Because of this pore size dilemma when using PE as a PS substrate—combined with the poor quantitation demonstrated by it and the ready availability of paper-based cartridges for the automated Velox 360 PS-MS source—paper was used as the substrate for the remainder of the tests in the development of a negative ionization method to avoid discharge.

Resistor-Aided Negative Ion Spray

Before optimizing the solvent, another method of discharge suppression was investigated, which was the inclusion of a 10-GΩ resistor in the high voltage line supplying the PS cartridge.[47-49] In a normal ESI circuit, the air gap through which the solution sprays is the only effective resistor; when discharge occurs, this component breaks down into a conductor, resulting in the noticeable rise in spray current. By including a 10-GΩ resistor as a discrete component in the circuit before the tip, a backup resistor is established that can maintain a consistent current even if the air gap begins to break down, circumventing discharge entirely. This was observed by the fact that discharge could not be induced at short gap lengths or at applied voltages up to 8 kV, although voltages between 5 and 6 kV had to be used to initiate the electrospray process in the first place. As described earlier, the applied voltage and the tip-to-inlet distance are two of the most troublesome factors when trying to avoid discharge, so the ability to operate comfortably within a larger working range of voltages and over a more variable gap length allows for a greater amount of flexibility when it comes to optimizing a negative ion PS-MS method.

Due to this impressive discharge suppressing ability, initial tests incorporating the resistor were performed to measure MS/MS signal, recovery, and ion suppression relative to a PS-MS setup excluding the resistor, all on manual cartridges. Stable sprays were

achieved in the latter setup by using a pure methanol solvent base on well-cut paper tips at 4.0 kV, achieving an average full-MS CO_3^- signal of 0.5% among those samples which did not exhibit discharge. The raw signals obtained for each of the five compounds tested—three analytes (ibuprofen, phenobarbital, and furosemide) at 10 µg/mL in the spotted sample and two ISTDs (ibufenac and phenobarbital-d5) at 1 µg/mL in the spray solvent—in both neat and human whole blood matrices are shown in Figure 8. As can be seen, use of the resistor saw a slight decrease in signal, but never by more than a factor of 2, demonstrating comparable sensitivity which could potentially be improved by optimizing the applied voltage. Discharge was never visually observed in any of the resistor-employing samples, with the measured full-MS CO_3^- signal never rising above 0.5% in those that saw constant TIC. However, because of the inability to easily incorporate the resistor into the electronic system of the Velox 360 PS source (see Future Work), it was not used for the optimization of a negative ion PS-MS method.

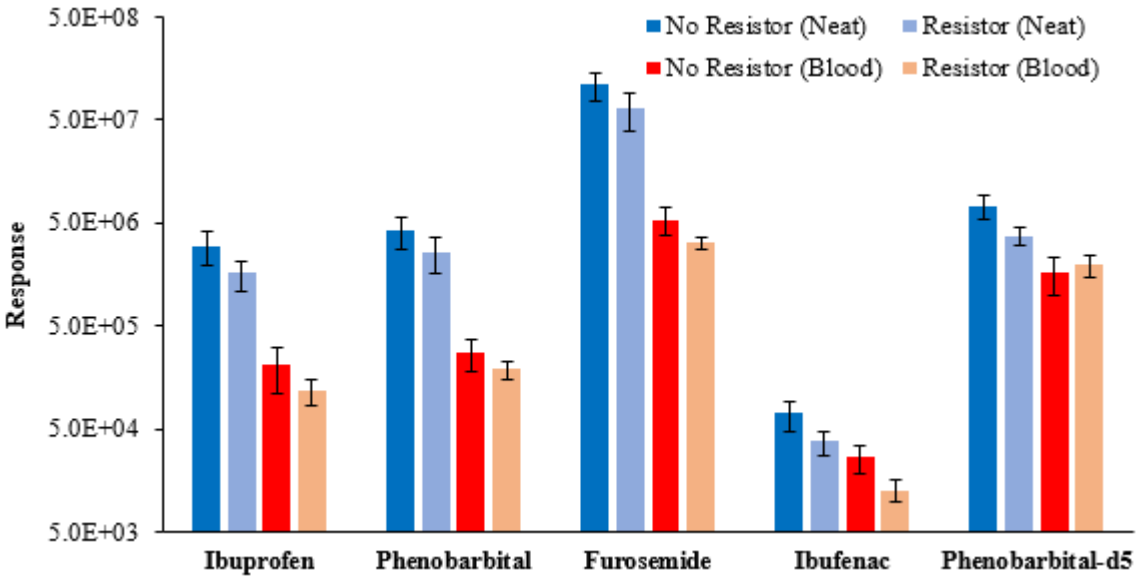

Figure 8. MS/MS fragment ion signal obtained for each of the five compounds in neat and whole blood matrices with and without use of the 10-GΩ resistor in the PS-MS circuit. Five replicates were run for each sample.

Discharge Susceptibility in Velox Sample Cartridges

To prepare for automation of PS-MS and eventual use of the Velox 360 PS source for the negative ion drug screen, a solvent composed of methanol with 0.01% NH_4OH was used in spraying samples from both the manual cartridges with paper tips (Figure 3a) and the VSCs (Figure 3b), comparing both the discharge susceptibility between the two types of cartridges and the resulting analyte MS/MS signal. Samples containing several analytes—ibuprofen at 10000 ng/mL, naproxen at 30000 ng/mL, furosemide at 1000 ng/mL, and three barbiturates, amobarbital, butabarbital, and butalbital, each at 500 ng/mL—were tested in both neat and whole blood matrices.

The raw MS/MS signals obtained for these six analytes' fragment ions are shown in Figure 9. Although the VSCs appeared to outperform the manual cartridges in a neat matrix, it should be noted that the spotting method for the latter only used 3.5 μL of sample while the former used 12 μL of sample, so the signal strength was comparable between the different cartridges overall. In spite of this, however, the barbiturates saw barely equivalent or lower signal, an effect more pronounced in blood. Samples diluted down to one-third and one-ninth of the screening cutoffs (see Table 1) produced similar trends in signals, but the barbiturates present in blood at 56 ng/mL were not detected at all when sprayed from the VSCs.

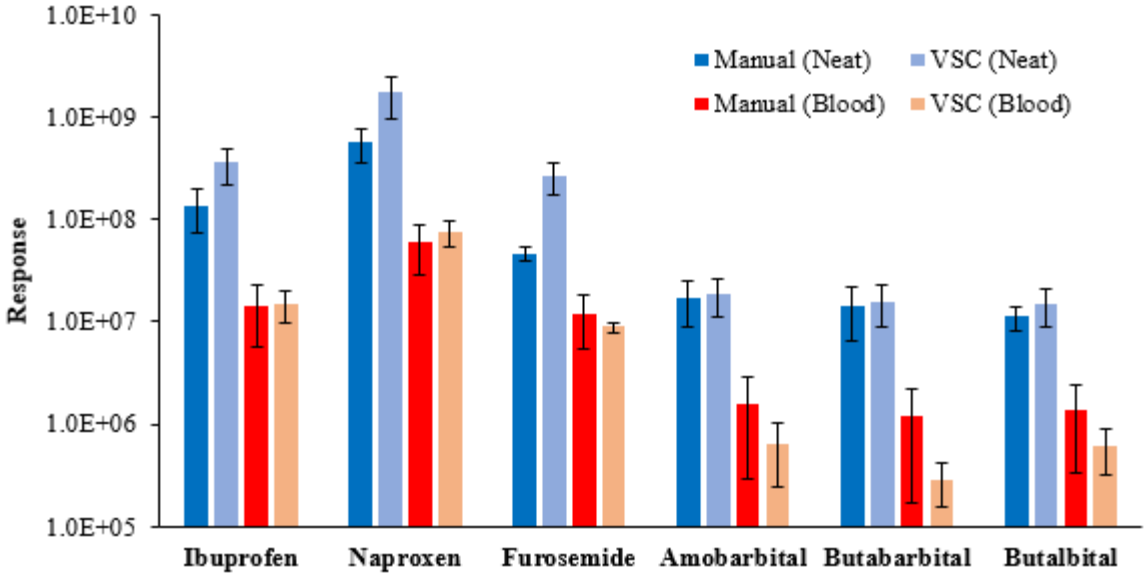

Figure 9. MS/MS fragment ion signal for ibuprofen (10000 ng/mL), naproxen (30000 ng/mL), furosemide (1000 ng/mL), amobarbital (500 ng/mL), butabarbital (500 ng/mL), and butalbital (500 ng/mL) in both neat and blood matrices, sprayed from manual cartridges and VSCs. All samples were run in triplicate.

One potential reason for lower signals may have been that the manual cartridges were sprayed at 4.0 kV while the VSCs were sprayed at 3.5 kV; the voltage had to be lowered by 500 V to accommodate the sharper paper tips in the VSCs, otherwise they would have only produced constant discharge. However, as can be seen in Table 2, discharge was still observed in both types of cartridges, even with a solvent base of pure methanol. The manual cartridges saw 14 of 36 samples discharge during acquisition, producing an average CO_3^- signal of 0.89%; those samples which did not discharge generated an average CO_3^- signal of 0.10%. The VSCs demonstrated a higher average CO_3^- signal of 2.19%, with 26 of 36 samples discharging during the spraying process.

Table 2. Experimental parameters and discharge diagnostic data for manual cartridges and VSCs.

Cartridge Type	Manual		VSC		VSC	
Velox Source	No		No		Yes	
Voltage [kV]	4.0		3.5		3.5	
Solvent [µL]	60		120[a]		142[b]	
Matrix	Neat	Blood	Neat	Blood	Neat	Blood
No. of Samples	18	18	18	18	18	17
No. Discharged	9	5	8	18	10	13
CO_3^- Signal [%]	0.93	0.85	2.22	2.16	0.81	8.15

[a]10 µL onto dried sample followed by 110 µL into the well of the VSC
[b]12 µL onto dried sample (in 3-µL increments with delays (in seconds) of 24,2,2,2) followed by 130 µL into the well of the VSC (in 10-µL increments, all with delays of 2 seconds)

Even though a lower voltage was used, a curious effect was observed with the VSCs wherein they frequently exhibited discharge only in the moments before the Taylor cone was established, spraying normally after that point. These quick discharges occurred in 22 of the 26 VSCs that discharged, leading to a range of full-MS CO_3^- signals between 0.01% and 10.24% depending on the length of the latent period before proper Taylor cone formation. The middle half of this distribution, though, saw more representative CO_3^- signals between 0.17% and 1.00%. While this wide spread of measurements may have artificially raised the amount of discharge measured in the VSCs, the fact that they discharged at all, even if only briefly, may explain the small drop in MS/MS signal. This phenomenon was also observed in some of the manual cartridges, although not nearly with the same frequency of occurrence and with a much weaker, more predictable effect on CO_3^- signal.

Using the same solvent system of methanol with 0.01% NH_4OH, the VSCs were also tested at 3.5 kV using the Velox source. This was done primarily to investigate the effects of both the solvent application via the source's pump programming and the inability to manually set the tip-to-inlet distance. Since the solvent base was purely organic, large delays had to be incorporated into the pump programming to avoid excessive solvent

evaporation before sample acquisition. A delay of 24 seconds was used before the first application of solvent to the dried sample, followed by 2-second delays for the remaining solvent dispensations. The tip-to-inlet distance, as already described, largely influences the strength of the electric field at the tip, which in turn influences discharge susceptibility; by utilizing the automated Velox source for PS-MS and positioning it up against the rim of its mounting flange, control over this variable is relinquished. Such lack of control can be desirable as it allows for easier automation without user expertise, but it is also troublesome because being able to set the gap length is one of the few immediate ways of controlling discharge in negative ESI studies, hence the need to quantify the discharge experienced when using the PS source.

The discharge exhibited by these fully automated VSC tests is reflected in Table 2. On average, neat samples saw less severe but more frequent discharge than the non-automated VSCs, but the discharge in blood samples was much more significant with an average CO_3^- signal of 8.15%. While the pre-cone discharge that plagued the non-automated VSCs was still observed with a similarly large range of discharge measurements, its frequency of occurrence was much lower, limited to only 4 of the 23 samples that discharged. And compared to the analyte MS/MS signal obtained without automation (Figure 9), the only appreciable and negative difference from automated spraying was seen in the blood samples owing to the more intense discharge they experienced.

Spray Solvent Optimization

When optimizing the spray solvent for PS-MS in negative ion mode, it was imperative to recognize that water should be excluded from the system entirely. The reason

for this is that including water increases the surface tension of the resulting mixture, which then requires higher onset voltages and field strengths to induce proper electrospray because stronger Coulombic forces are necessary to overcome the larger cohesive forces holding the solvent together.[36,54] However, the onset of corona discharge occurs at the same field strength regardless, so the onset voltage for electrospray of a water-containing solvent sits closer to levels that will only produce discharge, creating a very small window of operating voltages in which electrospray can occur without discharge; pure water solvents genuinely never see a stable electrospray without the presence of corona discharge, even in positive ion mode.[36] By only utilizing organic solvents as the base and adding trace amounts of modifiers as needed, the surface tension and, in turn, the onset potential for electrospray are kept low to maximize the range of operating voltages for stable spraying without incurring corona discharge.

As can be gathered from Table 2, it was apparent that despite the solvent base being pure methanol, discharge was still problematic for both manual cartridges and VSCs, especially so when automating the latter on the Velox PS source. Lowering the voltage further to 3.3 kV appeared to alleviate discharge and allow for consistency between samples, but the same experimental conditions on a different day saw constant discharge in every sample. This probably occurred because the applied voltage was close enough to the onset potential for corona discharge that slight day-to-day variances in operating parameters were significant—a more robust approach was clearly required. Electron-scavenging cosolvents, which actively suppress discharge by raising the onset potential at which it occurs, were turned to next. To this end, chlorine-containing solvents—primarily carbon tetrachloride (CCl_4)[2,45,46]—were paired with methanol and the discharge-

suppressing abilities of the resulting mixtures were investigated, with the results presented in Figure 9 and Table 2 serving as a baseline for measuring success in this regard. Chloroform ($CHCl_3$) was also tested as a potential cosolvent, but the discharge suppression it offered was not as strong as that of CCl_4, so only the latter was used in the solvent optimization.

Initially, solvents containing varying amounts of CCl_4—between 0.01% and 10%, with the rest of the solvent being composed of methanol and 0.01% NH_4OH—were tested against each other to gauge how much CCl_4 would be required to adequately suppress discharge. Run on manual cartridges with neat samples at 3.3 kV, the distributions of discharge measurements from these solvents are shown in Figure 10. Since a lower voltage was used than in Table 2, the spray solvent with no CCl_4 saw smaller measured amounts of discharge. The frequency of samples that discharged with this solvent, however, was still the same, with every other sample exhibiting discharge at some point during the acquisition.

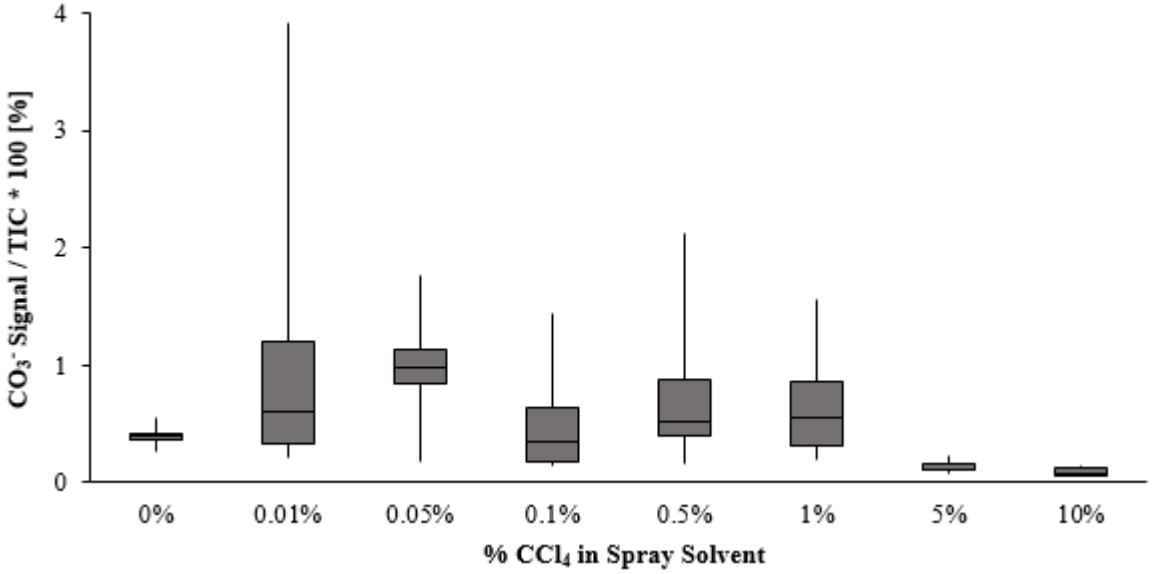

Figure 10. Full-MS CO_3^- measurement distributions for spray solvents containing different amounts of CCl_4. The remaining solvent consisted of methanol with 0.01% NH_4OH, spraying from neat samples on manual cartridges at 3.3 kV. Eight replicates were run with each spray solvent.

As can be seen, utilizing lower amounts of CCl_4 appeared to worsen the reproducibility between samples. While they generally saw a progressive decrease in the lower limit of the CO_3^- measurements, their average discharge measurement was higher than when CCl_4 was excluded from the solvent entirely. However, when CCl_4 was included at levels as high as 5% or 10%, the discharge suppression became readily apparent, generating average full-MS CO_3^- signals of 0.13% and 0.09%, respectively. Some of the samples tested with these two solvents did discharge, but those arose mainly from a lack of solvent rather than genuine spray instability, discharging only at the end when the spray solvent on the paper tip ran dry and the Taylor cone collapsed. To maintain good discharge prevention capabilities at applied voltages up to 4.0 kV, 10% CCl_4 was used for the remainder of the tests instead of 5% CCl_4.

When transferred to VSCs spotted with blood and run using the Velox 360 PS source (3.5 kV onset voltage, 142 μL of solvent), the capability of the 10% CCl_4 solvent in suppressing discharge became even more pronounced. Compared to the 8.15% CO_3^- signal seen in blood with a CCl_4-excluding solvent (Table 2), the 10% CCl_4 solvent's CO_3^- signal never rose above 0.01% across 29 samples, averaging out at 0.00%. Furthermore, none of the samples saw spray currents >1 μA, indicating that the solvent with 10% CCl_4 (90:10:0.01 methanol:CCl_4:NH_4OH)—when applied as 12 μL onto the DBS via pump A and 130 μL into the VSC well via pump B with appropriately set timing delays in the pump programming to avoid evaporation—was able to entirely prevent discharge over spraying times of at least 72 seconds, establishing it as the optimized solvent for negative ion PS-MS.

To highlight the effects of optimizing the solvent to include CCl_4 as a significant component, Figure 11 shows the amount of discharge (measured via CO_3^- signal) encountered compared to two other solvents—100:0.01 methanol:NH_4OH and 95:5:0.01 methanol:water:acetic acid—across 35 VSCs sprayed at 3.5 kV from the Velox 360 source. While methanol was able to lower the average discharge measured, it did not prevent all discharge, leading to some measurements >1%. When 10% CCl_4 was added to the solvent, all discharge measurements were <0.05% except for 2 of the 35, which still lay <0.5%. These exceptions were likely caused by imperfections on the VSCs' paper tips; if excluded, the distribution of discharge measurements for the optimized solvent would be narrower and the average would be shifted down. Nonetheless, the difference in discharge measurements provided by the optimized solvent as opposed to the methanol solvent was verified with a heteroscedastic t-test, where the former produced lower CO_3^- measurements with 95% confidence. Compared to the conventional solvent, it produced less discharge with >99% confidence.

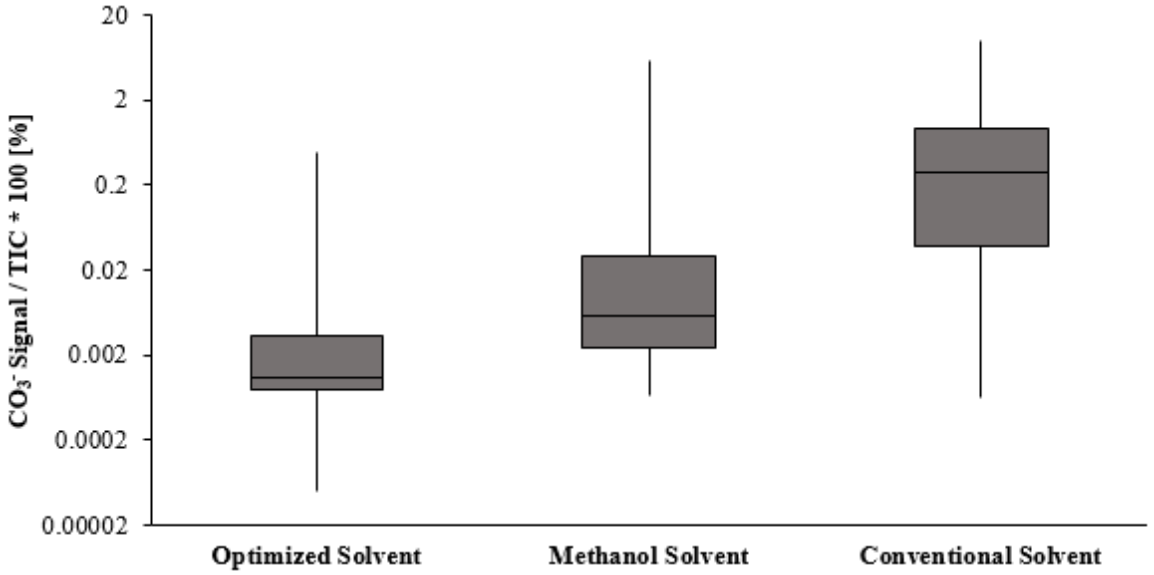

Figure 11. Comparison of discharge measurements between the optimized solvent (90:10:0.01 methanol:CCl_4:NH_4OH), a methanol solvent (100:0.01 methanol:NH_4OH), and a conventional PS solvent (95:5:0.01 methanol:water:acetic acid), all run at 3.5 kV on the Velox 360 source. 35 replicates were run with each spray solvent.

These same three solvents were also used to compare the precision of analyte/ISTD measurements between 30 VSCs spotted with blood samples containing hydrochlorothiazide, phenobarbital, and pentobarbital—all at their screening cutoffs (see Table 1) or lower—as well as the ISTDs ibufenac (for hydrochlorothiazide) and phenobarbital-d5 (for phenobarbital and pentobarbital). The distributions of these measurements are shown in Figure 12, with the optimized solvent prominently displaying lower RSDs for each drug. While the precisions of the other two solvents are not as important to take note of, it is worth drawing attention to the poor performance of barbiturates when sprayed with the methanol solvent compared to the conventional solvent; this was due to phenobarbital-d5 not being detected in many of the samples sprayed with methanol, subsequently returning values of zero for the phenobarbital/pentobarbital measurements. Regardless, the optimized solvent outperformed both of the other solvents at a single concentration.

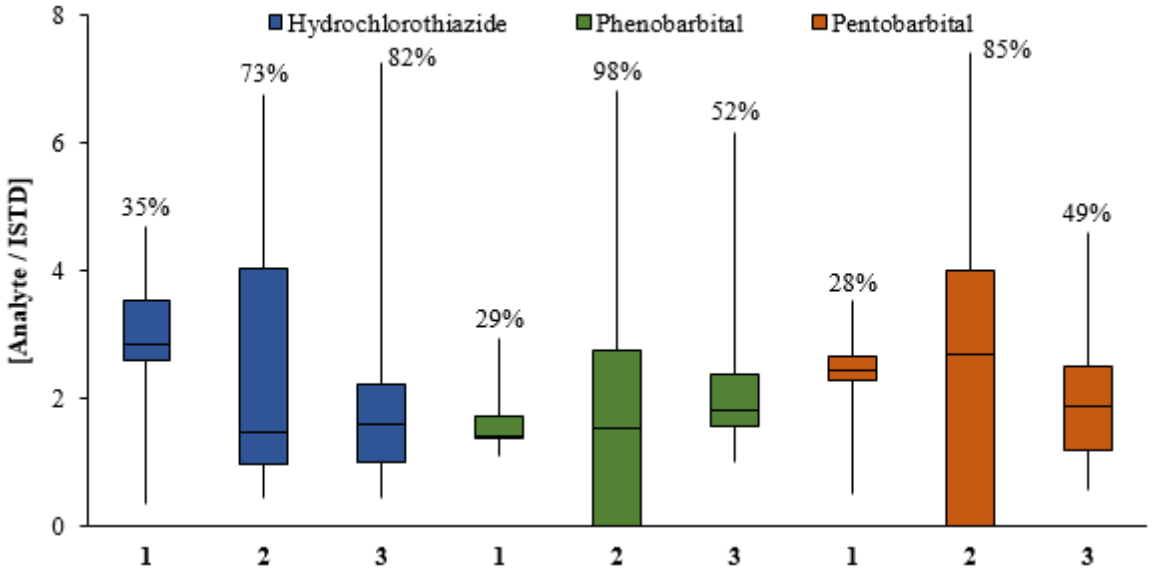

Figure 12. Ratio of analyte/ISTD signal for hydrochlorothiazide, phenobarbital, and pentobarbital acquired using (1) the optimized solvent (90:10:0.01 methanol:CCl_4:NH_4OH), (2) a pure methanol solvent (100:0.01 methanol:NH_4OH), and (3) a conventional PS solvent (95:5:0.01 methanol:water:acetic acid). 30 replicates were run with each solvent; RSDs are given above each plot.

To further test the quantitative capabilities of the optimized solvent, phenobarbital and warfarin were sprayed from manual cartridges at 3.5 kV in a similar manner to what was shown in Figure 7, this time comparing the solvent to a conventional one (95:5:0.01 methanol:water:acetic acid) using only paper tips. The results of these analyte/ISTD measurements in blood samples are shown in Figure 13. Through the three replicates that were tested at each concentration, the optimized solvent saw better RSDs in all but phenobarbital at 20000 ng/mL (10×), demonstrating its potential for more reliable quantitation, especially around lower concentrations.

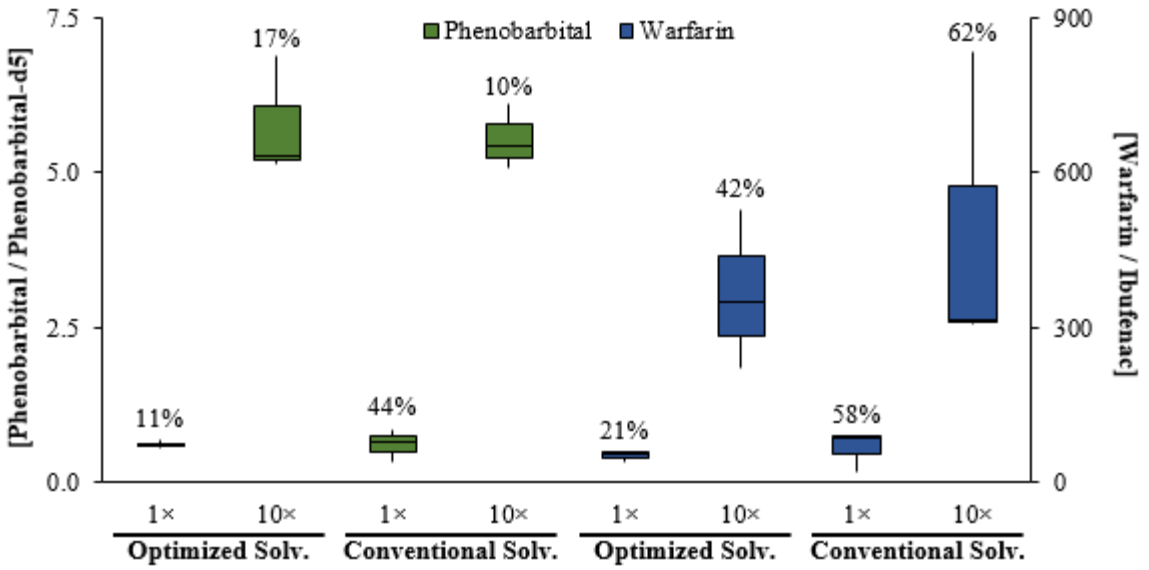

Figure 13. Ratio of analyte/ISTD signal for phenobarbital and warfarin at 1× and 10× their given concentrations of 2000 ng/mL and 500 ng/mL in blood, sprayed using the optimized solvent (90:10:0.01 methanol:CCl_4:NH_4OH) and a conventional solvent (95:5:0.01 methanol:water:acetic acid). All samples were run in triplicate; RSDs are given above each plot.

Additionally, through the inclusion of 10% CCl_4 in the spray solvent, the onset potential of corona discharge for the VSCs on the Velox source was effectively pushed up, allowing access to a greater range of operating voltages for normal, discharge-free ESI. At 4.0 kV—a voltage that caused nothing but constant discharge with a pure methanol solvent and generated full-MS CO_3^- measurements >25%—the optimized solvent succeeded at completely preventing discharge; of 20 blood-spotted VSCs that were tested at this heightened voltage, none saw discharge-level spray currents and all produced CO_3^- discharge measurements <0.1%. Paired with the strategy of setting large delays in the Velox 360 pump programming for dispensing 142 µL of solvent, this 90:10:0.01 methanol:CCl_4:NH_4OH solvent at 4.0 kV was treated as the fully optimized method for negative ion mode and as such was used for the negative ion PS-MS drug screen.

Negative Ion Drug Screen

The calibration curves generated from the negative ion drug screen are summarized in Table 3, with those of the barbiturates shown in Figure 14. As can be seen, with the exception of pentobarbital, the barbiturates performed well in this optimized negative ion PS-MS method, generating R^2 values >0.95 and relative errors in slope <7%. The likely limiting factor as regards their calculated LODs was the screening cutoff concentration used as the lowest calibrant (see Table 1); the selective and sensitive power of the Q-Exactive Focus mass spectrometer could potentially allow for even lower concentrations to be used and reliably detected in the calibration series, driving LODs down further. Altogether, these data indicate the success of utilizing phenobarbital-d5 not only as an ISTD, but as a general ISTD for all heterocyclic imides or structurally similar compounds.

Table 3. Calibration curve data for each analyte from the negative ion drug screen. Screening cutoffs can be found in Table 1.

Analyte	ISTD	LOD [ng/mL]	Rel. Error in Slope [%]	R^2
Butabarbital	Phenobarbital-d5	229	3	0.99
Butalbital	Phenobarbital-d5	263	4	0.98
Amobarbital	Phenobarbital-d5	321	5	0.97
Pentobarbital[a]	Phenobarbital-d5	1821	26	0.52
Phenobarbital	Phenobarbital-d5	502	4	0.98
Secobarbital	Phenobarbital-d5	286	4	0.98
Thiopental	Phenobarbital-d5	1100	4	0.98
Phenytoin	Phenobarbital-d5	919	7	0.95
Salicylic acid	Ibufenac	8572	7	0.94
Valproic acid	Ibufenac	24315	35	0.38
Levetiracetam	Ibufenac	8338	30	0.46
Ibuprofen	Ibufenac	3997	29	0.48
Naproxen	Ibufenac	3010	22	0.62
Hydrochlorothiazide	Ibufenac	130	9	0.90
Warfarin	Ibufenac	674	10	0.89
Furosemide	Ibufenac	1370	10	0.89
Tadalafil	Ibufenac	187	14	0.81
Ethyl sulfate	Ibufenac	125	9	0.90
Ethyl-beta-D-glucuronide	Ibufenac	461	34	0.41

[a]Run in a separate set of samples, the calibration curve for pentobarbital had a relative error in slope of 8% and an R^2 value of 0.94, generating a detection limit of 561 ng/mL

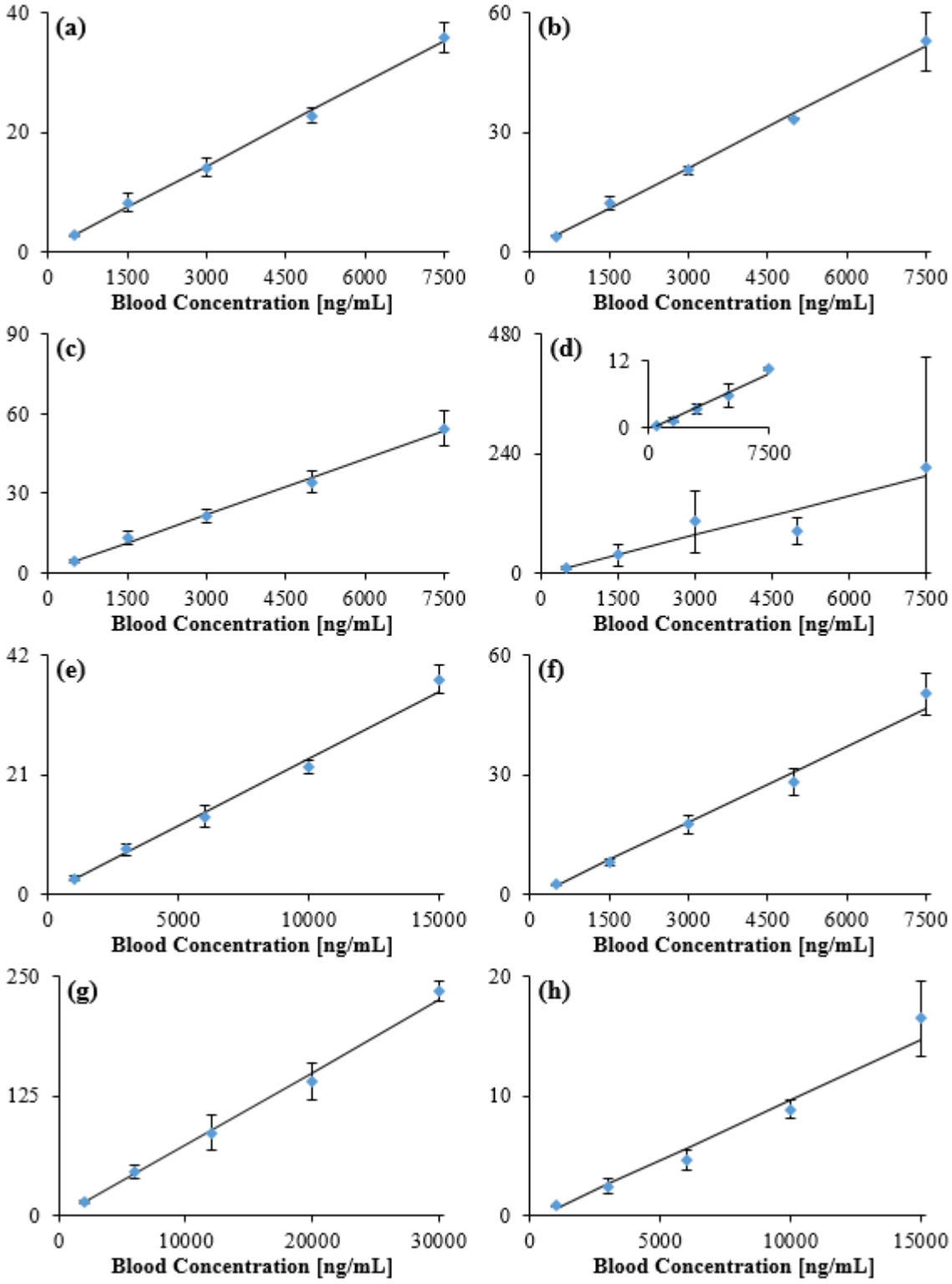

Figure 14. Calibration curves for (a) butabarbital, (b) butalbital, (c) amobarbital, (d) pentobarbital, (e) phenobarbital, (f) secobarbital, (g) thiopental, and (h) phenytoin. The y-axes are the ratio of the respective fragment ion signal to that of phenobarbital-d5, and each point is the average of three replicates of these measurements. Inset in (d) is a calibration curve for pentobarbital run from a different set of samples.

Comparatively, pentobarbital appeared to perform very poorly, owing largely to an exaggerated heteroscedastic effect observed in the analyte/ISTD measurements—the spread of the data at higher concentrations was noticeably disproportionate to the spread of the data at lower concentrations. Because of the poor quality of the calibration curve, the calculated LOD was almost 4× the screening cutoff of 500 ng/mL. While far from perfect, these results may simply be chalked up to poor individual data acquisitions rather than an incapability of the method in detecting pentobarbital for a number of reasons. First, there were no issues with detecting it at the screening cutoff, and it was not detected in the blank matrix at all. Secondly, amobarbital, which is a structural isomer to it and even fragments into the same daughter ion (Table 1), failed to see such shortcomings with its quantitative performance (Figure 14c). Thirdly, the other barbiturates which were present in the sample with pentobarbital—phenobarbital, secobarbital, thiopental, and phenytoin—did not appear to suffer from poor quantitation, indicating that the measured phenobarbital-d5 signal was not the source of the problem. And lastly, previous experiments using the same calibration series and data processing procedure saw significantly improved pentobarbital quantitation, as indicated after Table 3 and in the calibration curve inset in Figure 14d—the only difference was that a greater amount of ISTD was used. These reasons suggest that further experiments would likely not encounter this anomaly again.

Those analytes which used ibufenac as an ISTD saw generally worse performance in the drug screen than the barbiturates. While some of these compounds—namely salicylic acid, hydrochlorothiazide, warfarin, furosemide, tadalafil, and ethyl sulfate—saw adequate quantitation with relative errors in slope <15%, the rest displayed no ostensibly linear trend in the data. For example, ibuprofen, for which ibufenac was a direct structural analog and

therefore a theoretically acceptable ISTD, failed to produce any semblance of reliable quantitation, generating the calibration curve seen in Figure 15 with a relative error in slope of 29% and an R^2 value of 0.48.

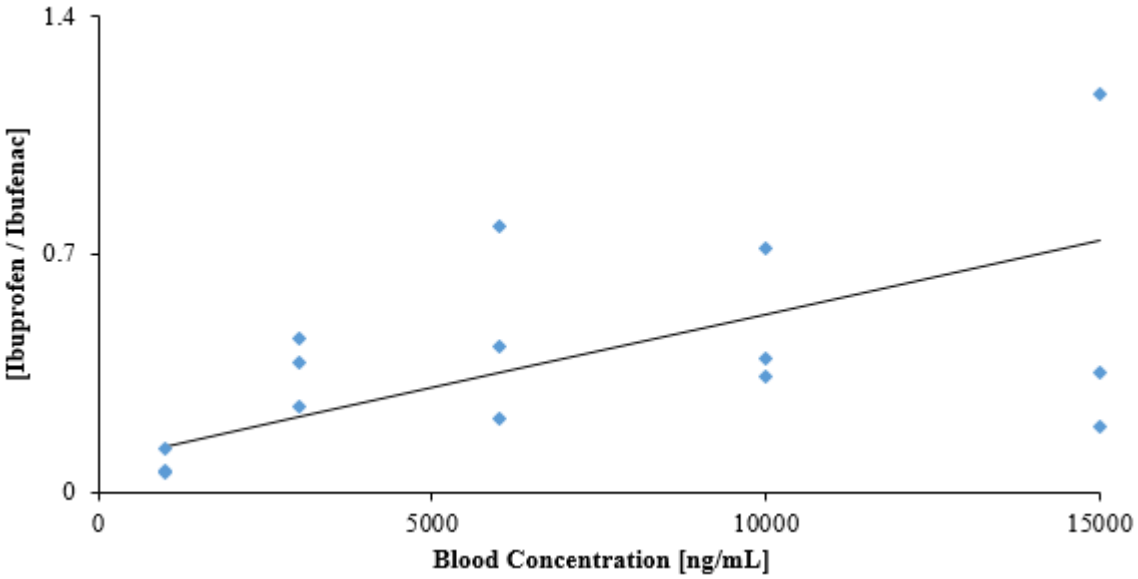

Figure 15. Calibration curve for ibuprofen in blood samples.

Most of the drugs that exhibited such poor quantitation did so either because the MS/MS signal did not noticeably change with concentration or because there was a high background signal in the matrix that obscured any true signal. As can be seen in Figure 16a, ibuprofen was not significantly detected in the blank matrix, but its signal effectively did not change over the concentration range tested. This may be a limitation of the method in that it cannot quantitatively detect such low concentrations of ibuprofen, requiring larger, more toxicologically relevant concentrations to obtain satisfactory calibration (see Future Work). Levetiracetam, on the other hand, saw high MS/MS signal in the blank matrix at about the same level as the calibration samples, as shown in Figure 16b; ethyl-beta-D-glucuronide, a metabolite of ethanol, experienced a similar problem. Ethyl sulfate, another ethanol metabolite, saw background signals as well, but they were not high enough to interfere with those generated by the calibration samples, leading to its acceptable

quantitation and the conclusion that it rather than the glucuronide may be better suited for biomonitoring of ethanol use.

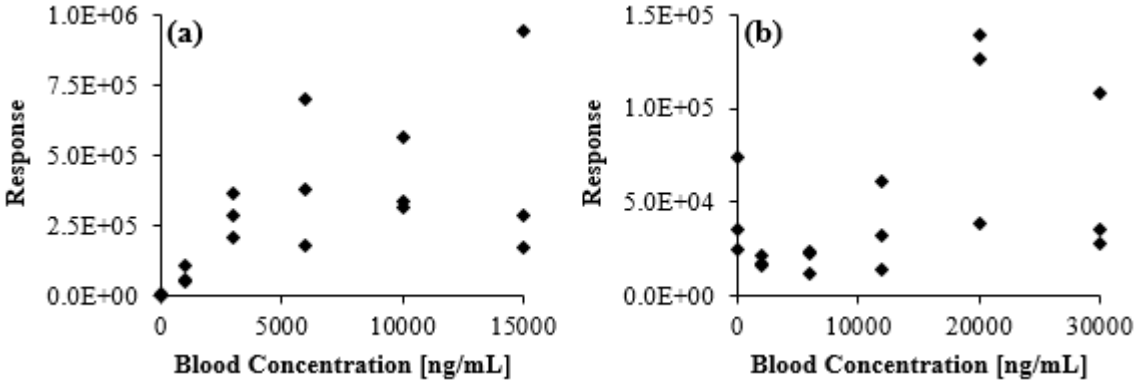

Figure 16. Raw MS/MS signal for (a) ibuprofen and (b) levetiracetam in the matrix blanks and calibration samples.

These high backgrounds at some of the observed fragment ions combined with the fact that certain compounds did not fragment well in the first place—valproic acid, for instance, did not fragment at all, so its precursor ion had to be used for all MS/MS measurements—suggests that the non-barbiturate side of the drug screen itself requires further optimization beyond just the negative ionization aspect of the method. Regardless of these poor calibration curves, though, the optimized method for PS-MS in negative ion mode was, if nothing else, demonstrated in the successful quantitation of barbiturates as well as several other acidic analytes.

Future Work

While including 10% CCl_4 in the spray solvent was shown to generate stable and reproducible sprays in negative ion mode, there are several drawbacks to its application outside of research, chief among those being that it is classified as an ozone-depleting substance under the Montreal Protocol as part of the Vienna Convention for the Protection of the Ozone Layer[55] and is regulated as such. Additionally, its acute toxicity poses not-

insignificant safety hazards to the user when aerosolized—it can metabolize and thermally degrade into phosgene, for example[56,57]—and it is considered a possible carcinogen by the International Agency for Research on Cancer (IARC).[58] And when processing a large number of samples that require bulk amounts of spray solvent—with the compound in question comprising 10% of it—there is an economic factor to be considered, which is made more dramatic when used for PS-MS, which is noted for its use of inexpensive materials designed for affordable replicate sampling.

Future research into bettering the performance of negative ion PS-MS could explore the inclusion of other analytes in the spray solvent that are not as regulated or hazardous as CCl_4 and can more efficiently suppress corona discharge, potentially requiring amounts totaling to less than 10% of the solvent volume. One such compound is 7,7,8,8-tetracyanoquinodimethane (TCNQ), which has an electron affinity of 2.8 eV.[59] Compared to the 0.8 eV electron affinity of CCl_4,[60] this suggests that it may act as a better and more efficient electron scavenger, further increasing the range of operating voltages that can be accessed in negative ion mode without seeing discharge. TCNQ has already been shown to generate reproducible negative ion sprays at higher-than-usual onset voltages with a solvent base of 98:2 acetone:acetonitrile,[44] indicating that it may be useful for further optimization of negative ion PS-MS.

Along these lines, other organic-soluble analytes with electron affinities >0.8 eV would be worthwhile to examine with respect to their discharge-suppressing capabilities. Another compound that might be useful in this regard is hexachloroethane, C_2Cl_6. Not regulated by the Montreal Protocol, this would follow in the veins of previous research into the use of chlorine-containing solvents for negative ESI.[2,45,46] While its precise electron

affinity is not confidently known and its chlorine content is about the same as $CHCl_3$, the larger amount of chlorine atoms alone may give it an advantage over CCl_4 in terms of its ability to suppress discharge. However, C_2Cl_6 is also classified as possibly carcinogenic to humans by the IARC[58] and has its own toxicity-related hazards, so its utility in negative ion PS-MS may need to be weighed against the associated safety risks.

In terms of the solvent base, different organic solvents could be tested to measure how well they suppress discharge and support analyte MS/MS signal. Isopropanol was briefly tested in this regard, and while its use as a solvent with 0.01% NH_4OH showed a decrease in full-MS precursor ion signals compared to a pure methanol solvent, a 50:50 mixture of methanol:isopropanol actually showed slightly improved sensitivity for certain MS/MS fragment ions when performing automated PS-MS. Furthermore, the CO_3^- discharge signal in this 50:50 methanol:isopropanol solvent was found to be less severe than when using a pure methanol solvent, with discharge occurring less frequently as well. It did not reach near the levels of discharge suppression that were achieved through the inclusion of 10% CCl_4 in the spray solvent (Figure 10 and Figure 11), but it may be worthwhile to investigate further to potentially lessen the amount of CCl_4 required to sufficiently quench the discharge problem.

Non-conventional substrates—not just PE—could also be further tested in the development of a negative ion PS-MS method. Initial experiments on the small-pore PE and paper using the optimized solvent did not see much of a change in quantitative capabilities compared to what was seen in Figure 7, but resolution of the pore size dilemma may prove otherwise. Additionally, as mentioned earlier, only operational voltages above 3 kV were used in these experiments, so lower voltages could be tested to determine if it

can prevent discharge as much as or more effectively than the optimized solvent and if it can achieve sensitivities and accurate quantitation for target compounds such as barbiturates in negative ion mode, for which the information contained in Table 3 will prove invaluable.

In light of the data shown for the inclusion of a 10-GΩ resistor in series with the high voltage line supplying the PS process, the technique to avoid discharge when operating in negative ion mode seemed to work without negatively affecting sensitivity. However, bearing in mind the desire to automate PS-MS, a major impediment to furthering this as an avenue of discharge suppression is that the required resistor modification would have to be a manufacturer-end addition. There are numerous ways this additional resistance could be worked into the current model of the Velox 360 PS source: inclusion in the source itself with a switch that can be flipped on or off depending on whether or not negative ionization is occurring; permanent incorporation into the circuitry in the source with the expectation of always operating at higher onset voltages when in use; or as an add-on that can be manually connected to the high-voltage line when negative ionization is desired. Regardless, the use of the resistor in these experiments was atypical of the type of user-end control designed for the PS source, which is meant to lie primarily with the solvent choice and its application to the cartridges through pump programming.

Regarding the negative ion PS-MS drug screen, additional work needs to be done to improve the performance of drugs such as ibuprofen, naproxen, levetiracetam, and valproic acid. Even when quantitated using phenobarbital-d5, these problematic analytes saw no improvement, signifying the problem as primarily analyte-based. It is worth mentioning that the given screening cutoffs for ibuprofen and naproxen were lowered by

10× and 30× for the purposes of generating these calibration curves—as opposed to the 1000 ng/mL used, the original cutoffs were 10000 ng/mL and 30000 ng/mL, respectively—to make their inclusion in blood samples along with other analytes more manageable, so they may see successful quantitation at such higher and more toxicologically relevant concentrations. Also, different matrices could be tested for quantitation, seeing if biofluids such as urine or blood plasma, or even a neat matrix, see as much trouble when quantitating drugs like ibuprofen, naproxen, levetiracetam, and valproic acid.

Conclusion

When using conventional PS-MS solvents in negative ion mode, there is a very narrow voltage range, nestled between the onset of electrospray and the onset of corona discharge, over which stable spray can be achieved, but even then only with questionable reproducibility. By using the CO_3^- (m/z 60) measurements in full-MS scans, discharge was effectively quantified to monitor how well any given technique suppressed it, provided the method generated a constant signal in the first place. While the use of PE as a substrate saw worse performance than paper, two techniques were found to sufficiently suppress discharge to allow for better sensitivity and accurate quantitation: (1) inclusion of a 10-GΩ resistor in the high voltage line supplying the PS source, and (2) optimization of the spray solvent to 90:10:0.01 methanol:CCl_4:NH_4OH. By altering the solvent to include larger amounts of CCl_4, the potential required to reach the onset of discharge was effectively pushed up, allowing for a larger working range of voltages that in turn improved the ability to spray consistently from sample to sample.

Using the optimized solvent alone as the discharge-preventing method, the ability to accurately quantitate several analytes was demonstrated using the automated Velox 360

PS source. Taking the problem with pentobarbital into consideration, the negative ion method worked exceptionally well for barbiturate detection, generating calibration curves with relative errors in slope <7% and LODs lower than the screening cutoffs, with suggested potential for better trace detection. Recoveries from blood relative to neat samples for the barbiturates were ~30%. Additional analytes such as salicylic acid, warfarin, furosemide, and ethyl sulfate showed adequate quantitation with ibufenac, exhibiting its adaptability as a generic ISTD, but, with the exception of salicylic acid, their calculated LODs still lay above the screening cutoffs. Ibuprofen, naproxen, levetiracetam, valproic acid, and ethyl-beta-D-glucuronide all saw poor calibration, a result of concentration-independent MS/MS signal, high background signal in the matrix, and poor fragmentation. These shortcomings, however, lie with the drug screen itself rather than the ionization method, and as such require attention beyond the intended purpose of this study.

In Chapter 3, this same negative ion PS-MS method, optimized to suppress discharge, will be applied to the detection of chemical warfare agent hydrolysis products, ultimately showing how well it compares to a positive ion PS-MS method.

CHAPTER 3. DETECTION OF CHEMICAL WARFARE AGENT HYDROLYSIS PRODUCTS USING PS-MS

Author's Note

The information contained within the Materials and Methods, Results and Discussion, and Conclusion sections has been reproduced from McKenna et al. (DOI: http://dx.doi.org/10.1039/C7AN00144D)[61] by permission of The Royal Society of Chemistry.

Introduction

Ever since their initial discovery and later weaponization in World Wars I and II as well as in the Iran-Iraq War in the 1980s,[62,63] the use of chemical warfare agents (CWAs) has been a subject of heated contention both politically and ethically. While attempts were made by the United Nations in the 1990s to curb the production, stockpiling, and use of CWAs through the Chemical Weapons Convention (CWC),[64] they still remain relevant today, as evidenced by their use in the Tokyo subway attacks perpetrated by the Aum Shinrikyo cult in 1995,[65-68] their suspected role in the assassination of a North Korean exile, Kim Jong-nam, in 2017,[69] and their recent reported use on Syrian civilians in both 2013 and 2017.[70-73]

CWAs are organized into several categories depending on their effects, such categories including riot-control agents, choking agents, blood agents, and blistering agents. Another family of CWAs are known as nerve agents, which are acutely toxic organophosphonate compounds that negatively affect the nervous system by inhibiting acetylcholinesterase activity; this leads to a buildup of acetylcholine in nerve cells and

prevents muscles from relaxing, ultimately causing death from respiratory paralysis.[74-76] Nerve agents are divided into two major categories: G- and V-series agents, which are differentiated primarily by their chemical structures, the former containing either a fluorine or cyanide substituent and the latter containing a thioalkyl substituent. Five such nerve agents—O-isopropyl methylphosphonofluoridate (GB, sarin), O-pinacolyl methylphosphonofluoridate (GD, soman), O-cyclohexyl methylphosphonofluoridate (GF, cyclosarin), O-ethyl-S-(2-diisopropylamino)ethyl methylphosphonothiolate (VX), and O-isobutyl-S-(2-diethylamino)ethyl methylphosphonothiolate (VR, "Russian VX")—are shown in Figure 17.

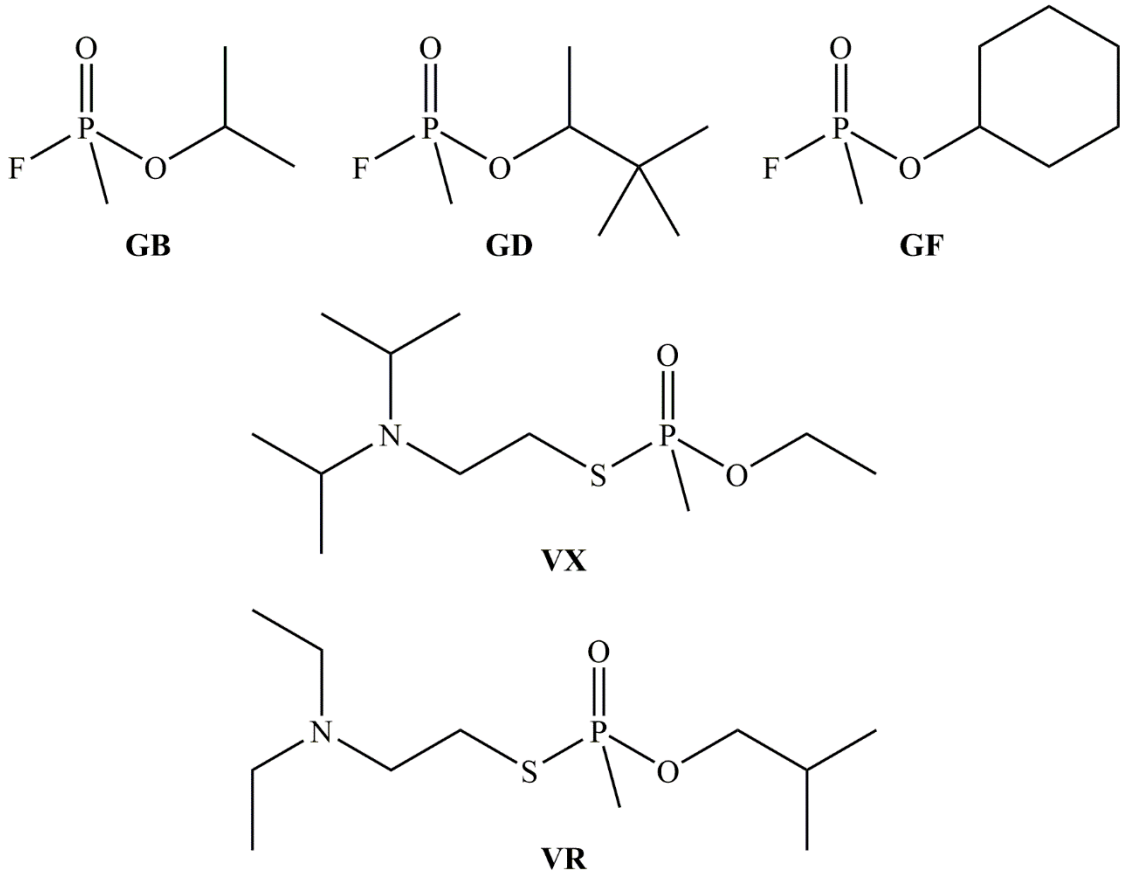

Figure 17. Chemical structures of five nerve agents: GB (sarin), GD (soman), GF (cyclosarin), VX, and VR ("Russian VX").

Detection of CWAs in biological and environmental samples is important for several reasons. In the event of exposure to such toxic compounds, rapid identification of the agent responsible is crucial both to providing immediate and appropriate medical treatment for any victims[77,78] as well as to directing emergency response in the handling and management of the attack site.[79] Monitoring adherence to the CWC, especially along the lines of destroying weapon stockpiles and investigating suspected sites of mass CWA production, is necessary for maintaining international agreements and relationships. Additionally, biomonitoring of personnel responsible for decontaminating and cleaning up CWA production sites is vital to ensuring that proper and sufficient safety protocols are being followed.

Over the past 20 years, numerous methods—most utilizing MS—have been shown to be successful in the detection of CWAs. LC-MS has been effective in analyzing CWAs present in environmental samples such as water and soil, with liquid extractions usually performed on solid samples.[80,81] However, since intact CWAs are volatile and thermally stable, they are particularly well-suited for GC-MS analyses; while a typical extraction from a soil sample followed by GC-MS was on par with LC-MS detection,[80] solid-phase microextraction (SPME) sampling coupled with GC-MS analysis was able to achieve LODs down to 0.05-1 ng/mL from environmental water samples.[82] Ambient ionization techniques have also been appealing in CWA analysis, predominantly because of the minimal requirements in the way of sample preparation and the fieldability of the instrumentation. To this end, atmospheric pressure chemical ionization (APCI) MS has been used for air samples[83,84] and DART-MS has shown good quantitation from both clean and muddy water samples.[6,85] DESI-MS has also proven useful when combined with SPME

sampling from office media (i.e., carpet, upholstery, printer paper, cotton swabs), demonstrating detection of CWAs at 1 μg/g quantities and lower as well as showing contaminant identification from a munitions-grade sample of VX.[86,87]

Aside from the analysis of pesticides and herbicides—which are chemically similar to CWAs—from food and environmental samples,[28,88] no work has been done toward using PS-MS for the detection of CWAs. A recent study, however, examined the nerve agent simulants dimethyl methylphosphonate (DMMP), diisopropyl methylphosphonate (DIMP), and trimethyl phosphate (TMP) using PS-MS and quantitated their detection in biological samples.[61] The paper spray technique was capable of detecting these simulants at concentrations between 1-25 ng/mL in urine and 10-40 ng/mL in blood. Furthermore, the authors demonstrated that successful quantitation could be achieved without any direct sample preparation at all, achieving comparable LODs and linear calibration curves when the ISTDs were spiked directly onto the dried sample spot on the VSC rather than spiking them into the sample before spotting.

While detecting intact CWAs is important, it is often not feasible when testing real biological samples due to chemical degradation. All CWAs shown in Figure 17, when present in bodily fluids, quickly undergo hydrolysis according to the first reaction in Figure 18, producing alkyl methylphosphonic acids (alkyl MPAs) depending on the identity of the R group. To this end, sarin produces isopropyl MPA (IMPA), soman produces pinacolyl MPA (PinMPA), cyclosarin produces cyclohexyl MPA (CHMPA), VX produces ethyl MPA (EMPA), and VR produces isobutyl MPA (iBuMPA).[76] These alkyl MPAs then undergo further hydrolysis to form MPA via the second, much slower reaction shown in Figure 18. Because of this rapid hydrolysis of the intact nerve agents, they are rarely ever

detected in biological samples, instead making the hydrolysis products useful for any analyses. For example, in blood samples collected from victims of the Tokyo subway sarin attack 1.5-2.5 hours after exposure, sarin itself was not detected in the serum, but IMPA was detected at concentrations ranging from 2-135 ng/mL.[67]

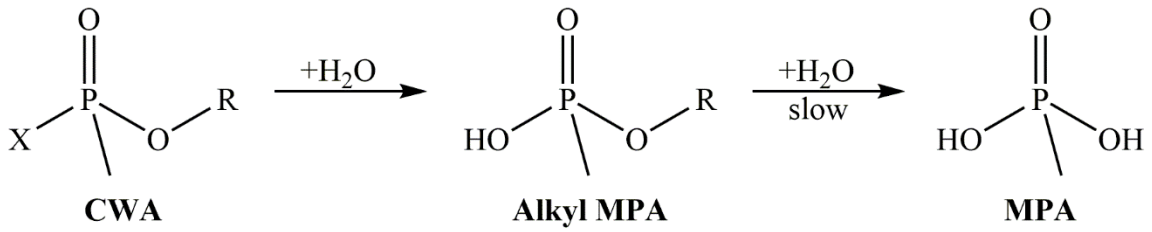

Figure 18. Successive hydrolysis reactions of a CWA, where X = F or $S(CH_2)_2NR'_2$ and R = C_2-C_6.

The detection of these hydrolysis products in several media has been previously shown using several methods. Unlike the intact CWAs, though, they do not volatilize well, making GC-MS analyses difficult because they require derivatization first, which is both time-consuming and complicates attempted quantitation.[89,90] With derivatization, GC-MS was able to detect the alkyl MPAs in soil and diesel samples down to absolute quantities of 200-500 pg.[91] Although they generally see worse quantitative performance than their GC counterparts—achieving LODs between 10-100 ng/mL—LC- and HPLC-MS techniques have more frequently been used for qualitative detection of the alkyl MPAs from environmental samples.[92-96] An ambient ionization technique, reactive DESI-MS was used in the detection of EMPA, IMPA, and MPA from biological and complex matrices on glass and polytetrafluoroethylene surfaces, achieving sub-ng detection limits for all.[97] No studies, however, have investigated the detection of the CWA hydrolysis products using PS-MS.

Since the alkyl MPAs are acidic, the goal of this study was to take the optimized negative ion method from Chapter 2 and apply it to the PS-MS detection of EMPA, IMPA,

iBuMPA, CHMPA, and PinMPA in biological samples. These five compounds were also detected using positive ionization for purposes of comparison and to determine which polarity offered superior sensitivity and quantitative accuracy. The potential is demonstrated for the application of PS-MS detection of CWA hydrolysis products to fieldable instrumentation, which would allow for rapid analyses of biological samples to provide valuable information when responding to nerve agent attacks.

Materials and Methods

Chemical Materials

Ultra-high-performance liquid chromatography (UHPLC) grade methanol, Optima grade ammonium hydroxide, and formic acid were purchased from Fisher Scientific (Pittsburgh, PA, USA). Anhydrous carbon tetrachloride was purchased from Sigma Aldrich (St. Louis, MO, USA). Mixtures of EMPA, IMPA, iBuMPA, CHMPA, and PinMPA dissolved in water were purchased from Cerilliant (Round Rock, TX, USA—product number NAx8-CAL). A mixture of SIL analogs of the hydrolysis products—d_5EMPA, $^{13}C_3$IMPA, $^{13}Cd_3$iBuMPA, $^{13}C_6$CHMPA, and $^{13}C_6$PinMPA dissolved in water—was also purchased from Cerilliant (product number NAx8-IS). Human whole blood and urine were provided by a single donor.

Sample Preparation

Solutions containing the CWA hydrolysis products were purchased in concentrations of 5000, 2500, 1250, 625, 250, 125, 63, and 25 ng/mL. Calibration standards were then prepared in blood or urine at concentrations of 250, 125, 62.5, 31.25, 12.5, 6.25, 3.15, and 1.25 ng/mL by performing 1:20 dilutions of the aqueous working solutions in the

biological matrix. A 5-μL aliquot of an aqueous ISTD solution was spiked into a 100-μL aliquot of each biological sample; the ISTD solution contained 525 ng/mL of each of the five SIL CWA hydrolysis products.

Paper Spray Ionization

All samples were spotted (12 μL) on VSCs and sprayed using the Velox 360 automated PS source (Prosolia, Indianapolis, IN, USA). When using positive ionization, 95:5:0.01 methanol:water:formic acid was used as the spray solvent. To reduce the propensity for discharge and encourage ion formation when operating in negative ion mode, 90:10:0.01 methanol:CCl_4:NH_4OH was used as the spray solvent. Pump A was programmed to dispense 3 μL four times and pump B was programmed to dispense 10 μL thirteen times, using 142 μL of solvent total. For both polarities of ionization, the solvent pump programming was spread out over the course of 1.4 minutes, with the negative ion mode program utilizing smaller delays between subsequent pumps to prevent excessive solvent evaporation.

Mass Spectrometry

All data were acquired on a Q-Exactive Focus orbitrap mass spectrometer (Thermo Fisher Scientific, San Jose, CA, USA) with the S-lens set to 50 and capillary temperature set to either 325°C or 320°C for positive or negative ion modes, respectively. The instrument methods were both 1.4 minutes long with the spray voltage on at +4.0 kV or −4.0 kV (depending on the method-specified polarity) from 0–1.1 min, the voltage then being set to 0 kV from 1.1–1.4 min; the spray voltage was turned off to give zero-intensity scans, a requirement for automatic peak integration. The mass spectrometer was operated solely in MS/MS mode using an inclusion list with an isolation width of ±0.5 m/z in the

first quadrupole to filter precursor ions. The precursor and fragment ions for the five hydrolysis products and their SIL analogs, as well as the optimized CE for each fragmentation, can be found in Table 4, and the negative ion transitions are shown in Figure 19.

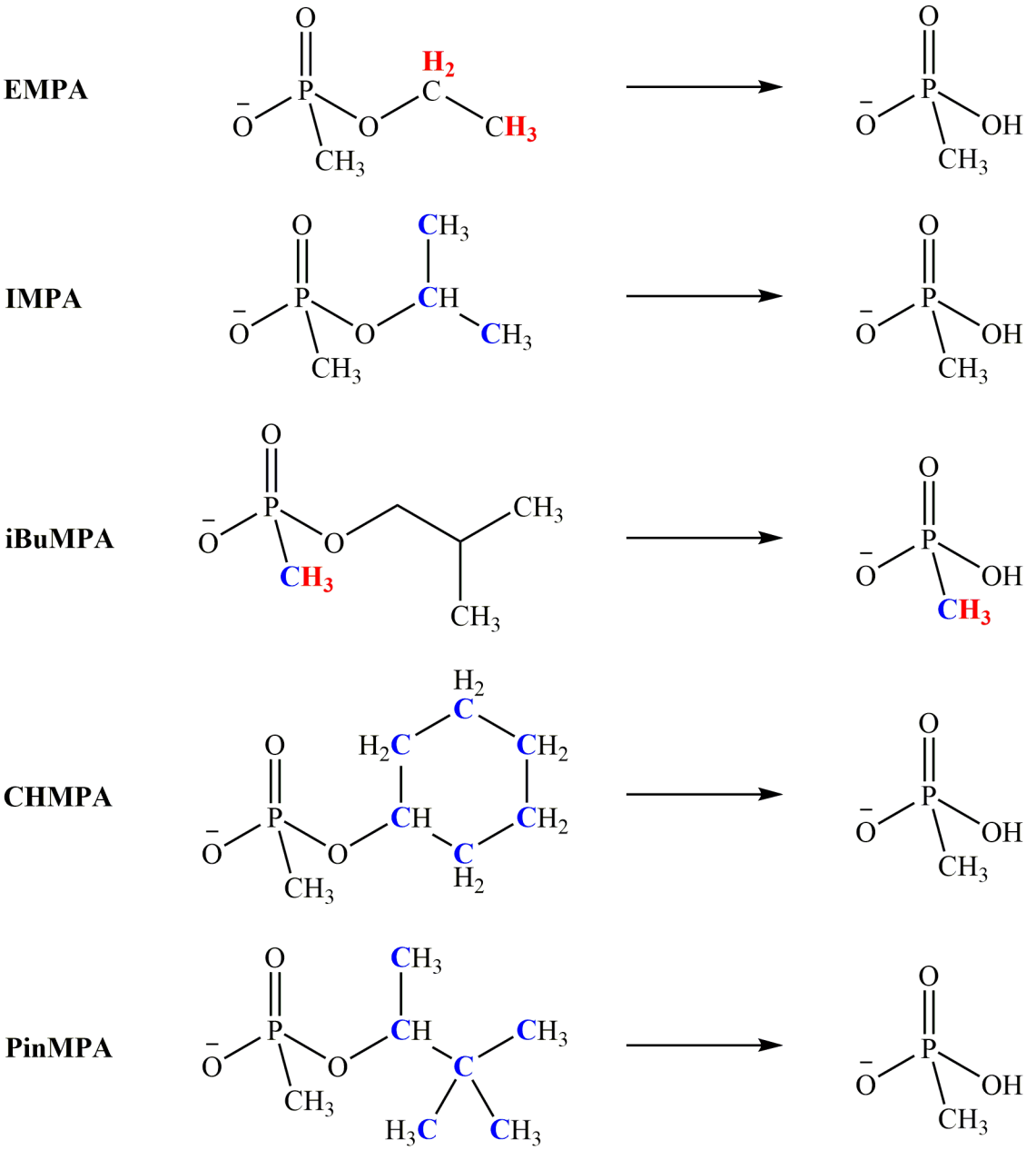

Figure 19. Negative ion transitions of the five CWA hydrolysis products. Red and blue bolded atom labels indicate the locations of the ^{2}H (d) and ^{13}C isotopes, respectively, in the SIL analogs.

Table 4. Fragmentation of each CWA hydrolysis product and their SIL ISTDs for both positive and negative ion MS/MS, the latter of which is highlighted.

Compound	Adduct	Precursor Ion [m/z]	Fragment Ion [m/z]	CE [V]
EMPA	+H	125.0364	97.0055	10
	-H	123.0212	94.9896	12
d_5EMPA	+H	130.0679	98.0117	11
	-H	128.0529	94.9897	14
IMPA	+H	139.0506	97.0055	10
	-H	137.0371	94.9896	14
$^{13}C_3$IMPA	+H	142.0619	97.0055	12
	-H	140.0473	94.9896	14
iBuMPA	+H	153.0675	97.0055	16
	-H	151.0528	94.9895	16
$^{13}Cd_3$iBuMPA	+Na	179.0719	73.0292	13
	-H	155.0752	99.0118	15
CHMPA	+Na	201.0650	118.9872	13
	-H	177.0683	94.9896	23
$^{13}C_6$CHMPA	+Na	207.0851	118.9871	10
	-H	183.0885	94.9896	20
PinMPA	+Na	203.0808	118.9871	12
	-H	179.0840	94.9896	21
$^{13}C_6$PinMPA	+Na	209.1007	118.9871	10
	-H	185.1042	94.9896	19

Data Processing

All data were automatically processed using TraceFinder v. 3.3 (Thermo Fisher Scientific). Peaks within a 5-ppm window of the target compound's fragment ion were integrated. The analyte peak area was divided by the area of the corresponding fragment ion of the appropriate ISTD. Each calibration point was run in triplicate and the ratios of analyte signal to ISTD signal were plotted against their known concentrations to generate the calibration curve, which was linearly fit using 1/x weighted least squares. LODs for the CWA hydrolysis products were determined by multiplying the standard error of the y-intercept by 3.3 and dividing by the slope of the curve; for positive ion mode, some of these calculated LODs were lower than the lowest-detected calibration samples, in which case the concentration of the first reliably detected calibration level was reported as the LOD.

Results and Discussion

The CWA hydrolysis products can be detected in positive ion mode as both protonated and sodiated ions, but they also form intense $[M-H]^-$ ions in negative ion mode because they all contain an acidic phosphonic acid moiety, so the quantitative performance of the five organophosphonate compounds in both positive and negative ion modes was compared. Using positive ionization with the optimized solvent system as determined with the intact CWA simulants[61]—95:5:0.01 methanol:water:formic acid—calibration curves could be generated in both blood and urine matrices, which are shown in Figure 20. Detection limits, relative errors in the slope, and correlation coefficients obtained from the ten calibration curves are shown in Table 5.

Table 5. Comparison of quantitative capabilities of positive and negative ionization in the detection of CWA hydrolysis products in blood and urine matrices.

	Positive Ion Mode			Negative Ion Mode		
	LOD [ng/mL]	**Rel. error in slope [%]**	**R^2**	**LOD [ng/mL]**	**Rel. error in slope [%]**	**R^2**
Blood						
EMPA	3	2	0.99	1.2	2	0.994
IMPA	10	26	0.46	0.9	2	0.997
iBuMPA	10	12	0.90	0.9	1	0.996
CHMPA	10	7	0.97	0.8	1	0.998
PinMPA	25	3	0.98	0.5	1	0.995
Urine						
EMPA	0.7	1	0.99	1.2	3	0.982
IMPA	6	10	0.72	1.2	2	0.994
iBuMPA	3	8	0.84	1.1	2	0.996
CHMPA	3	5	0.98	0.6	1	0.999
PinMPA	6	4	0.97	0.4	1	0.998

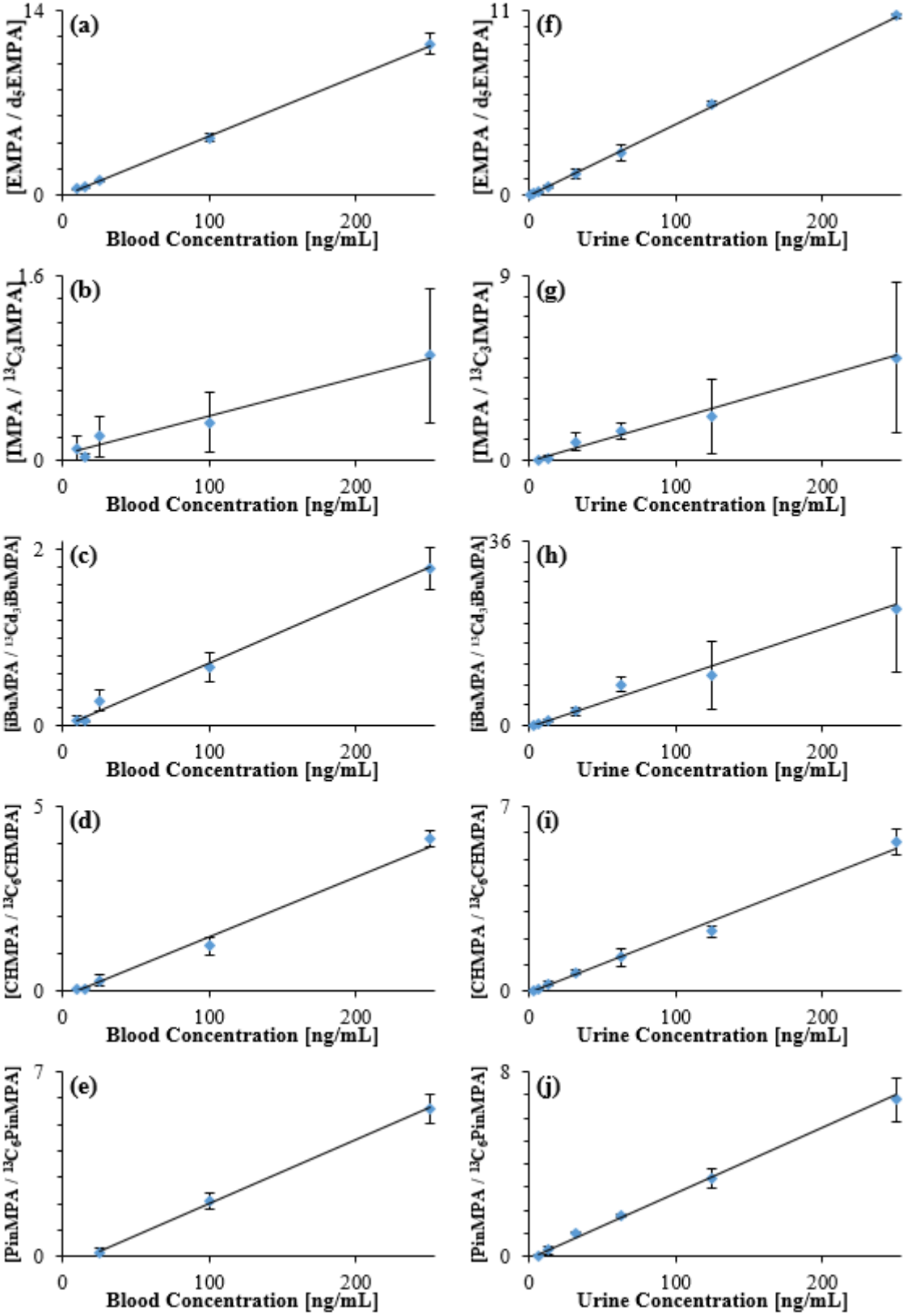

Figure 20. Positive ion calibration curves for EMPA, IMPA, iBuMPA, CHMPA, and PinMPA in both blood (a-e) and urine (f-j) matrices. Each data point is the average of three replicates.

Overall, detection of the CWA hydrolysis products as positive ions was complicated by their poor fragmentation in MS/MS mode. Despite good intensities for the positive molecular ions, the signal strength of their corresponding fragment ions was typically 10-100× lower than their negative ion counterparts, making quantitative analysis for positive ionization generally less sensitive. Furthermore, fragmentation for some of the hydrolysis products in positive ion mode was found to be unreliable, resulting in poor precision of analyte/ISTD measurements, as demonstrated for IMPA in Figure 21a.

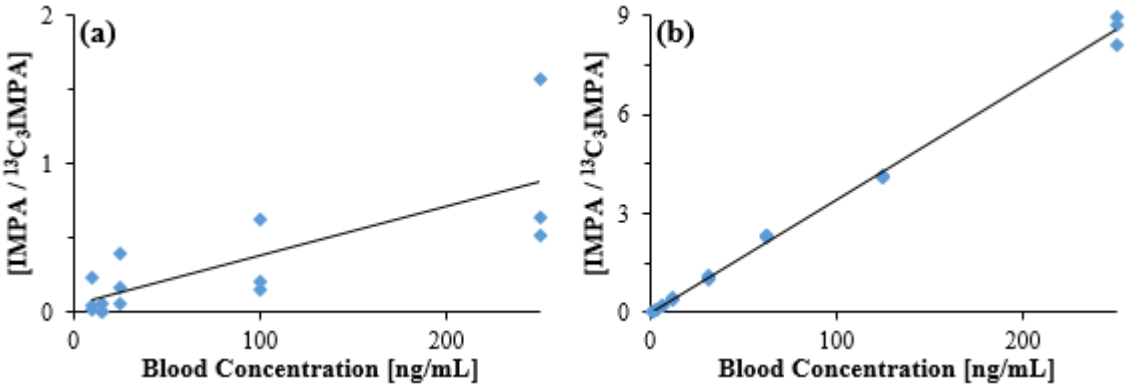

Figure 21. (a) Positive and (b) negative ion calibration curves for IMPA in blood, showing each individual analyte/ISTD measurement against its known concentration.

When operating in negative ion mode, however, $[M-H]^-$ molecular ions formed readily and fragmentation by high-energy collisional dissociation (HCD) in the q-orbitrap was efficient. By utilizing the optimized solvent from chapter 2—90:10:0.01 methanol:CCl_4:NH_4OH—discharge could reliably be circumvented, allowing for greater precision of measurements and better quantitation. The negative ion calibration curves generated for EMPA, IMPA, iBuMPA, CHMPA, and PinMPA in blood and urine matrices are shown in Figure 22, with the quantitative measures summarized in Table 5 next to those obtained when spraying in positive ion mode.

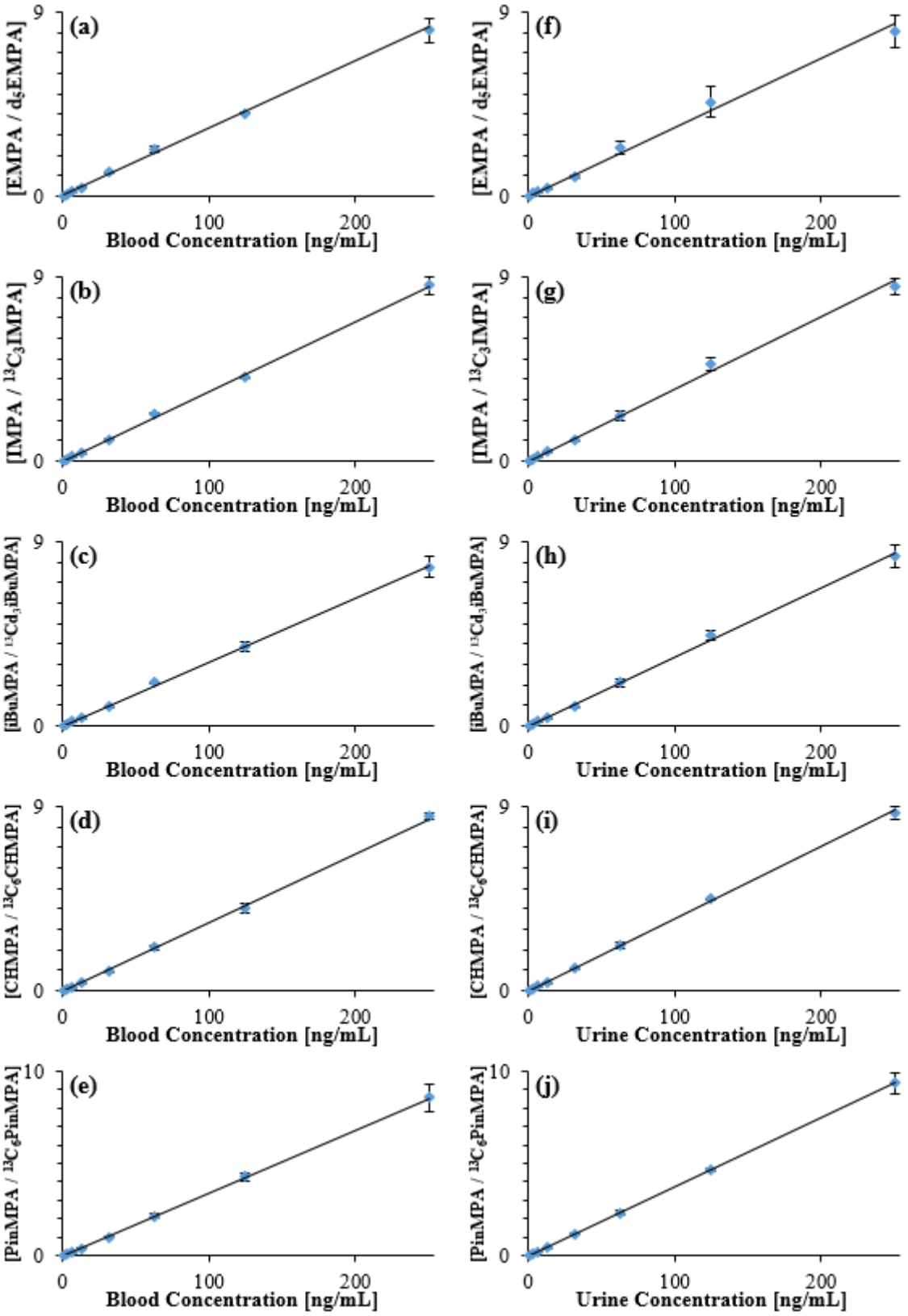

Figure 22. Negative ion calibration curves for EMPA, IMPA, iBuMPA, CHMPA, and PinMPA in both blood (a-e) and urine (f-j) matrices. Each data point is the average of three replicates.

In general, detection limits in negative ion mode improved with increasing analyte weight, achieving sub-ng/mL LODs for most compounds—down to 0.55 ng/mL in blood and 0.36 ng/mL in urine for PinMPA, respectively 50- and 15-fold improvements over its detection in positive ion mode. These LODs lie below the range measured from real victims of sarin exposure, where IMPA was present at concentrations between 2-135 ng/mL.[67] The hydrolysis products demonstrated better quantitation overall when moving from positive ionization to negative ionization. IMPA and iBuMPA especially showed marked improvement in linearity of the calibration curve and sample- to-sample precision, exemplified by IMPA in Figure 21. EMPA showed comparable quantitation between positive and negative ion modes for blood and urine (Table 5). Furthermore, the resolving power of the orbitrap mass analyzer was capable of significantly reducing matrix interference as a potential problem for these analytes; blank biofluid showed no signal within the 5-ppm m/z window for the fragment ions.

Conclusion

The PS-MS analysis of five CWA hydrolysis products—EMPA, IMPA, iBuMPA, CHMPA, and PinMPA—was capably demonstrated using both positive and negative ionization. Their detection in positive ion mode is useful because the intact CWAs generally ionize better under positive polarities, but analyzing them in negative ion mode afforded higher sensitivities and more linear calibration curves. LODs down to 0.4-1.2 ng/mL—corresponding to absolute quantities between 5-15 pg—were achieved with negative ionization. Since concentrations were able to be detected from biological samples that were lower than those in real exposure victims, it shows promise for this as a direct

method of screening for nerve agent exposure, which could be vital in providing immediate medical attention and treatment in a first-responder scenario.

MS-based techniques are highly regarded in terms of specificity and sensitivity, but they traditionally require significant sample handling and processing procedures typically in a “brick and mortar” laboratory. Furthermore, most MS detection techniques, especially if they required extensive processing, could take as long as 24 hours to get interpretable results. Using PS-MS, quantitative results can be obtained in as little as one minute. This technology and approach could have immediate utility since analytical grade mass spectrometers such as the orbitrap are currently used in field-forward, portable laboratories such as the US Army’s JUPITR program.

CHAPTER 4. APPLYING A PS-MS/MS DRUG SCREEN TO POSTMORTEM BLOOD SAMPLES

Introduction

High-Resolution Mass Spectrometry

Almost all of the data presented herein were acquired on a mass spectrometer with an orbitrap mass analyzer. When combined with tandem mass spectrometric analysis, this instrument is capable of providing excellent selectivity for compound identification. An orbitrap is a type of ion trap—based on a simpler model proposed by Kingdon in which ions were trapped in orbit around a central filament electrode[98]—that provides a means of obtaining high-resolution mass spectra by measuring ions' exact masses.[99,100] Such high mass accuracy can often signify a single molecular formula with a good degree of reliability, identifying the elemental composition of any given MS signal.

Instruments that are capable of measuring m/z with a high degree of accuracy—typically on the ppm level—encompass a field that is appropriately known as high-resolution MS (HR-MS). There are three major types of mass analyzing techniques that can accomplish such high-resolution measurements: orbital trapping (orbitrap), Fourier transform ion cyclotron resonance (FT-ICR),[101,102] and time-of-flight (TOF).[103] As they were not implemented in any of these studies, the mechanisms behind FT-ICR-MS and TOF-MS will only be mentioned in brief.

Geometrically, orbitraps consist of two coaxial electrodes, one of which is spindle-shaped and surrounded by the other, which is shaped like a barrel (see Figure 23). When a potential difference is applied between these electrodes, injected ions that tangentially approach the central electrode begin to orbit it due to electrostatically attractive forces.

While maintaining these orbits, the ions also oscillate harmonically along the principal axis; the frequency of these axial oscillations is independent of the initial energy and position of the ions, but it is inversely proportional to the square root of the m/z of each ion.[100] As they pass back and forth along the axis with their given frequencies of oscillation, the ions produce an image current on the outer electrode which is detected and transformed using fast Fourier algorithms to generate a high-resolution mass spectrum. Similar Fourier transform techniques can be applied to induced oscillations in standard quadrupole ion trap mass analyzers, but they do not achieve as high of a resolution as orbitraps.[104,105]

FT-ICR-MS utilizes the induced circular motion of moving ions in a static magnetic field, excited to larger and more measurable radii by electric fields, to generate its high-resolution mass spectra.[106] Similar to how detection in the orbitrap works, the ions rotate with a frequency that produces an image current on opposing electrodes in the system, which is then processed via fast Fourier transformations. TOF-MS, on the other hand, operates on the principles of kinematics, measuring the flight times of ions accelerated through a fixed-distance drift space. While not a source of great resolution in and of itself, the advent of the reflectron[107] and eventually multipass instrumentation[108,109] increased ion drift lengths and flight times while maintaining coherence of the traveling ion pulses. When paired with orthogonal acceleration from a continuous source of ions,[110,111] TOF mass spectrometers can attain sufficiently high resolutions for exact-mass measurements.

Of the three mass analyzers, orbitraps typically fall in the middle in terms of resolving potential, achieving resolutions ~5× above TOF but ~10× below FT-ICR.[112] By drastically extending drift lengths and flight times in TOF-MS, resolutions can be generated in excess of those normally attainable with orbitraps;[108] however, the resolving

power necessary for identifying small molecules without error is around the limit of most TOF instruments.[113] It should also be noted that, compared to orbital trapping, TOF mass analysis experiences less resolution decay with increasing m/z, so its mass-discriminating advantages lie with larger molecules rather than smaller ones. FT-ICR-MS can routinely achieve ppb-level exact-mass measurements,[114,115] but the instrumentation required to supply the magnetic field is more demanding mechanistically and economically than most other mass spectrometers. As such, orbitraps provide a simpler means of accomplishing sufficient mass accuracy, especially for the small molecules presented throughout this work.

Comparisons of mass resolving power aside, HR-MS techniques in general offer several other advantages. One of those is the multiplex advantage, which arises from their ability to scan all ion masses simultaneously rather than having to scan over each mass individually.[116] Because of this, full mass spectra are acquired instead of singly monitored ions, enabling retrospective analyses for target compounds which may have been unoptimized or even unidentified at the time of acquisition.[117-119] Another advantage of HR-MS instrumentation is the capability of running data-dependent acquisitions.[120,121] Instrument methods can be set up such that if any mass is detected above a given limit, it is selected for fragmentation and analysis via full-scan MS/MS. These benefits, on top of the already-selective exact-mass measurements provided, have aided the implementation of HR-MS for both targeted and non-targeted screening.[112,122]

Drug Screening

Both clinical and forensic toxicology rely on the accurate detection of drugs—pharmaceutical or otherwise—within a person's body. While the former suggests

physiological implications and is frequently used in therapeutic drug monitoring for medical treatments, the latter has potential legal implications and can mean the difference between determining a person's innocence or guilt in a crime. To complicate matters further, the sheer number of evidentiary biological samples that pass through the legal system necessitates the use of large-panel drug screens that target many drugs simultaneously. While not completely comprehensive in the absolute sense, most screens used today employ analytical techniques to separate, identify, and even quantitate drugs from their native samples. For example, one screening method utilizes LC-TOF-MS to scan for 124 doping agents in urine samples within the span of 30 minutes.[123] Newly developing methods strongly trend toward simpler and more efficient testing while still maintaining a high standard of analytical robustness.

Because it utilizes small amounts of sample, involves little-to-no sample preparation, and can produce reviewable results within minutes, PS-MS lends itself well to screening techniques. And considering the fact that much of the foundation of PS was built on the analysis and detection of small molecules such as drugs,[10,11,24-26] this ambient ionization technique is a promising candidate for drug screening using MS. The main issue with using it for such purposes, however, is that it does not include an analytical separation, the closest analog being the rough extraction performed by the solvent when it passes through the sample. MS/MS can be used to make up for this selectivity loss, but large-panel screens run into problems when other extracted matrix components are detected in addition to the target analytes.

Low-resolution triple quadrupole mass spectrometers can be used for PS-MS/MS drug screens by monitoring two separate fragment ions as well as their relative

abundance.[33,34] However, because of the low mass accuracy they provide—identifying ions within a ±0.5 m/z ratio range, otherwise known as unit resolution—such instruments occasionally experience substantial background noise over the analytical signal, impacting the selectivity of MS/MS and worsening the overall performance of the screen. On the other hand, the mass accuracy provided by orbitraps—typically measuring m/z down to ±0.0005 units—decreases this selectivity problem while still maintaining comparable sensitivity. Although they are more expensive than triple quadrupole instruments and require daily mass calibration, this advantage can play a critical role in improving the performance of PS-based screens.

The Q-Exactive series of mass spectrometers from Thermo Fisher Scientific used throughout this work utilizes a hybrid quadrupole-orbitrap design, which is detailed in Figure 23. The S-lens, flatapoles, and octopole primarily serve the purpose of ion optics, focusing the ion beam introduced into the system and conveying it through the differentially pumped sections of the instrument. Because of the nature of their operation, orbitraps cannot accept a continuous stream of ions into their space. It is for this reason that curved linear traps (C-traps) must be employed when using continuous ionization techniques such as ESI and PS; the C-trap accumulates ions as they pass through the instrument and then injects them orthogonally into the orbitrap in discrete packets, or pulses, for analysis.[124,125]

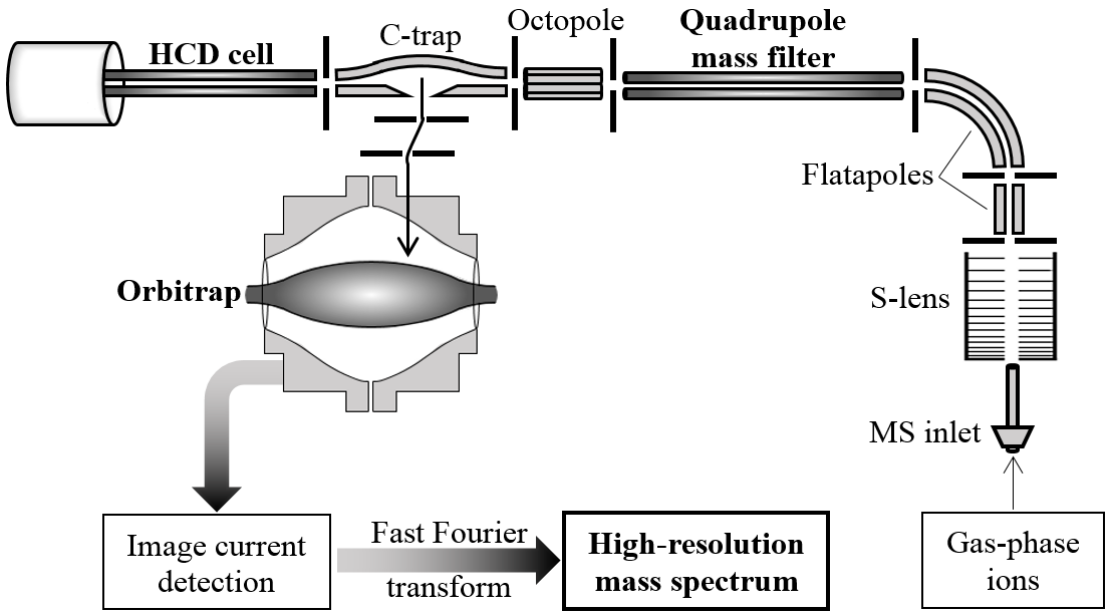

Figure 23. Schematic diagram of a Q-Exactive mass spectrometer from Thermo Fisher Scientific, which utilizes a hybrid quadrupole-orbitrap to achieve high mass resolution.

While HR-MS scans of intact ions have been shown to be as effective as MS/MS scans in lower-resolution instruments,[126] the inclusion of a quadrupole gives the Q-Exactive a greater degree of versatility. Through this quadrupole, precursor ions can be filtered by mass for either selected ion monitoring (SIM) or fragmentation in the HCD cell with subsequent MS/MS analysis. Because MS/MS itself is already powerful in selectively detecting target compounds, coupling it with high mass-discriminating capabilities often results in no background signal whatsoever at the observed fragment ion(s). Overall, this quadrupole-orbitrap hybridity with MS/MS methodology helps to provide the selectivity that PS-MS inherently lacks due to it not being a chromatographic technique, thereby increasing its potential effectiveness as a technique for simple and rapid drug screening.

A PS-MS/MS screening method has already been developed for 137 drugs with 11 SIL ISTDs for quantitation, and initial work into it was performed on a triple quadrupole mass spectrometer.[33,34] The goal of the following work was to adapt this PS-based screen to a quadrupole-orbitrap mass spectrometer and test the method on samples which are

routinely collected in death investigations: unknown, postmortem blood samples. After their analysis with PS, the results were compared to those of a more established screening method to evaluate the qualitative and quantitative performance of the PS-MS/MS screen.

Materials and Methods

Chemical Materials

Glacial acetic acid and HPLC-grade methanol, acetonitrile, isopropanol, and acetone were all purchased from Fisher Scientific (Pittsburgh, PA, USA). The human whole blood used in preparing the calibration samples was provided by a single donor. 30 different postmortem (PM) blood samples—to be analyzed as unknowns in the drug screen—were received from Axis Forensic Toxicology (Indianapolis, IN, USA). Most of the 137 drugs and 11 SIL ISTDs used in the drug screen were purchased as analytical standards from Cerilliant (Round Rock, TX, USA) at concentrations of either 1.0 mg/mL or 100 μg/mL in methanol. Acetaminophen, amlodipine, aripiprazole, benztropine, bupivacaine, carbamazepine, donepezil, etomidate, fluvoxamine, hydroxyzine, labetalol, metaxalone, methocarbamol, metoclopramide, papaverine, and ropinirole were all purchased as powders from Sigma Aldrich (St. Louis, MO, USA) and dissolved in 95:5 methanol:water to create standard solutions.

Sample Preparation

The 137 analytes were first divided up into 16 separate groups to maintain low organic content in the blood samples and to prevent structural isomers from interfering with individual analyses when generating the calibration curves. For most of these groups, spiking solutions were created by diluting the analyte standards to 1000× their screening

cutoff in 50:50 methanol:water, which were then diluted in the same matrix according to the series 2:5, 1:2, 2:5, and 1:4; each of these spiking solutions was then diluted 1:20 in blood to generate the calibrant samples. Six of the sixteen mixtures had to be prepared directly in the biological matrix, for which the analyte standards were spiked into blood to generate concentrations either 250× or 500× the screening cutoff, followed by serial dilution using the same series of 2:5, 1:2, 2:5, and 1:4.

All calibrant and PM samples were mixed 1:3 (v:v) with an aqueous ISTD mixture before spotting. The concentrations of each ISTD in this mixture were: 65 ng/mL of alprazolam-d5 (A); 650 ng/mL of benzoylecgonine-d8 (B), cocaine-d3 (C), and methamphetamine-d11 (I); 260 ng/mL of flunitrazepam-d7 (D), hydrocodone-d3 (F), and trimipramine-d3 (J); 1300 ng/mL of gabapentin-d10 (E); 2600 ng/mL of metaxalone-d6 (G); 325 ng/mL of methadone-d3 (H); and 130 ng/mL of zolpidem-d6 (K). For ease of reporting, the ISTDs—in alphabetical order—were given labels A-K.

Paper Spray Ionization

Paper spray was achieved using VSCs on the automated Velox 360 source from Prosolia (Indianapolis, IN, USA); 12 μL of sample were spotted on the cartridges and allowed to dry at room temperature before spraying. The spray solvent used was 85:10:5:0.01 acetonitrile:acetone:water:acetic acid. In total, 136 μL of solvent were gradually applied to each cartridge—6 μL directly onto the DBS via pump A and 130 μL into the solvent well via pump B—over the course of 2.43 minutes.

Mass Spectrometry

All data were acquired on a Q-Exactive Focus orbitrap mass spectrometer (Thermo Fisher Scientific, San Jose, CA, USA) with the S-lens set to 75 and capillary temperature

set to 320°C. The instrument method was 2.43 minutes long, operating in positive ion mode at +5.0 kV for the first 1.6 min before turning the voltage off to 0 kV for the next 0.83 min. In the final 0.2 min, the instrument was switched to negative ionization at -4.0 kV to prevent charge buildup on the S-lens. The voltage was turned off for 0.83 min at the end of the run to generate zero-intensity scans for each drug, which were required for automated data processing in Thermo's TraceFinder.

The mass spectrometer was operated solely in MS/MS mode using an inclusion list with an isolation width of ±0.5 m/z in the first quadrupole to filter precursor ions; a maximum injection time of 50 ms was used to accommodate the number of scans required for reliable signal detection across all compounds in the method. In the event where the precursor ions of two or more drugs were close enough in mass to have both passed through the first quadrupole and into the orbitrap mass analyzer, a single scan event was used for both and the same CE was used for fragmentation. The precursor ions, fragment ions, and optimized CEs for all 137 drugs and the 11 SIL ISTDs can be found in Table 6. For norpropoxyphene, norsertraline, and propoxyphene, the precursor ions fragmented within the first quadrupole, and since these primary fragment ions demonstrated higher signal than the precursors in full-MS mode, they were selected for further fragmentation via MS/MS.

Table 6. Fragmentation of each analyte and SIL ISTD used in the PS-MS/MS drug screen. The fragment ion indicated was the primary fragment ion used for quantitation.

Compound	Precursor Ion [m/z]	Fragment Ion [m/z]	CE [V]
6-Monoacetylmorphine	328.1543	211.0753	25
7-Aminoclonazepam	286.1000	121.0760	30
7-Aminoflunitrazepam	284.1194	135.0915	30
9-Hydroxyrisperidone	427.2140	207.1127	33
Acetaminophen	152.0706	110.0602	20
Alfentanil	417.2609	268.1763	20
Alpha-PVP	232.1696	126.1276	22
Alprazolam	309.0902	281.0712	45
Amitriptyline	278.2000	191.0852	28

Table 6 (continued)

Compound	Precursor Ion [m/z]	Fragment Ion [m/z]	CE [V]
Amlodipine	409.1525	238.0625	15
Amphetamine	136.1121	119.0858	10
Aripiprazole	448.1553	285.0910	30
Atenolol	267.1700	145.0646	26
Baclofen	214.0629	116.0620	32
Benzoylecgonine	290.1387	168.1015	20
Benztropine	308.1850	167.0850	35
Benzylpiperazine	177.1386	91.0546	20
Brompheniramine	319.1400	274.0215	20
Bupivacaine	289.1000	140.1430	33
Buprenorphine	468.3108	414.2630	42
Bupropion	240.1150	131.0728	30
Buspirone	386.2551	122.0710	35
Carbamazepine	237.1022	194.0961	26
Carbamazepine-10,11-epoxide	253.0972	180.0806	24
Carisoprodol	283.1628	200.1644	16
Chlordiazepoxide	300.1000	227.0489	21
Chlorpheniramine	275.1000	230.0726	19
Chlorpromazine	319.1030	197.1361	30
Citalopram	325.1711	109.0449	24
Clomipramine	315.1623	86.0969	50
Clonazepam	316.0484	214.0416	45
Clozapine	327.1371	270.0786	25
Cocaethylene	318.1700	196.1328	25
Cocaine	304.1543	182.1170	30
Codeine	300.1594	215.1064	30
Cyclobenzaprine	276.1747	215.0853	60
Demoxepam	287.0582	219.1569	23
Desalkylflurazepam	289.1000	140.0260	33
Desipramine	267.1700	72.0813	26
Dextromethorphan	272.2009	147.0801	32
Diazepam	285.1000	154.0415	33
Diltiazem	415.1686	178.0315	23
Diphenhydramine	256.1000	167.0851	25
Donepezil	380.2220	243.1373	28
Doxepin	280.1696	107.0493	25
Doxylamine	271.1805	182.0962	18
Duloxetine	298.1260	267.0836	15
EDDP	278.1903	234.1271	38
Ephedrine/Pseudoephedrine	166.1226	115.0544	26
Etomidate	245.1285	113.0346	30
Felbamate	239.1026	117.0702	10
Fentanyl	337.2274	188.1431	25

Table 6 (continued)

Compound	Precursor Ion [m/z]	Fragment Ion [m/z]	CE [V]
Flecainide	415.1451	301.0284	46
Flunitrazepam	314.0936	239.0975	40
Fluoxetine	310.1413	168.0890	35
Flurazepam	388.1586	315.0685	28
Fluvoxamine	319.1400	71.0497	20
Gabapentin	172.1332	137.0959	17
Haloperidol	376.1474	123.0242	55
Hydrocodone	300.1594	199.0752	30
Hydromorphone	286.1000	185.0594	30
Hydroxychloroquine	336.1837	179.0370	20
Hydroxyzine	375.1834	201.0461	20
Ketamine	238.0993	125.0152	20
Labetalol	329.1860	162.0545	25
Lamotrigine	256.1000	210.9821	25
Levetiracetam	171.1128	126.0914	20
Lidocaine	235.1805	86.0967	20
Lorazepam	321.0192	275.0129	32
MDA	180.1019	133.0647	15
MDMA	194.1176	135.0438	25
MDPV	276.1594	126.1276	27
Meperidine	248.1645	174.1274	20
Mephedrone	178.1226	145.0883	25
Meprobamate	219.1100	162.0915	12
Mescaline	212.1281	180.0780	20
Metaxalone	222.1125	161.0960	10
Methadone	310.2165	265.1580	18
Methamphetamine	150.1277	91.0546	10
Methocarbamol	242.1023	118.0500	10
Methylone	208.0968	160.0754	20
Methylphenidate	234.1489	84.0811	20
Metoclopramide	300.1000	227.0575	21
Metoprolol	268.1907	116.1070	20
Midazolam	326.0855	244.0320	30
Mirtazapine	266.1500	195.0914	24
Morphine	286.1000	201.0905	30
Naproxen	231.1016	185.0963	20
Norbuprenorphine	414.2639	83.0861	60
Norclomipramine	301.1466	72.0813	20
Norclozapine	313.1300	270.0783	26
Nordiazepam	271.0633	140.0259	34
Nordoxepin	266.1500	107.0493	24
Norfluoxetine	296.1257	100.1124	20
Norketamine	224.0837	125.0151	15

Table 6 (continued)

Compound		Precursor Ion [m/z]	Fragment Ion [m/z]	CE [V]
Normeperidine		234.1489	160.1118	15
Norpropoxyphene (fragment)		308.2009	143.0856	25
Norsertraline (fragment)		275.1000	158.9759	19
Nortramadol		250.1802	189.1274	15
Nortriptyline		264.1800	191.0853	28
Norvenlafaxine		264.1800	107.0494	28
o-/m-Chlorophenylpiperazine		197.0840	154.0416	26
Olanzapine		313.1300	256.0893	26
Oxazepam		287.0582	241.0521	23
Oxycodone		316.1543	241.1089	33
Oxymorphone		302.1387	227.0934	35
Papaverine		340.1543	202.0858	28
Paroxetine		330.1500	192.1179	22
PCP		244.2060	159.1166	13
Pentazocine		286.2165	218.1535	20
Phenytoin		253.0972	182.0965	24
Pregabalin		160.1332	124.1118	12
Primidone		219.1100	162.0912	12
Promethazine		285.1000	198.0369	33
Propoxyphene (fragment)		266.1500	143.0854	24
Propranolol		260.1645	116.1070	20
Quetiapine		384.1740	253.0795	25
Ranitidine		315.1485	176.0484	18
Risperidone		411.2191	191.1172	35
Ropinirole		261.1961	114.1277	24
Sertraline		306.1000	158.9760	29
Sildenafil		475.2122	283.1183	45
Temazepam		301.0738	255.0677	36
TFMPP		231.1104	188.0679	32
Topiramate		362.0880	265.1047	18
Tramadol		264.1958	58.0659	10
Trazodone		372.1586	176.0814	25
Triazolam		343.0512	315.0318	35
Trimipramine		295.2169	100.1123	25
Vardenafil		489.2279	169.0968	50
Venlafaxine		278.2000	121.0648	28
Verapamil		455.2904	165.0906	30
Zaleplon		306.1000	236.0927	29
Ziprasidone		413.1197	194.0362	30
Zolpidem		308.1850	235.1224	35
Zonisamide		213.0328	150.0548	22
Zopiclone		389.1123	217.0270	40
Alprazolam-d5	**A**	314.1215	314.1215	45

Table 6 (continued)

Compound		Precursor Ion [m/z]	Fragment Ion [m/z]	CE [V]
Benzoylecgonine-d8	**B**	298.2000	171.1208	25
Cocaine-d3	**C**	307.1732	307.0732	30
Flunitrazepam-d7	**D**	321.1375	321.1375	40
Gabapentin-d10	**E**	182.1960	182.1960	17
Hydrocodone-d3	**F**	303.1783	303.1783	30
Metaxalone-d6	**G**	228.1501	228.1501	10
Methadone-d3	**H**	313.2354	313.2354	18
Methamphetamine-d11	**I**	161.1968	161.1968	10
Trimipramine-d3	**J**	298.2000	298.2357	25
Zolpidem-d6	**K**	314.2134	314.2134	35

Data Processing

All data were automatically processed using TraceFinder v. 3.3 (Thermo Fisher Scientific). Peaks within a 5-ppm window of the target compound's fragment ion were integrated. The analyte peak area was then divided by the area of the corresponding fragment ion of the appropriate ISTD. Each calibration point was run in duplicate and the ratios of analyte signal to ISTD signal were plotted against their known concentrations to generate the calibration curve, which was linearly fit using 1/x weighted least squares. Limits of reporting (LORs) were determined by the lowest reliably detected calibrator above noise.

Postmortem Sample Drug Screen

All 30 unknown PM samples were run in triplicate alongside the calibration samples, and each analyte/ISTD measurement was plotted on the corresponding calibration curve to semi-quantitatively determine the amount of drug present. The results of this PS-MS/MS drug screen were then compared to those of a more established screening method using HPLC-MS, which was run off-site and independently by Axis Forensic Toxicology.

Results and Discussion

Paper Spray Screening on a Quadrupole-Orbitrap Mass Spectrometer

When screening for a relatively large number of targets using an MS/MS inclusion list, the settings of the mass spectrometer must be adjusted to ensure an adequate number of scans are obtained for each target within the time the cartridge is spraying; in this screen, 5 scans per target was chosen as a standard for achieving accurate m/z measurements and ion ratios as well as acceptable quantitative performance. When using a single VSC with the Velox 360 PS source, though, spraying times are limited by the amount of applied spray solvent, which is in turn limited by the volume that can be retained by the paper tip and in the solvent well. Since it is not currently possible to apply solvent during an acquisition on the automated source, the finite amount applied to the cartridge beforehand limits the length of the spraying process to about 90 seconds, so an injection time of 50 ms was accordingly used to allow for the collection of the 5 scans for each target.

An example of the total ion chronogram acquired using the described instrument method is shown in Figure 24a, where each stick is an individual MS/MS scan. A full cycle of these scans, encompassing all target compounds, completed within ~0.3 minutes. 5 or 6 scans were acquired for each MS/MS scan filter followed by a zero-intensity scan at the end, which was obtained by turning off the spray voltage 1.6 minutes into the acquisition. Such zero-scans were necessary for automatic peak integration through the TraceFinder software. The extracted ion chronogram for cocaine—the filter for which fragmented precursor ions at m/z 304.1543 ±0.5—is shown in Figure 24b, demonstrating the number and frequency of MS/MS scans as well as the zero-scan.

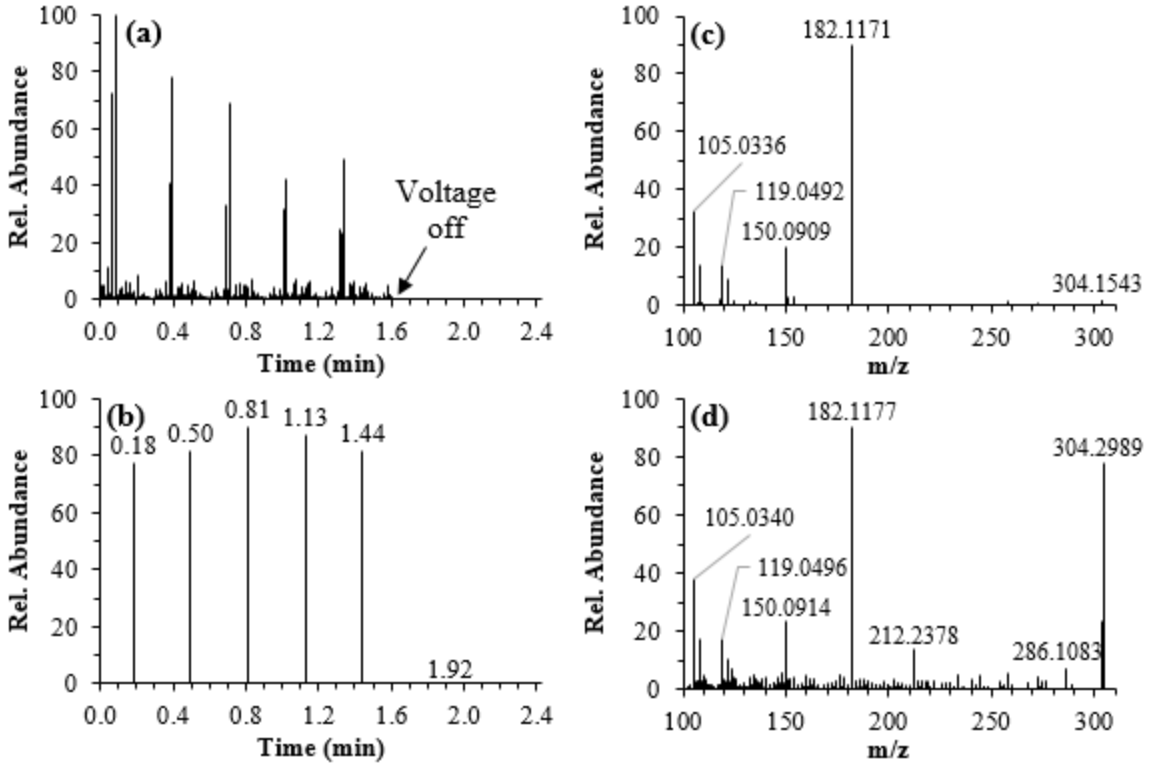

Figure 24. (a) Total ion chronogram (all scans combined). (b) Extracted ion chronogram from MS/MS scans of cocaine. (c) Tandem mass spectrum for a neat standard of cocaine at 200 ng/mL, infused via commercial ESI. (d) Tandem mass spectrum for blood spiked with 16 ng/mL cocaine (0.33× its cutoff), sprayed via paper spray.

The injection time is an instrument parameter analogous to dwell time in triple quadrupole mass spectrometers, and as such it affects the amount of signal detected; using larger injection times, for example, improves sensitivity by allowing more ions into the orbitrap and more completely filling it. For all but six of the drugs screened here, detection at the cutoff was sufficient with an injection time of 50 ms, and increasing it allowed for better detection of the six that failed at their cutoff. However, since 5-6 scans were desired, attempting to increase the injection time would lead to a total acquisition time of around 5-6 minutes, which would not be possible with paper spray unless spray solvent could be continuously applied to the cartridge.

On top of sensitivity, selectivity is another concern of any screening technique. As stated before and can be seen in Figure 24d for the MS/MS spectrum of cocaine, analytes

can be confidently detected straight from blood samples—even at concentrations below the screening cutoff—owing to the high mass accuracy provided by the orbitrap mass analyzer. And while the biomatrix generates extraneous peaks not seen in neat matrices (Figure 24c), the selectivity provided by the exact-mass measurements was enough to identify the prominent peaks at m/z 182.117 and below as indicative of the presence of cocaine.

The instrument resolution used here was 35,000, which lies in the middle of the range offered by the instrument; to avoid increasing the scan times and worsening any sensitivity problems, the highest resolution was not used. Together with the 5-ppm detection window used in data processing, the selectivity afforded by the instrument was sufficient for all targets, making sensitivity the primary limiting factor, and even then only for those drugs whose signal at the cutoff was genuinely not high enough for detection.

Almost all drugs screened saw the production of more than one fragment ion. In such cases, the weaker ions could be used as confirmatory ions for positive detection, bolstering specificity, while the strongest ion would be used for quantitation measurements; in this study, however, only the strongest ion was utilized for both purposes of identification and quantitation.

For more non-exhaustive screens, where the number of target compounds is few in comparison, the determination of instrumental parameters is more flexible and can be readily altered to improve detection. But for the 148-target (including ISTDs) screen employed here—spread out over 130 unique MS/MS scan events—these parameters were set to strike a balance between sensitivity and selectivity, all within the short sampling period supported by paper spray. As such, further improvement of the screen could not be

accomplished solely by altering instrument-side variables, but rather had to be done chemically by altering the method itself, which mostly consisted of the spray solvent used.

Method Optimization for Postmortem Samples

Previous work into developing this positive ion PS-MS/MS drug screen saw the spiking of 10 μL of the ISTD mixture into 200 μL of each sample as well as the utilization of 95:5:0.01 methanol:water:acetic acid as the spray solvent, operated at an onset voltage of 4.0 kV. However, this method had only been used in the generation of analyte calibration curves and had not been tested with any of the PM blood samples. When making the transition from a single living blood donor to multiple deceased blood donors—coupled with differing levels of coagulation—matrix effects started to become more noticeable. As can be seen in Figure 25, the measured ISTD MS/MS signal from the PM samples was typically weaker than the calibrant samples, showing inconsistency between the unknowns themselves as well as the samples used in generating the calibration curves, which would impede the accuracy of any attempted quantitation. Of the ISTDs, metaxalone-d6 suffered the most from the effects of these diverse chemical backgrounds, remaining completely undetected in over half of the PM samples. To address this problem, new methods were investigated to mitigate the ion suppressing effects of the different matrices by increasing ISTD sensitivity and achieving consistent signal strength between the PM and calibrant samples.

Acetonitrile was tested as an alternative organic phase in the spray solvent. Previous work[127] demonstrated that acetonitrile-based solvents show lower ion suppression than methanol solvents, presumably because of lower solubility of salts and lipids. However, the use of acetonitrile-water mixtures is problematic as they are less capable than methanol-

water mixtures in permeating and fully wetting DBSs, which completely stymies the spraying process. Isopropanol and acetone were both investigated as cosolvents to increase the ability of the spray solvent to penetrate the DBS; to the same end, thinning the blood samples—either by mixing them 1:1 (v:v) with 0.9% saline solution before spiking in the ISTD or by mixing them up to 1:9 (v:v) directly with the aqueous ISTD mixture—before spotting was also tested. Of these different sample preparation and spray solvent combinations, spraying with 85:10:5:0.01 acetonitrile:acetone:water:acetic acid at a 5.0 kV onset voltage allowed for proper and consistent spraying across multiple different samples, but only if the blood samples had been mixed 1:3 (v:v) with an aqueous ISTD mixture before spotting.

The results of this new method tested against the original method are demonstrated through the raw ISTD MS/MS signals shown in Figure 25 and summarized in Table 7. When using the new method, there were no issues with the detection of any ISTDs from any of the PM samples, and almost all of them experienced a notable increase in sensitivity over the original method. Furthermore, the signal achieved using the new method was much more stable and comparable across the different PM and calibrant samples. These facts taken together indicate that the new method of sample preparation as well as the new solvent would allow for more reliable quantitative conclusions to be drawn regarding analyte detection in the PM samples.

Table 7. Raw ISTD MS/MS signal in the PM and calibrant samples when sprayed using the new method (85:10:5:0.01 acetonitrile:acetone:water:acetic acid with thinned blood samples) as compared to the original method (95:5:0.01 methanol:water:acetic acid).

ISTD		Original Method		New Method	
		PM Samples	Calibrants	PM Samples	Calibrants
Alprazolam-d5					
	AUC	6.67×10^{8}	8.84×10^{8}	3.50×10^{8}	3.14×10^{8}
	RSD	38%	36%	46%	26%
Benzoylecgonine-d8					
	AUC	1.52×10^{7}	1.34×10^{8}	3.56×10^{8}	3.06×10^{8}
	RSD	48%	54%	28%	27%
Cocaine-d3					
	AUC	3.71×10^{8}	5.78×10^{8}	6.79×10^{8}	5.65×10^{8}
	RSD	28%	32%	28%	24%
Flunitrazepam-d7					
	AUC	3.72×10^{5}	1.38×10^{6}	4.00×10^{7}	2.30×10^{7}
	RSD	75%	38%	32%	27%
Gabapentin-d10					
	AUC	1.79×10^{6}	4.13×10^{6}	3.52×10^{7}	3.59×10^{7}
	RSD	80%	38%	42%	31%
Hydrocodone-d3					
	AUC	9.17×10^{6}	2.23×10^{7}	6.97×10^{7}	8.61×10^{7}
	RSD	45%	35%	30%	28%
Metaxalone-d6					
	AUC	5.05×10^{4}	5.62×10^{6}	2.41×10^{7}	2.96×10^{7}
	RSD	260%	94%	32%	24%
Methadone-d3					
	AUC	1.00×10^{9}	9.58×10^{8}	9.39×10^{8}	8.56×10^{8}
	RSD	38%	43%	50%	32%
Methamphetamine-d11					
	AUC	1.05×10^{8}	3.23×10^{8}	6.85×10^{8}	8.97×10^{8}
	RSD	54%	41%	38%	35%
Trimipramine-d3					
	AUC	2.21×10^{8}	4.13×10^{8}	6.19×10^{8}	5.82×10^{8}
	RSD	34%	33%	48%	27%
Zolpidem-d6					
	AUC	1.22×10^{7}	1.97×10^{7}	2.26×10^{7}	1.88×10^{7}
	RSD	28%	33%	29%	26%

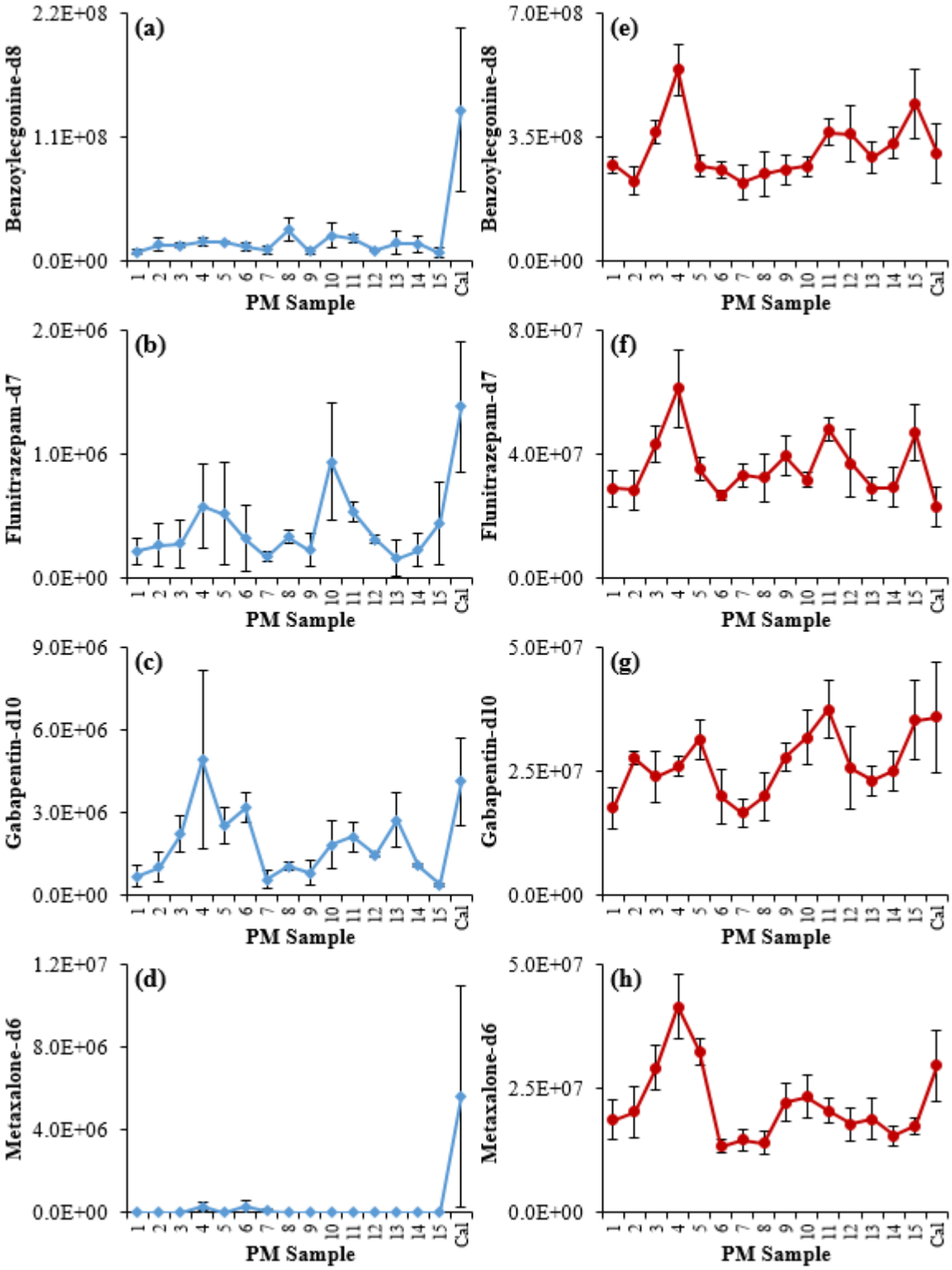

Figure 25. MS/MS signals between the original (a-d) and new (e-h) methods of sample preparation and spraying for the ISTDs benzoylecgonine-d8, flunitrazepam-d7, gabapentin-d10, and metaxalone-d6. Average values for half of the PM samples, run in triplicate, are shown along with an average value for calibrants run alongside them, with the error bars indicating one standard deviation above and below these values.

Limits of Reporting

Using this new method, all samples were prepared in a similar fashion and run concurrently, spraying each calibrant sample in duplicate to generate the calibration curves used in quantitating the amount of each analyte detected in the PM samples, which were all run in triplicate. The calibration curves are summarized in Table 8 and the results of the drug screen are given in Table 9.

For most drugs, no signal was detected when blank matrix was sprayed, but some saw high blank signal. To calculate signal-to-blank ratios (S/B), the average analyte MS/MS signal at the LOR was divided by either the average blank signal or an estimate of the electrical noise produced by the mass spectrometer ($\sim 1 \times 10^5$)—whichever was higher. When combined with the results of the calibration curves, an estimate can be made as to which drugs could potentially be screened for at lower concentrations; for example, bupivacaine, carbamazepine, lidocaine, and papaverine all demonstrated such potential.

Table 8. Quantitative measurements for each of the analyte calibration curves which ran concurrently with the PM samples in the PS-MS/MS drug screen.

Analyte	ISTD	LOR [ng/mL]	S/B at LOR	Rel. Error in Slope [%]	R^2
6-Monoacetylmorphine	**F**	20	5	3	0.993
7-Aminoclonazepam	**F**	25	34	3	0.994
7-Aminoflunitrazepam	**F**	20	52	3	0.992
9-Hydroxyrisperidone	**F**	10	155	7	0.963
Alfentanil	**K**	50	257	7	0.961
Alpha-PVP	**K**	50	214	9	0.936
Alprazolam	**A**	5	3	2	0.996
Amitriptyline	**J**	20	72	3	0.994
Amlodipine	**F**	20	2	7	0.959
Amphetamine	**I**	80	3	5	0.984
Aripiprazole	**H**	50	111	8	0.951
Atenolol	**F**	100	48	3	0.993
Benzoylecgonine	**B**	50	7	1	0.998
Benztropine	**H**	10	303	6	0.972
Benzylpiperazine	**F**	50	2	2	0.997
Brompheniramine	**H**	25	83	13	0.877
Bupivacaine	**H**	250	4696	5	0.983

Table 8 (continued)

Analyte	ISTD	LOR [ng/mL]	S/B at LOR	Rel. Error in Slope [%]	R^2
Buprenorphine	**H**	10	6	4	0.986
Bupropion	**K**	50	156	11	0.915
Buspirone	**H**	6	69	33	0.528
Carbamazepine	**J**	1000	5925	9	0.940
Chlordiazepoxide	**K**	50	120	5	0.981
Chlorpheniramine	**H**	15	145	5	0.977
Chlorpromazine	**J**	50	42	5	0.983
Citalopram	**H**	10	63	10	0.926
Clomipramine	**J**	20	35	3	0.993
Clonazepam	**A**	30	2	4	0.984
Clozapine	**K**	50	542	8	0.951
Cocaethylene	**C**	50	136	2	0.997
Cocaine	**C**	50	36	12	0.903
Codeine	**F**	20	7	3	0.992
Cyclobenzaprine	**J**	10	208	2	0.997
Demoxepam	**D**	50	58	5	0.980
Desalkylflurazepam	**A**	50	64	6	0.972
Desipramine	**J**	20	195	4	0.990
Dextromethorphan	**H**	10	78	8	0.952
Diazepam	**A**	50	97	3	0.995
Diltiazem	**K**	50	129	11	0.910
Diphenhydramine	**H**	25	7	4	0.986
Donepezil	**H**	45	47	4	0.989
Doxepin	**J**	20	128	5	0.977
Doxylamine	**K**	25	60	6	0.974
Duloxetine	**H**	400	1	10	0.963
EDDP	**H**	25	141	6	0.973
Ephedrine/Pseudoephedrine	**I**	50	17	2	0.996
Etomidate	**A**	100	9	5	0.982
Fentanyl	**C**	1	10	4	0.988
Flecainide	**K**	250	549	5	0.981
Flunitrazepam	**D**	20	5	4	0.989
Fluoxetine	**H**	20	3	3	0.992
Flurazepam	**H**	25	182	5	0.979
Fluvoxamine	**K**	15	7	9	0.933
Gabapentin	**E**	250	39	7	0.966
Haloperidol	**H**	10	264	7	0.963
Hydrocodone	**F**	20	35	2	0.998
Hydromorphone	**F**	20	11	6	0.973
Hydroxychloroquine	**K**	2000	336	12	0.899
Hydroxyzine	**K**	10	82	4	0.985
Ketamine	**H**	100	370	7	0.963
Labetalol	**F**	45	50	5	0.983

Table 8 (continued)

Analyte	ISTD	LOR [ng/mL]	S/B at LOR	Rel. Error in Slope [%]	R^2
Levetiracetam	**G**	2000	3	4	0.984
Lidocaine	**K**	250	4303	3	0.993
Lorazepam	**D**	25	5	6	0.970
MDA	**I**	100	8	4	0.984
MDMA	**I**	45	79	3	0.994
MDPV	**K**	45	360	4	0.987
Meperidine	**K**	25	137	5	0.980
Mephedrone	**I**	45	64	5	0.983
Meprobamate	**B**	1000	3	11	0.910
Mescaline	**F**	100	3	6	0.971
Metaxalone	**G**	1000	37	7	0.966
Methadone	**H**	15	165	5	0.980
Methamphetamine	**I**	45	70	2	0.995
Methylone	**I**	45	17	5	0.983
Methylphenidate	**K**	20	464	2	0.997
Metoclopramide	**F**	100	726	5	0.982
Metoprolol	**F**	45	131	3	0.993
Midazolam	**K**	45	65	4	0.987
Mirtazapine	**K**	45	572	4	0.985
Morphine	**F**	30	3	5	0.980
Naproxen	**B**	14994	3	14	0.878
Norbuprenorphine	**H**	100	11	13	0.880
Norclomipramine	**J**	36	276	2	0.998
Norclozapine	**J**	45	140	3	0.993
Nordiazepam	**A**	50	133	5	0.978
Nordoxepin	**J**	20	65	4	0.985
Norfluoxetine	**H**	20	38	2	0.997
Norketamine	**F**	91	114	5	0.978
Normeperidine	**F**	25	297	6	0.972
Norpropoxyphene (fragment)	**H**	50	16	3	0.995
Nortramadol	**K**	1000	1	8	0.953
Nortriptyline	**J**	20	66	3	0.994
Norvenlafaxine	**K**	25	2	52	0.312
o-/m-Chlorophenylpiperazine	**F**	20	89	4	0.989
Olanzapine	**K**	50	164	7	0.966
Oxazepam	**D**	50	41	4	0.987
Oxycodone	**F**	50	18	3	0.992
Oxymorphone	**F**	15	5	5	0.981
Papaverine	**K**	250	2064	3	0.994
Paroxetine	**K**	15	57	7	0.959
PCP	**H**	25	1	12	0.901
Pentazocine	**H**	50	425	4	0.987
Pregabalin	**E**	250	7	7	0.958

Table 8 (continued)

Analyte	ISTD	LOR [ng/mL]	S/B at LOR	Rel. Error in Slope [%]	R^2
Primidone	**B**	750	3	11	0.910
Promethazine	**H**	25	61	5	0.978
Propoxyphene (fragment)	**H**	50	39	3	0.994
Propranolol	**K**	50	194	2	0.996
Quetiapine	**K**	50	579	5	0.983
Ranitidine	**F**	250	231	5	0.981
Risperidone	**K**	10	48	7	0.961
Ropinirole	**K**	10	144	5	0.982
Sertraline	**H**	100	18	6	0.971
Sildenafil	**F**	100	14	3	0.994
Temazepam	**D**	50	86	2	0.997
TFMPP	**K**	50	386	3	0.992
Tramadol	**K**	100	8	3	0.991
Trazodone	**K**	100	539	3	0.995
Triazolam	**A**	20	19	5	0.982
Trimipramine	**J**	20	179	3	0.993
Vardenafil	**F**	100	39	4	0.989
Venlafaxine	**F**	50	3	4	0.984
Verapamil	**H**	50	267	4	0.987
Zaleplon	**D**	15	3	4	0.986
Ziprasidone	**H**	40	49	9	0.944
Zolpidem	**K**	10	169	1	0.999

Table 9. Results from the PS-MS/MS drug screen for each of the 30 PM samples.

PM Sample	Drug (Concentration [ng/mL])
#1	None detected
#2	7-Aminoclonazepam (95); benztropine (20); bupropion (308); fluoxetine (31); quetiapine (130); risperidone (15); tramadol (1346)
#3	Hydrocodone (82); lidocaine (544)
#4	Donepezil (84); gabapentin (781); nortramadol (987)
#5	Hydrocodone (38); norbuprenorphine (21)
#6	Alprazolam (28); amlodipine (34); gabapentin (13679); hydrocodone (253); nordiazepam (106)
#7	None detected
#8	Bupropion (366); chlorpheniramine (41); codeine (128); dextromethorphan (146); gabapentin (26882); hydrocodone (29); promethazine (37)
#9	Gabapentin (14981); mirtazapine (176); sertraline (128)
#10	None detected
#11	Bupropion (253); diphenhydramine (67); gabapentin (4781)
#12	Diazepam (154); metoclopramide (160); nordiazepam (194)
#13	Alprazolam (136); Nordiazepam (173); oxycodone (152); oxymorphone (57)
#14	6-Monoacetylmorphine (348); codeine (21); hydromorphone (88); morphine (937)
#15	Diphenhydramine (160)
#16	Cyclobenzaprine (59); EDDP (114); methadone (669)
#17	None detected
#18	None detected
#19	Citalopram (580); gabapentin (1056)
#20	Amitriptyline (926); metoclopramide (254); morphine (217); naproxen (135781); nortriptyline (1894); paroxetine (796); pregabalin (1378)
#21	9-Hydroxyrisperidone (46)
#22	Bupropion (97); buspirone (464); diazepam (247); gabapentin (33397); mirtazapine (141); nordiazepam (335); zolpidem (35)
#23	None detected
#24	Citalopram (462); hydrocodone (31)
#25	Amphetamine (254)
#26	Alprazolam (34); doxepin (421); gabapentin (8358); methadone (362); nordoxepin (342)
#27	Alprazolam (35); benzoylecgonine (206); citalopram (763); hydroxyzine (362)
#28	Diphenhydramine (97); doxylamine (73); hydrocodone (50)
#29	None detected
#30	Amphetamine (199); methamphetamine (5761); morphine (52)

For almost all drugs tested, the LOR given was the concentration in the lowest calibrant; as long as they lay above this LOR value and within the range of the calibration

curve, the calculated concentrations of such drugs in the PM samples were as reliable as the calibration itself. Duloxetine, norbuprenorphine, and nortramadol, though, were exceptions to this—their LORs were increased because the raw MS/MS signal provided by lower concentrations was not enough to distinguish it from the blank signal. This was important to bear in mind when interpreting the results of the drug screen on the PM samples. For example, nortramadol, the calibration curve of which spanned the range from 250 ng/mL to 12500 ng/mL, was detected in one of the PM samples and quantitated at a concentration of 987 ng/mL. However, it was not able to be reliably discerned from blank signal in the calibrant samples until 1000 ng/mL, indicating that, despite the linearity of its calibration curve, all measurements below this value would be difficult to accurately quantitate. Similar detection concerns arise from the other two drugs whose LORs were increased.

Evaluating the PS-MS/MS Drug Screen

Several general HPLC-MS drug screens were performed on PM samples from the same 30 donors to detect and quantitate the amount of each drug present. These results in addition to those presented in Table 9 were used as a basis for evaluating the integrity of the PS-MS/MS drug screen by monitoring the occurrence of true positives (TPs) and negatives (TNs) as well as, more importantly, false positives (FPs) and negatives (FNs).

Because of the superior selectivity afforded by using MS/MS coupled with the high resolution from the orbitrap mass analyzer, the background for many of the observed fragment ions was zero. (It was for this reason that 1×10^5 had to be used as an estimate of blank noise in the S/B measurements shown in Table 8.) Therefore, any reliably detected signal could be interpreted as originating from the analyte itself. In a few cases, such no-

background targets were clearly detected in the PM samples, signifying the analyte's presence, but their calculated concentrations were lower than the established LOR; these were accordingly not reported as quantitative results, but only as qualitatively detected drugs. This biased detection toward positive results (both TPs and FPs) was used to demonstrate the capability of the PS-MS/MS screen in detecting as many drugs as possible.

Of the 137 drugs screened for across each of the 30 PM samples—either passing (present) or failing (absent) detection—a total of 4110 qualitative and binary results were obtained. These results are summarized in Table 10 for both screening methods. PS-MS/MS detected a total of 91 drugs across all samples, with 10 of them failing detection via the HPLC-MS screens (the FPs). 88 drugs were detected using HPLC, but 7 of them were not caught with the PS method (the FNs). In total, 4012 drugs were confirmed to be absent from the PM samples by both screening methods.

Table 10. Qualitative results of the HPLC- and PS-based drug screens.

Qualitative Result	**Detection Criteria**		**Frequency**
	HPLC	**PS**	
True Positive (TP)	Positive	Positive	81
False Positive (FP)	Negative	Positive	10
True Negative (TN)	Negative	Negative	4012
False Negative (FN)	Positive	Negative	7

Qualitatively, the rates of occurrence for positive and negative results can be used in measuring a method's sensitivity, specificity, positive predictive value (PPV), and negative predictive value (NPV). These values are defined as:[128]

$$\text{Sensitivity} = \frac{\text{TP}}{\text{TP} + \text{FN}} \cdot 100 = 92.0\% \quad (1)$$

$$\text{Specificity} = \frac{\text{TN}}{\text{TN} + \text{FP}} \cdot 100 = 99.8\% \quad (2)$$

$$\mathrm{PPV} = \frac{\mathrm{TP}}{\mathrm{TP} + \mathrm{FP}} \cdot 100 = 89.0\% \quad (3)$$

$$\mathrm{NPV} = \frac{\mathrm{TN}}{\mathrm{TN} + \mathrm{FN}} \cdot 100 = 99.8\% \quad (4)$$

Put in context, qualitative sensitivity is a measure of how often the presence of a drug is accurately detected by the technique. Specificity is the opposite, measuring how often a drug's absence is accurately indicated. The predictive values are used to measure how often a drug is correctly detected (or not detected) among the positive (or negative) results. Expressed as percentages, the sensitivity of the PS-MS/MS screen was 92.0% while the specificity was 99.8%. 89.0% of all positive PS hits were drugs which were genuinely present in the samples, and 99.8% of all undetected drugs were confirmed to be absent in the samples.

The quantitative results of those drugs which were detected by both methods are shown plotted against each other—HPLC on the x-axis and PS on the y-axis—in Figure 26. In two methods with instrument responses that are directly proportional to changing concentrations, the slope of the regression line would be close to 1 and the calculated concentrations would directly correlate (the dashed line). However, in comparing PS-MS/MS and HPLC-MS, the former tended to overestimate the actual concentration; at 95% confidence, the slope of the regression lay between 1.05-1.30, indicating that PS-determined concentrations were biased high compared to HPLC. On average, the calculated concentrations based on the PS method were 58% different from the HPLC-determined concentrations. Important to note, though, is the fact that the PS method was developed solely as a screening method, whereas the HPLC method was a comprehensive assay meant for quantitative and confirmatory testing. Despite this, the concentrations

determined by PS-MS/MS still correlated well with those determined by HPLC-MS, generating a Pearson correlation coefficient of 0.996. This indicates the utility of PS-MS/MS in not only qualitative screening but also semi-quantitative analyses.

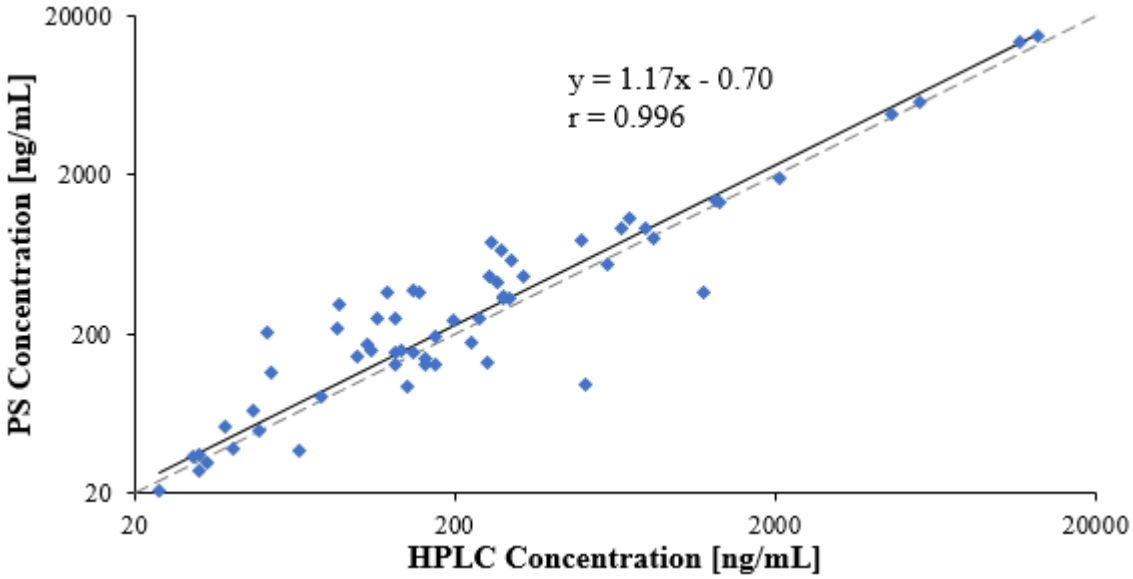

Figure 26. Comparison of concentrations for the drugs detected and quantitated from the PM samples by both HPLC- and PS-based screening methods. The dashed line represents two methods whose quantitative performances are identical.

Future Work

All analyses presented here relied solely on the detection of a single fragment ion in MS/MS mode. In most cases, the drugs fragmented into more than one ion when undergoing CID, but for purposes of maximizing method sensitivity, only the most abundant fragment ion was used for quantitation. To increase the specificity of this drug screen, one or more of these additional fragment ions could be included in the processing method to further streamline and automate analyses, which would allow the method to provide more reliable drug identifications without as much of a risk of false positives.[129]

Bearing in mind the work presented in Chapter 2, this positive ion drug screen could also be combined with a negative ion drug screen to create a much more comprehensive

technique for rapidly obtaining toxicologically relevant information. Currently, due to the differences in spray solvent needs between the two modes of ionization, they would have to be run separately, which is not ideal and would require running and processing unknown samples at least twice. However, if a universal solvent could be used for both polarities along with a unified sample preparation method that works for a wide variety of biological matrices, both acidic and basic drugs could be scanned for and processed simultaneously. Such a technique would be able to provide probative quantitation for 154 individual drugs in the span of three to four minutes, which would be an invaluable tool in an investigator's arsenal.

Conclusion

A PS-MS/MS drug screen was applied to the analysis of PM blood samples. Adjusting the spray solvent to 85:10:5:0.01 acetonitrile:acetone:water:acetic acid as well as mixing the samples with a larger volume of aqueous ISTD solution both proved to be critical modifications to the method to eliminate relative matrix effects. These adjustments were shown to lessen the ion suppression experienced by the ISTDs, producing more uniform signals across the calibrants and the 30 unknown PM samples than was previously achievable by the original method. Calibration curves were generated—establishing LORs and good linearity for almost all 137 analytes—and several drugs were able to be identified and quantitated from the PM samples.

The results from the PS-based drug screen were compared to those obtained independently via HPLC-MS. From the drugs which were identified and quantitated by both methods, concentrations determined by PS tended to slightly overestimate the true values; however, they showed a good overall correlation (R^2 = 0.9924) with their

corresponding HPLC concentrations, indicating the semi-quantitative capabilities of PS-MS/MS on top of its intended purposes for screening. Furthermore, the rates of false positives and negatives were worked out, and their effects on the diagnostic reliability of the technique were investigated. Because the scale of the screen was so large and most drugs screened for were absent from the samples, the number of negative results indicated an almost perfect NPV and specificity for PS. A much smaller number by comparison, the positive results led to a qualitative sensitivity of 92.0% and a PPV of 89.0%. Despite these disparities, though, these are still promising results that demonstrate the capability of PS-MS/MS in screening for drugs on a level that rivals HPLC-MS, accomplishing the same task in a significantly simpler and quicker way. By comparing the newer technique to the older and more established technique of HPLC, PS-based drug screens further develop toward real-world application, where they could ultimately be used for rapid, effective, and cheap biomonitoring and toxicology.

REFERENCES

1. Gohlke, R. S.; McLafferty, F. W. Early gas chromatography/mass spectrometry. *Journal of the American Society for Mass Spectrometry* **1993**, *4*, 367-371.
2. Hiraoka, K.; Kudaka, I. Electrospray interface for liquid chromatography/mass spectrometry. *Rapid Communications in Mass Spectrometry* **1990**, *4*, 519-526.
3. Whitehouse, C. M.; Dreyer, R. N.; Yamashita, M.; Fenn, J. B. Electrospray interface for liquid chromatographs and mass spectrometers. *Analytical Chemistry* **1985**, *57*, 675-679.
4. Yamashita, M.; Fenn, J. B. Electrospray ion source. Another variation on the free-jet theme. *The Journal of Physical Chemistry* **1984**, *88*, 4451-4459.
5. Takáts, Z.; Wiseman, J. M.; Gologan, B.; Cooks, R. G. Mass spectrometry sampling under ambient conditions with desorption electrospray ionization. *Science* **2004**, *306*, 471-473.
6. Cody, R. B.; Laramée, J. A.; Durst, H. D. Versatile new ion source for the analysis of materials in open air under ambient conditions. *Analytical Chemistry* **2005**, *77*, 2297-2302.
7. Alberici, R. M.; Simas, R. C.; Sanvido, G. B.; Romão, W.; Lalli, P. M.; Benassi, M.; Cunha, I. B. S.; Eberlin, M. N. Ambient mass spectrometry: Bringing MS into the "real world". *Analytical and Bioanalytical Chemistry* **2010**, *398*, 265-294.
8. Tepper, G.; Kessick, R. Nanoelectrospray aerosols from microporous polymer wick sources. *Applied Physics Letters* **2009**, *94*, 084106.
9. Liu, J.; Wang, H.; Manicke, N. E.; Lin, J.-M.; Cooks, R. G.; Ouyang, Z. Development, characterization, and application of paper spray ionization. *Analytical Chemistry* **2010**, *82*, 2463-2471.
10. Manicke, N. E.; Abu-Rabie, P.; Spooner, N.; Ouyang, Z.; Cooks, R. G. Quantitative analysis of therapeutic drugs in dried blood spot samples by paper spray mass spectrometry: An avenue to therapeutic drug monitoring. *Journal of the American Society for Mass Spectrometry* **2011**, *22*, 1501-1507.
11. Manicke, N. E.; Yang, Q.; Wang, H.; Oradu, S.; Ouyang, Z.; Cooks, R. G. Assessment of paper spray ionization for quantitation of pharmaceuticals in blood spots. *International Journal of Mass Spectrometry* **2011**, *300*, 123-129.
12. Wang, H.; Liu, J.; Cooks, R. G.; Ouyang, Z. Paper spray for direct analysis of complex mixtures using mass spectrometry. *Angewandte Chemie* **2010**, *122*, 889-892.
13. Wang, H.; Manicke, N. E.; Yang, Q.; Zheng, L.; Shi, R.; Cooks, R. G.; Ouyang, Z. Direct analysis of biological tissue by paper spray mass spectrometry. *Analytical Chemistry* **2011**, *83*, 1197-1201.

14. Zhang, Z.; Xu, W.; Manicke, N. E.; Cooks, R. G.; Ouyang, Z. Silica coated paper substrate for paper-spray analysis of therapeutic drugs in dried blood spots. *Analytical Chemistry* **2012**, *84*, 931-938.

15. Narayanan, R.; Sarkar, D.; Cooks, R. G.; Pradeep, T. Molecular ionization from carbon nanotube paper. *Angewandte Chemie International Edition* **2014**, *53*, 5936-5940.

16. Wong, M. Y.-M.; Man, S.-H.; Che, C.-M.; Lau, K.-C.; Ng, K.-M. Negative electrospray ionization on porous supporting tips for mass spectrometric analysis: Electrostatic charging effect on detection sensitivity and its application to explosive detection. *Analyst* **2014**, *139*, 1482-1491.

17. Wong, M. Y.-M.; Tang, H.-W.; Man, S.-H.; Lam, C.-W.; Che, C.-M.; Ng, K.-M. Electrospray ionization on porous spraying tips for direct sample analysis by mass spectrometry: Enhanced detection sensitivity and selectivity using hydrophobic/hydrophilic materials as spraying tips. *Rapid Communications in Mass Spectrometry* **2013**, *27*, 713-721.

18. Hu, B.; So, P.-K.; Chen, H.; Yao, Z.-P. Electrospray ionization using wooden tips. *Analytical Chemistry* **2011**, *83*, 8201-8207.

19. Liu, J.; Wang, H.; Cooks, R. G.; Ouyang, Z. Leaf spray: Direct chemical analysis of plant material and living plants by mass spectrometry. *Analytical Chemistry* **2011**, *83*, 7608-7613.

20. Li, M.; Zhang, J.; Jiang, J.; Zhang, J.; Gao, J.; Qiao, X. Rapid, in situ detection of cocaine residues based on paper spray ionization coupled with ion mobility spectrometry. *Analyst* **2014**, *139*, 1687-1691.

21. Soparawalla, S.; Tadjimukhamedov, F. K.; Wiley, J. S.; Ouyang, Z.; Cooks, R. G. In situ analysis of agrochemical residues on fruit using ambient ionization on a handheld mass spectrometer. *Analyst* **2011**, *136*, 4392-4396.

22. Li, L.; Chen, T.-C.; Ren, Y.; Hendricks, P. I.; Cooks, R. G.; Ouyang, Z. Mini 12, miniature mass spectrometer for clinical and other applications—introduction and characterization. *Analytical Chemistry* **2014**, *86*, 2909-2916.

23. Snyder, D. T.; Pulliam, C. J.; Ouyang, Z.; Cooks, R. G. Miniature and fieldable mass spectrometers: Recent advances. *Analytical Chemistry* **2016**, *88*, 2-29.

24. Espy, R. D.; Teunissen, S. F.; Manicke, N. E.; Ren, Y.; Ouyang, Z.; van Asten, A.; Cooks, R. G. Paper spray and extraction spray mass spectrometry for the direct and simultaneous quantification of eight drugs of abuse in whole blood. *Analytical Chemistry* **2014**, *86*, 7712-7718.

25. Su, Y.; Wang, H.; Liu, J.; Wei, P.; Cooks, R. G.; Ouyang, Z. Quantitative paper spray mass spectrometry analysis of drugs of abuse. *Analyst* **2013**, *138*, 4443-4447.

26. Wang, H.; Ren, Y.; McLuckey, M. N.; Manicke, N. E.; Park, J.; Zheng, L.; Shi, R.; Cooks, R. G.; Ouyang, Z. Direct quantitative analysis of nicotine alkaloids from biofluid samples using paper spray mass spectrometry. *Analytical Chemistry* **2013**, *85*, 11540-11544.

27. Salentijn, G. I. J.; Permentier, H. P.; Verpoorte, E. 3D-printed paper spray ionization cartridge with fast wetting and continuous solvent supply features. *Analytical Chemistry* **2014**, *86*, 11657-11665.

28. Zhang, Z.; Cooks, R. G.; Ouyang, Z. Paper spray: A simple and efficient means of analysis of different contaminants in foodstuffs. *Analyst* **2012**, *137*, 2556-2558.

29. Zhang, Y.; Li, H.; Ma, Y.; Lin, J.-M. Paper spray mass spectrometry-based method for analysis of droplets in a gravity-driven microfluidic chip. *Analyst* **2014**, *139*, 1023-1029.

30. Yang, Q.; Manicke, N. E.; Wang, H.; Petucci, C.; Cooks, R. G.; Ouyang, Z. Direct and quantitative analysis of underivatized acylcarnitines in serum and whole blood using paper spray mass spectrometry. *Analytical and Bioanalytical Chemistry* **2012**, *404*, 1389-1397.

31. Amador, V. S.; Pereira, H. V.; Sena, M. M.; Augusti, R.; Piccin, E. Paper spray mass spectrometry for the forensic analysis of black ballpoint pen inks. *Journal of the American Society for Mass Spectrometry* **2017**, 1-12.

32. da Silva Ferreira, P.; Fernandes de Abreu e Silva, D.; Augusti, R.; Piccin, E. Forensic analysis of ballpoint pen inks using paper spray mass spectrometry. *Analyst* **2015**, *140*, 811-819.

33. Jett, R. (2017). *Paper spray mass spectrometry for rapid drug screening* (Master's thesis). Purdue University (Indianapolis, IN).

34. Jett, R.; Skaggs, C.; Manicke, N. Drug screening method development for paper spray coupled to a triple quadrupole mass spectrometer. *Analytical Methods* **2017**.

35. Espy, R. D.; Muliadi, A. R.; Ouyang, Z.; Cooks, R. G. Spray mechanism in paper spray ionization. *International Journal of Mass Spectrometry* **2012**, *325–327*, 167-171.

36. Ikonomou, M. G.; Blades, A. T.; Kebarle, P. Electrospray mass spectrometry of methanol and water solutions suppression of electric discharge with SF6 gas. *Journal of the American Society for Mass Spectrometry* **1991**, *2*, 497-505.

37. Goldman, M.; Goldman, A., in *Gaseous Electronics, Volume I: Electrical Discharges*, Hirsh, M. N.; Oskam, H. J., Eds. (Academic Press, New York, NY, 1978), 219-290.

38. Raizer, Y. P., in *Gas Discharge Physics*, Allen, J. E., Ed. (Springer-Verlag, Berlin, 1991), 324-377.

39. Skalny, J. D.; Mikoviny, T.; Matejcik, S.; Mason, N. J. An analysis of mass spectrometric study of negative ions extracted from negative corona discharge in air. *International Journal of Mass Spectrometry* **2004**, *233*, 317-324.

40. Faircloth, D. C. Technological aspects: High voltage. *CERN Yellow Report* **2013**, *2013*, 381-419.

41. Loeb, L. B. *Electrical Coronas: Their Basic Physical Mechanisms*. (University of California Press, Berkeley, CA, 1965).

42. Busch, K. Space charge in mass spectrometry. *Spectroscopy* **2004**, *19*, 35-38.

43. Wampler, F. M.; Blades, A. T.; Kebarle, P. Negative ion electrospray mass spectrometry of nucleotides: Ionization from water solution with SF6 discharge suppression. *Journal of the American Society for Mass Spectrometry* **1993**, *4*, 289-295.

44. Yamashita, M.; Fenn, J. B. Negative ion production with the electrospray ion source. *The Journal of Physical Chemistry* **1984**, *88*, 4671-4675.

45. Cole, R. B.; Harrata, A. K. Charge-state distribution and electric-discharge suppression in negative-ion electrospray mass spectrometry using chlorinated solvents. *Rapid Communications in Mass Spectrometry* **1992**, *6*, 536-539.

46. Hiraoka, K.; Kudaka, I. Negative-mode electrospray-mass spectrometry using nonaqueous solvents. *Rapid Communications in Mass Spectrometry* **1992**, *6*, 265-268.

47. Cech, N. B.; Enke, C. G. Practical implications of some recent studies in electrospray ionization fundamentals. *Mass Spectrometry Reviews* **2001**, *20*, 362-387.

48. Jackson, G. S.; Enke, C. G. Electrical equivalence of electrospray ionization with conducting and nonconducting needles. *Analytical Chemistry* **1999**, *71*, 3777-3784.

49. Jaworek, A.; Sobczyk, A.; Czech, T.; Krupa, A. Corona discharge in electrospraying. *Journal of Electrostatics* **2014**, *72*, 166-178.

50. López-Muñoz, F.; Ucha-Udabe, R.; Alamo, C. The history of barbiturates a century after their clinical introduction. *Neuropsychiatric Disease and Treatment* **2005**, *1*, 329-343.

51. Ikonomou, M. G.; Blades, A. T.; Kebarle, P. Investigations of the electrospray interface for liquid chromatography/mass spectrometry. *Analytical Chemistry* **1990**, *62*, 957-967.

52. Diaz, A. F.; Felix-Navarro, R. M. A semi-quantitative tribo-electric series for polymeric materials: The influence of chemical structure and properties. *Journal of Electrostatics* **2004**, *62*, 277-290.

53. Wleklinski, M.; Li, Y.; Bag, S.; Sarkar, D.; Narayanan, R.; Pradeep, T.; Cooks, R. G. Zero volt paper spray ionization and its mechanism. *Analytical Chemistry* **2015**, *87*, 6786-6793.

54. Smith, D. P. H. The electrohydrodynamic atomization of liquids. *IEEE Transactions on Industry Applications* **1986**, *IA-22*, 527-535.

55. Conference of Plenipotentiaries on the Protocol on Chlorofluorocarbons to the Vienna Convention for the Protection of the Ozone Layer. *Amendment to the Montreal Protocol on substances that deplete the ozone layer* **1990**. United Nations (London, United Kingdom).

56. Hamilton, A. Formation of phosgene in thermal decomposition of carbon tetrachloride. *Industrial & Engineering Chemistry* **1933**, *25*, 539-541.

57. Kubic, V. L.; Anders, M. W. Metabolism of carbon tetrachloride to phosgene. *Life Sciences* **1980**, *26*, 2151-2155.

58. International Agency for Research on Cancer. *List of classifications* **2017**. United Nations (Lyon, France).

59. Compton, R. N.; Cooper, C. D. Negative ion properties of tetracyanoquinodimethan: Electron affinity and compound states. *The Journal of Chemical Physics* **1977**, *66*, 4325-4329.

60. Staneke, P. O.; Groothuis, G.; Ingemann, S.; Nibbering, N. M. M. Formation, stability and structure of radical anions of chloroform, tetrachloromethane and fluorotrichloromethane in the gas phase. *International Journal of Mass Spectrometry and Ion Processes* **1995**, *142*, 83-93.

61. McKenna, J.; Dhummakupt, E. S.; Connell, T.; Demond, P. S.; Miller, D. B.; Nilles, J. M.; Manicke, N. E.; Glaros, T. Detection of chemical warfare agent simulants and hydrolysis products in biological samples by paper spray mass spectrometry. *Analyst* **2017**, *142*, 1442-1451.

62. Benschop, H. P.; van der Schans, G. P.; Noort, D.; Fidder, A.; Mars-Groenendijk, R. H.; de Jong, L. P. A. Verification of exposure to sulfur mustard in two casualties of the Iran-Iraq conflict. *Journal of Analytical Toxicology* **1997**, *21*, 249-251.

63. Black, R. M.; Clarke, R. J.; Read, R. W.; Reid, M. T. J. Application of gas chromatography-mass spectrometry and gas chromatography-tandem mass spectrometry to the analysis of chemical warfare samples, found to contain residues of the nerve agent sarin, sulphur mustard and their degradation products. *Journal of Chromatography A* **1994**, *662*, 301-321.

64. Organisation for the Prohibition of Chemical Weapons. *Convention on the prohibition of the development, production, stockpiling and use of chemical weapons and on their destruction* **1993**. United Nations (New York, NY).

65. Matsuda, Y.; Nagao, M.; Takatori, T.; Niijima, H.; Nakajima, M.; Iwase, H.; Kobayashi, M.; Iwadate, K. Detection of the sarin hydrolysis product in formalin-fixed brain tissues of victims of the Tokyo subway terrorist attack. *Toxicology and Applied Pharmacology* **1998**, *150*, 310-320.

66. Nagao, M.; Takatori, T.; Matsuda, Y.; Nakajima, M.; Iwase, H.; Iwadate, K. Definitive evidence for the acute sarin poisoning diagnosis in the Tokyo subway. *Toxicology and Applied Pharmacology* **1997**, *144*, 198-203.

67. Noort, D.; Hulst, A. G.; Platenburg, D. H. J. M.; Polhuijs, M.; Benschop, H. P. Quantitative analysis of O-isopropyl methylphosphonic acid in serum samples of Japanese citizens allegedly exposed to sarin: Estimation of internal dosage. *Archives of Toxicology* **1998**, *72*, 671-675.

68. Tu, A. T. Aum Shinrikyo's chemical and biological weapons: More than sarin. *Forensic Science Review* **2014**, *26*, 115-120.

69. Berlinger, J. VX nerve agent used to kill Kim Jong Nam, police say. *CNN* **2017**. http://www.cnn.com/2017/02/23/asia/kim-jong-nam-vx-nerve-agent/.

70. Dewan, A.; Alkashali, H. Syria chemical attack: Authority finds 'incontrovertible' evidence of sarin. *CNN* **2017**. http://www.cnn.com/2017/04/20/middleeast/syria-chemical-attack-sarin-opcw/.

71. Hakeem, O.; Jabri, S. Adverse birth outcomes in women exposed to Syrian chemical attack. *The Lancet Global Health* **2015**, *3*, e196.

72. Pita, R.; Domingo, J. The use of chemical weapons in the Syrian conflict. *Toxics* **2014**, *2*, 391-402.

73. Rosman, Y.; Eisenkraft, A.; Milk, N.; Shiyovich, A.; Ophir, N.; Shrot, S.; Kreiss, Y.; Kassirer, M. Lessons learned from the Syrian sarin attack: Evaluation of a clinical syndrome through social media. *Annals of Internal Medicine* **2014**, *160*, 644-648.

74. Bajgar, J. Organophosphates/nerve agent poisoning: Mechanism of action, diagnosis, prophylaxis, and treatment. *Advances in Clinical Chemistry* **2004**, *38*, 151-216.

75. Ganesan, K.; Raza, S.; Vijayaraghavan, R. Chemical warfare agents. *Journal of Pharmacy And Bioallied Sciences* **2010**, *2*, 166-178.

76. Munro, N. B.; Talmage, S. S.; Griffin, G. D.; Waters, L. C.; Watson, A. P.; King, J. F.; Hauschild, V. The sources, fate, and toxicity of chemical warfare agent degradation products. *Environmental Health Perspectives* **1999**, *107*, 933-974.

77. Cannard, K. The acute treatment of nerve agent exposure. *Journal of the Neurological Sciences* **2006**, *249*, 86-94.

78. Noeller, T. P. Biological and chemical terrorism: Recognition and management. *Cleveland Clinic Journal of Medicine* **2001**, *68*, 1001-1016.

79. Murray, V.; Goodfellow, F. Mass casualty chemical incidents—towards guidance for public health management. *Public Health* **2002**, *116*, 2-14.

80. D'Agostino, P. A.; Hancock, J. R.; Provost, L. R. Determination of sarin, soman and their hydrolysis products in soil by packed capillary liquid chromatography–electrospray mass spectrometry. *Journal of Chromatography A* **2001**, *912*, 291-299.

81. John, H.; Worek, F.; Thiermann, H. LC-MS-based procedures for monitoring of toxic organophosphorus compounds and verification of pesticide and nerve agent poisoning. *Analytical & Bioanalytical Chemistry* **2008**, *391*, 97-116.

82. Lakso, H.-Å.; Ng, W. F. Determination of chemical warfare agents in natural water samples by solid-phase microextraction. *Analytical Chemistry* **1997**, *69*, 1866-1872.

83. Ketkar, S. N.; Dulak, J. G.; Fite, W. L.; Buchner, J. D.; Dheandhanoo, S. Atmospheric pressure ionization tandem mass spectrometric system for real-time detection of low-level pollutants in air. *Analytical Chemistry* **1989**, *61*, 260-264.

84. Seto, Y.; Kanamori-Kataoka, M.; Tsuge, K.; Ohsawa, I.; Iura, K.; Itoi, T.; Sekiguchi, H.; Matsushita, K.; Yamashiro, S.; Sano, Y.; Sekiguchi, H.; Maruko, H.; Takayama, Y.; Sekioka, R.; Okumura, A.; Takada, Y.; Nagano, H.; Waki, I.; Ezawa, N.; Tanimoto, H.; Honjo, S.; Fukano, M.; Okada, H. Sensitive monitoring of volatile chemical warfare agents in air by atmospheric pressure chemical ionization mass spectrometry with counter-flow introduction. *Analytical Chemistry* **2013**, *85*, 2659-2666.

85. Nilles, J. M.; Connell, T. R.; Durst, H. D. Quantitation of chemical warfare agents using the direct analysis in real time (DART) technique. *Analytical Chemistry* **2009**, *81*, 6744-6749.

86. D'Agostino, P. A.; Hancock, J. R.; Chenier, C. L.; Lepage, C. R. J. Liquid chromatography electrospray tandem mass spectrometric and desorption electrospray ionization tandem mass spectrometric analysis of chemical warfare agents in office media typically collected during a forensic investigation. *Journal of Chromatography A* **2006**, *1110*, 86-94.

87. D'Agostino, P. A.; Chenier, C. L.; Hancock, J. R.; Lepage, C. R. J. Desorption electrospray ionisation mass spectrometric analysis of chemical warfare agents from solid-phase microextraction fibers. *Rapid Communications in Mass Spectrometry* **2007**, *21*, 543-549.

88. Reeber, S. L.; Gadi, S.; Huang, S.-B.; Glish, G. L. Direct analysis of herbicides by paper spray ionization mass spectrometry. *Analytical Methods* **2015**, *7*, 9808-9816.

89. Black, R. M.; Muir, B. Derivatisation reactions in the chromatographic analysis of chemical warfare agents and their degradation products. *Journal of Chromatography A* **2003**, *1000*, 253-281.

90. Sng, M. T.; Ng, W. F. In-situ derivatisation of degradation products of chemical warfare agents in water by solid-phase microextraction and gas chromatographic–mass spectrometric analysis. *Journal of Chromatography A* **1999**, *832*, 173-182.

91. Rohrbaugh, D. K.; Sarver, E. W. Detection of alkyl methylphosphonic acids in complex matrices by gas chromatography–tandem mass spectrometry. *Journal of Chromatography A* **1998**, *809*, 141-150.

92. Black, R. M.; Read, R. W. Application of liquid chromatography-atmospheric pressure chemical ionisation mass spectrometry, and tandem mass spectrometry, to the analysis and identification of degradation products of chemical warfare agents. *Journal of Chromatography A* **1997**, *759*, 79-92.

93. Liu, Q.; Hu, X.; Xie, J. Determination of nerve agent degradation products in environmental samples by liquid chromatography–time-of-flight mass spectrometry with electrospray ionization. *Analytica Chimica Acta* **2004**, *512*, 93-101.

94. Owens, J.; Vu, A.; Koester, C. Analysis of phosphonic acids: Validation of semi-volatile analysis by HPLC-MS/MS by EPA method MS999. *Lawrence Livermore National Laboratory* **2008**. https://e-reports-ext.llnl.gov/pdf/367241.pdf.

95. Read, R. W.; Black, R. M. Rapid screening procedures for the hydrolysis products of chemical warfare agents using positive and negative ion liquid chromatography–mass spectrometry with atmospheric pressure chemical ionisation. *Journal of Chromatography A* **1999**, *862*, 169-177.

96. Black, R. M.; Read, R. W. Analysis of degradation products of organophosphorus chemical warfare agents and related compounds by liquid chromatography–mass spectrometry using electrospray and atmospheric pressure chemical ionisation. *Journal of Chromatography A* **1998**, *794*, 233-244.

97. Song, Y.; Cooks, R. G. Reactive desorption electrospray ionization for selective detection of the hydrolysis products of phosphonate esters. *Journal of Mass Spectrometry* **2007**, *42*, 1086-1092.

98. Kingdon, K. H. A method for the neutralization of electron space charge by positive ionization at very low gas pressures. *Physical Review* **1923**, *21*, 408-418.

99. Hu, Q.; Noll, R. J.; Li, H.; Makarov, A.; Hardman, M.; Cooks, R. G. The Orbitrap: A new mass spectrometer. *Journal of Mass Spectrometry* **2005**, *40*, 430-443.

100. Makarov, A. Electrostatic axially harmonic orbital trapping: A high-performance technique of mass analysis. *Analytical Chemistry* **2000**, *72*, 1156-1162.

101. Comisarow, M. B.; Marshall, A. G. Fourier transform ion cyclotron resonance spectroscopy. *Chemical Physics Letters* **1974**, *25*, 282-283.

102. Comisarow, M. B.; Marshall, A. G. Frequency-sweep Fourier transform ion cyclotron resonance spectroscopy. *Chemical Physics Letters* **1974**, *26*, 489-490.

103. Cotter, R. J. Peer reviewed: The new time-of-flight mass spectrometry. *Analytical Chemistry* **1999**, *71*, 445A-451A.

104. Wong, P. S. H.; Cooks, R. G. Ion trap mass spectrometry. *Current Separations* **1997**, *16*, 85-92.

105. Soni, M.; Frankevich, V.; Nappi, M.; Santini, R. E.; Amy, J. W.; Cooks, R. G. Broad-band Fourier transform quadrupole ion trap mass spectrometry. *Analytical Chemistry* **1996**, *68*, 3314-3320.

106. Marshall, A. G.; Hendrickson, C. L.; Jackson, G. S. Fourier transform ion cyclotron resonance mass spectrometry: A primer. *Mass Spectrometry Reviews* **1998**, *17*, 1-35.

107. Mamyrin, B. A.; Karataev, V. I.; Shmikk, D. V.; Zagulin, V. A. The mass-reflectron, a new nonmagnetic time-of-flight mass spectrometer with high resolution. *Journal of Experimental and Theoretical Physics* **1973**, *37*, 45-48.

108. Toyoda, M.; Okumura, D.; Ishihara, M.; Katakuse, I. Multi-turn time-of-flight mass spectrometers with electrostatic sectors. *Journal of Mass Spectrometry* **2003**, *38*, 1125-1142.

109. Yavor, M.; Verentchikov, A.; Hasin, J.; Kozlov, B.; Gavrik, M.; Trufanov, A. Planar multi-reflecting time-of-flight mass analyzer with a jig-saw ion path. *Physics Procedia* **2008**, *1*, 391-400.

110. Dawson, J. H. J.; Guilhaus, M. Orthogonal-acceleration time-of-flight mass spectrometer. *Rapid Communications in Mass Spectrometry* **1989**, *3*, 155-159.

111. Verentchikov, A. N.; Ens, W.; Standing, K. G. Reflecting time-of-flight mass spectrometer with an electrospray ion source and orthogonal extraction. *Analytical Chemistry* **1994**, *66*, 126-133.

112. Krauss, M.; Singer, H.; Hollender, J. LC–high resolution MS in environmental analysis: From target screening to the identification of unknowns. *Analytical and Bioanalytical Chemistry* **2010**, *397*, 943-951.

113. Rajski, Ł.; Gómez-Ramos, M. d. M.; Fernández-Alba, A. R. Large pesticide multiresidue screening method by liquid chromatography-Orbitrap mass spectrometry in full scan mode applied to fruit and vegetables. *Journal of Chromatography A* **2014**, *1360*, 119-127.

114. Savory, J. J.; Kaiser, N. K.; McKenna, A. M.; Xian, F.; Blakney, G. T.; Rodgers, R. P.; Hendrickson, C. L.; Marshall, A. G. Parts-per-billion Fourier transform ion cyclotron resonance mass measurement accuracy with a "walking" calibration equation. *Analytical Chemistry* **2011**, *83*, 1732-1736.

115. Shi, S. D. H.; Hendrickson, C. L.; Marshall, A. G. Counting individual sulfur atoms in a protein by ultrahighresolution Fourier transform ion cyclotron resonance mass spectrometry: Experimental resolution of isotopic fine structure in proteins. *Proceedings of the National Academy of Sciences* **1998**, *95*, 11532-11537.

116. Marshall, A. G.; Hendrickson, C. L. High-resolution mass spectrometers. *Annual Review of Analytical Chemistry* **2008**, *1*, 579-599.

117. Bateman, K. P.; Kellmann, M.; Muenster, H.; Papp, R.; Taylor, L. Quantitative–qualitative data acquisition using a benchtop orbitrap mass spectrometer. *Journal of the American Society for Mass Spectrometry* **2009**, *20*, 1441-1450.

118. Gómez-Ramos, M. M.; Ferrer, C.; Malato, O.; Agüera, A.; Fernández-Alba, A. R. Liquid chromatography-high-resolution mass spectrometry for pesticide residue analysis in fruit and vegetables: Screening and quantitative studies. *Journal of Chromatography A* **2013**, *1287*, 24-37.

119. Zhang, N. R.; Yu, S.; Tiller, P.; Yeh, S.; Mahan, E.; Emary, W. B. Quantitation of small molecules using high-resolution accurate mass spectrometers – a different approach for analysis of biological samples. *Rapid Communications in Mass Spectrometry* **2009**, *23*, 1085-1094.

120. Hogenboom, A. C.; van Leerdam, J. A.; de Voogt, P. Accurate mass screening and identification of emerging contaminants in environmental samples by liquid chromatography–hybrid linear ion trap Orbitrap mass spectrometry. *Journal of Chromatography A* **2009**, *1216*, 510-519.

121. Lim, H.-K.; Chen, J.; Sensenhauser, C.; Cook, K.; Subrahmanyam, V. Metabolite identification by data-dependent accurate mass spectrometric analysis at resolving power of 60000 in external calibration mode using an LTQ/Orbitrap. *Rapid Communications in Mass Spectrometry* **2007**, *21*, 1821-1832.

122. Alder, L.; Steinborn, A.; Bergelt, S. Suitability of an orbitrap mass spectrometer for the screening of pesticide residues in extracts of fruits and vegetables. *Journal of AOAC International* **2011**, *94*, 1661-1673.

123. Kolmonen, M.; Leinonen, A.; Pelander, A.; Ojanperä, I. A general screening method for doping agents in human urine by solid phase extraction and liquid chromatography/time-of-flight mass spectrometry. *Analytica Chimica Acta* **2007**, *585*, 94-102.

124. Hardman, M.; Makarov, A. A. Interfacing the orbitrap mass analyzer to an electrospray ion source. *Analytical Chemistry* **2003**, *75*, 1699-1705.

125. Olsen, J. V.; de Godoy, L. M. F.; Li, G.; Macek, B.; Mortensen, P.; Pesch, R.; Makarov, A.; Lange, O.; Horning, S.; Mann, M. Parts per million mass accuracy on an orbitrap mass spectrometer via lock mass injection into a C-trap. *Molecular & Cellular Proteomics* **2005**, *4*, 2010-2021.

126. Kaufmann, A.; Dvorak, V.; Crüzer, C.; Butcher, P.; Maden, K.; Walker, S.; Widmer, M.; Schürmann, A. Study of high-resolution mass spectrometry technology as a replacement for tandem mass spectrometry in the field of quantitative pesticide residue analysis. *Journal of AOAC International* **2012**, *95*, 528-548.

127. Vega, C.; Spence, C.; Zhang, C.; Bills, B. J.; Manicke, N. E. Ionization suppression and recovery in direct biofluid analysis using paper spray mass spectrometry. *Journal of the American Society for Mass Spectrometry* **2016**, *27*, 726-734.

128. Akobeng, A. K. Understanding diagnostic tests 1: Sensitivity, specificity and predictive values. *Acta Pædiatrica* **2007**, *96*, 338-341.

129. Pozo, Ó. J.; Sancho, J. V.; Ibáñez, M.; Hernández, F.; Niessen, W. M. A. Confirmation of organic micropollutants detected in environmental samples by liquid chromatography tandem mass spectrometry: Achievements and pitfalls. *Trends in Analytical Chemistry* **2006**, *25*, 1030-1042.

VITA

Josiah McKenna graduated from D.C. Everest High School (Weston, WI) as a valedictorian in 2011. He went on to pursue a B.S. in Chemistry as well as minors in Theatre Arts and English from Carroll University (Waukesha, WI). In summer 2014, he was awarded the Thronson Fellowship, which gave him the opportunity to do research under Dr. John Parkinson at the University of Strathclyde (Glasgow, Scotland), focusing on method development for nuclear magnetic resonance spectroscopy. After graduating summa cum laude from Carroll University in 2015, he began graduate school at Indiana University – Purdue University Indianapolis (Indianapolis, IN), performing research in mass spectrometry under Dr. Nick Manicke. In 2017, he obtained his M.S. in Forensic Science.